Physiological Relevance of Novel Lysosomal Ion Channels

by

Ce Wang

A dissertation submitted in partial fulfillment
of the requirements for the degree of
Doctor of Philosophy
(Molecular, Cellular, and Developmental Biology)
in the University of Michigan
2021

Doctoral Committee:

Professor Richard Hume, Chair
Professor Robert Fuller
Professor Daniel Klionsky
Professor Yanzhuang Wang

Ce Wang

cerwang@umich.edu

ORCID: 0000-0003-1932-0218

© Ce Wang 2021

DEDICATION

To my family and my friends,

For their love, support, and encouragement.

ACKNOWLEDGEMENTS

This thesis would not be possible without the help and support of many people throughout my Ph.D. study and I appreciate all of them.

First and foremost, I would like to extend my sincere gratitude to my Ph.D. advisor Dr. Haoxing Xu. Dr. Xu is incredibly smart, hard-working and his passion towards science has always inspired me and pushed me forward. During these years, Dr. Xu always provides professional and inspiring instructions, sharp critiques, and encouragement towards my thinking and research abilities. More importantly, Dr. Xu teaches me how to deal with difficulties and frustrations, and from him I have gained the confidence and courage in my abilities to embrace any future challenges.

I would like to thank Dr. Richard Hume as my co-advisor for his support in maintaining the lab during the hard times and for his dedication of time and effort in assisting my research projects and thesis writing.

I would also like to express my sincere thanks to my thesis committee members, Dr. Richard Hume, Dr. Yanzhuang Wang, Dr. Daniel Klionsky, and Dr. Robert Fuller for all the perceptive suggestions, invaluable suggestions and critiques along the progress of my thesis. I would like to thank Dr. Yanzhuang Wang for generously sharing all reagents and equipment as a wonderful neighbor through all the difficult times of the lab.

I would like to thank Dr. Laura Buttita and all the people in her lab. I enjoyed my rotation in the Buttita lab, and I appreciate her guidance as well as the help with flow cytometry. I also want to thank many people in MCDB for making my graduate work possible, especially Dr.

Kenneth Cadigan, who helped me go through the hard transition; Dr. Ursula Jakob, who helped with my prelim preparation; Mary Carr, who helped in every aspect of my graduate life; and Gregg Sobocinski, who always helped to solve problems with microscopes and other instruments.

I would also like to thank all the Xu lab members, who I always feel so lucky to work with. I appreciate all great scientific conversations, all fun and sad moments we have shared together. I would like to thank Dr. Xiaoli Zhang, for not only providing me with so many brilliant scientific suggestions but also for being a loyal friend. I thank Dr. Ping Li, Dr. Meiqin Hu and Dr. Lu Yu for the discussions, suggestions, and collaborations. I thank Dr. Mingxue Gu, Wei Chen, Qi Geng, Shiyu Xiao, Kaiyuan Tang, Shiyi Wang for being helpful and supportive as labmates as well as friends all the time. I also thank undergraduate researchers Spring Gao and Prateek Pinchi for helping me with genotyping and data analysis.

I thank all my friends that I have made over the years here at Michigan as well as all old friends, with whom I have shared all the struggles and happy moments. They can always turn my sadness and struggles into motivations, and make my happy time unforgettable. I have learned so much from my friends.

Finally, to my family, for always providing me with their unconditional love and support throughout my life. I thank my parents, who are always open-minded and always cheer me up whenever I feel upset. I also thank my sister, who is a smart scientist, for all enthusiasm about science she has ever shared with me and all the memorable trips during my vacation in the past few years. Without them, I could not have made it this far.

PREFACE

The work reported in this thesis resulted from the highly collaborative research environment of the Xu lab. I have permission from my co-authors to report their portions of these studies in this thesis.

The results presented in Chapter II are drawn from a recently published paper (Li et al 2020) with some modifications. Ping Li initiated the project and is first author. I am the co-second author. Ping Li generated most of the electrophysiology data, with Meiqin Hu also making a contribution. I designed and carried out most of the cell culture based imaging experiments. Details of who contributed to each figure are shown in Table I.

The results presented in Chapter III are drawn from a manuscript currently under review entitled "TMEM175 encodes a proton-activated, proton channel of lysosomes." Meiqin Hu, Ping Li and I are listed as co-first authors. Meiqin Hu and Ping Li generated all of the electrophysiology data. I designed and carried out most of the cell biology experiments. Details of who contributed to each figure and the full list of authors of this manuscript and their affiliations are shown in Table II.

The literature review presented in Chapter I was written by me, with editing provided by my thesis co-advisor Professor Richard Hume. The writing in chapters 2 and 3 represents a collaborative effort between me, the other two major co-authors, (Meiqin Hu and Ping Li) and my two thesis advisors, Professor Haoxing Xu and Professor Richard Hume. The final summary in chapter IV was written by me with editing provided by my thesis co-advisor Professor Richard Hume.

Table I. Source of the data in Chapter II (from Li et al 2020)	
Figure #	Person who was responsible for the illustrated experiment
2.1	The experiments were designed in collaboration with Ping Li. Data collection and analysis were done as follows: Panel a by me; Panels b-e by Ping Li
2.2	Ping Li collected the data and did the analysis
2.3	Ping Li collected the data and did the analysis
2.4	Ping Li collected the data and did the analysis
2.5	Data collection and analysis were done as follows: Panel a by Meiqin Hu; Panels b-c by me
2.6	The experiments were designed in collaboration with Ping Li. All data in this figure was collected and analyzed entirely by me
2.7	The experiments were designed in collaboration with Ping Li. Mutant construct was made by me. Data collection and analysis were done as follows: Panels a-b by me; Panels c-i by Ping Li
2.8	Data collection and analysis were done as follows: Panels a, b, e by me; Panels c, d, f by Ping Li
2.9	Data collection and analysis were done as follows: Panels a, c, d, e by me; Panels b, f, g by Ping Li
2.10	Data collection and analysis were done as follows: Panels a, f by me; Panels b, c, d, e, f, g by Ping Li
2.11	Drawn by Yexin Yang

Table II. Source of the data in Chapter III (paper under review)	
Authors	Meiqin Hu[1,2*], Ping Li[1,2], Ce Wang[1], Xinghua Feng[2], Qi Geng[1], Wei Chen[1], Matangi Marthi[3], Wenlong Zhang[1,4], Chenlang Gao[1], Whitney Reid[1], Joel Swanson[3], Wanlu Du[1], Richard I. Hume[1], and Haoxing Xu[1]
Author affiliations	[1]Department of Molecular, Cellular, and Developmental Biology, University of Michiga 4114 Biological Sciences Building (BSB), 1105 N. University Ave, Ann Arbor, MI 48109, USA. [2]Collaborative Innovation Center of Yangtze River Delta Region Green Pharmaceutical College of Pharmaceutical Sciences, Zhejiang University of Technology, Hangzhou 310014, China. [3]Department of Microbiology & Immunology, University of Michigan Medical School, 6750 Med Sci II, 1150 W. Medical Center Drive, Ann Arbor, MI 48109, USA.

	[4]College of Veterinary Medicine, Northeast Agricultural University, 600 Changjiang Road, Harbin 150030, China.
Figure #	Person who was responsible for the illustrated experiment
3.1	Meiqin Hu and Ping Li collected the data and did the analysis
3.2	Data collection and analysis were done as follows: Panels a, b by Meiqin Hu; Panels c-f by Ping Li, Panel g by Wei Chen
3.3	The experiments were designed in collaboration with Meiqin Hu. Data collection and analysis were done as follows: Panels a-d by Meiqin Hu; Panels [illegible]
3.4	The experiments were designed in collaboration with Meiqin Hu. Data collection and analysis were done as follows: Panels a-b by Meiqin Hu; Panels c-d by Ping Li; Panels e-g by me
3.5	The experiments were designed in collaboration with Meiqin Hu. Data collection and analysis were done as follows: Panels a, g, h by me; Panels b-c by Wenlong Zhang; Panels d-f by Meiqin Hu
3.6	The experiments were designed in collaboration with Meiqin Hu. Data collection and analysis were done as follows: Panel a by Meiqin Hu; Panels b-i by me
3.7	The experiments were designed in collaboration with Meiqin Hu. All data in this figure was collected and analyzed entirely by me
3.8	Drawn by me

TABLE OF CONTENTS

DEDICATION ..... **ii**

ACKNOWLEDGEMENTS ..... **iii**

PREFACE ..... **v**

LIST OF FIGURES ..... **x**

LIST OF TABLES ..... **xii**

LIST OF ABBREVIATIONS ..... **xiii**

ABSTRACT ..... **xv**

CHAPTER I

Introduction

I-1 Overview of lysosomes **1**
1.1 Basic properties of lysosomes 1
1.2 Creating and maintaining the lysosome acidic environment 5
1.3 Lysosomal channel and transporters 7
1.4 Lysosome function and disease 12

I-2 Volume regulated anion channels (VRACs) **14**
2.1 Cell volume is essential to maintain normal cell homeostasis 14
2.2 Regulated cell volume decrease under hypotonic conditions 15
2.3 Milestones in understanding the role of VRAC 16
2.4 Channel structure of VRAC 16
2.5 Permeability and gating properties of VRAC 17

I-3 TMEM175 as a lysosomal potassium channel **19**
3.1 Milestones in understanding the role of TMEM175 19
3.2 Permeability and gating properties of TMEM175 22
3.3 TMEM175 channel structure 23
3.4 TMEM175 linked pathology 26

CHAPTER II

LRRC8 Family Proteins Within Lysosomes Regulate Cellular Osmoregulation and Enhance Cell Survival to Hypotonic Stress

II-1 Abstract **30**

II-2 Introduction **31**

II-3 Results **33**
3.1 Lysosomes are highly osmosensitive organelles in many types of mammalian cells. ... 33
3.2 Lysosome-derived vacuoles express chloride channels gated by low ionic strength. 35
3.3 The Lyso-VRAC current is mediated by LRRC8 proteins 36

3.4 Lyso-VRAC requires a double-leucine motif of LRRC8A. 38
3.5 Lyso-VRAC plays a critical role in lysosome vacuolation. 39
3.6 Lysosomes maintain intracellular water homeostasis 40
3.7 Lyso-VRACs protect cells from necrotic cell death in response to hypo-osmotic stress 42

II-4 Discussion 43

II-5 Methods 45

II-6 Figures 56

CHAPTER III

TMEM175 Encodes a Proton-Activated, Proton Channel of Lysosomes

III-1 Abstract 77

III-2 Introduction 78

III-3 Results 79
3.1 A proton "leak" channel exists in endosomes and lysosomes 79
3.2 Lysosomal membrane protein TMEM175 is required for LyPAP currents 79
3.3 TMEM175 acts as a proton-activated, proton selective channel. 80
3.4 Activation of TMEM175 induces lysosome H^+ release. 82
3.5 A single pore mutation in TMEM175 selectively eliminates its H^+ permeability without altering the K^+ permeability. 83
3.6 H^+ conductance through TMEM175 is required for lysosomal pH homeostasis. 83
3.7 TMEM175 is required for normal lysosome hydrolase activity. 84

III-4 Discussion 85

III-5 Methods 87

III-6 Figures 93

Chapter IV

Summary and Future Directions

IV-1 Summary of the study and significance 109

IV-2 Potential Future Directions 112
2.1 Lyso-VRAC and cell death 112
2.2 The Role of TMEM175 113

References 115

LIST OF FIGURES

CHAPTER I

Figure 1.1 VRAC channel structure ……..17
Figure 1.2 hTMEM175 channel structure…….....….24

CHAPTER II

Figure 2.1 Vacuoles are derived from late endosomes and lysosomes under hypotonicity……..56
Figure 2.2 Lysosomes are highly osmosensitive organelles…….....….58
Figure 2.3 Lysosome-derived vacuoles express chloride channels gated by low ionic strength …….....…60
Figure 2.4 LRRC8A is required for Lyso-VRAC currents…….....62
Figure 2.5 LRRC8A are localized on lysosomes…….....64
Figure 2.6 Intracellular LRRC8 proteins are localized on the perimeter membrane of lysosomes ……..……....65
Figure 2.7 A double-leucine motif is required for lysosomal localization of LRRC8A to mediate Lyso-VRAC…….....67
Figure 2.8 Lyso-VRAC is required for hypotonicity-induced lysosomal vacuolation……..69
Figure 2.9 Lysosomes store and expel intracellular water to regulate cytosolic RVD……..71
Figure 2.10 Lyso-VRACs protect cells from necrotic cell death in response to hypo-osmotic stress ……..73
Figure 2.11 Working model for how Lyso-VRAC-mediated lysosome osmoregulation behavior is protective for cell survival……..75

CHAPTER III

Figure 3.1 A proton “leak” channel exists in endosomes and lysosome…….....97
Figure 3.2 Lysosomal membrane protein TMEM175 is required for LyPAP currents…….....99
Figure 3.3 TMEM175 acts as a proton-activated, proton-selective channel…….....101
Figure 3.4 Activation of TMEM175 induces lysosome H^+ release…….....103
Figure 3.5 A single pore mutation in TMEM175 selectively eliminates its H^+ permeability without altering the K^+ permeability …….……..… 104

Figure 3.6 H^+ conductance through TMEM175 is required for lysosomal pH homeostasis ……106
Figure 3.7 TMEM175 is required for normal lysosome hydrolase activity…….....….108
Figure 3.8 Model for the role of TMEM175 in lysosomal pH homeostasis and lysosomal degradation……..…….....….109

LIST OF TABLES

Table 1.1 Conserved TMEM175 in representative species in three domains of life..... 21
Table 1.2 Animal models of PD.....27

LIST OF ABBREVIATIONS

AA	*Amino Acids*
AAVs	*Adeno-associated viral vectors*
AD	*Alzheimer's disease*
Baf-A1	*Bafilomycin-A1*
BK	*Big-conductance Ca^{2+}-activated potassium channel*
BMMs	*Bone marrow macrophages*
cryo-EM	*Cryo-electron microscopy*
DCPIB	*4-(2-butyl-6,7-dichloro-2-cyclopentyl-indan-1-on-5-yl) oxobutyric acid*
D_2O	*Deuterated water*
DUF	*Domain of Unknown Function*
EEA1	*Early endosomal marker*
EE	*Early Endosome*
ER	*Endoplasmic reticulum*
E_{rev}	*Reversal potential*
GAA	*α-glucosidase*
GBA	*Glucocerebrosidase*
GWASs	*Genome-wide association studies*
KI	*Knock-in*
KO	*Knockout*
LAMP	*Lysosomal-associated membrane protein*
LDH	*Lactate dehydrogenase*
LL	*Double-leucine*
LMP	*Lysosomal membrane proteins*
LRRC8	*Leucine-rich repeat containing protein 8*
LRRK2	*Leucine rich repeat kinase 2*

LSDs	*Lysosomal storage disorders*
LY-Dextran	*Lucifer yellow dextran*
Lyso-VRAC	*Lysosomal Volume-Regulated Anion Channel*
MCOLN1	*Transient receptor mucolipin 1*
MEFs	*Mouse embryonic fibroblasts*
MSA^-	*Methanesulfonic acid*
$NMDG^+$	*N-methyl-D-glucamine*
PD	*Parkinson's Disease*
PFF	*Preformed α-synuclein fibrils*
pH_C	*Cytosolic pH*
$pH_{E/L}$	*Extracellular pH*
pH_L	*Luminal pH*
PI	*Propidium iodide*
PINK1	*Phosphatase and tensin homolog (PTEN)-induced novel kinase 1*
PM-VRAC	*Plasma membrane Volume-Regulated Anion Channel*
RVD	*Regulatory volume decrease*
TMEM175	*Transmembrane protein 175*
TPC	*Two-pore channels*
TRPMLs	*Transient receptor potential mucolipins*
SNP	*Single nucleotide polymorphism*
STED	*Stimulated Emission depletion*
V-ATPase	*Vacuolar-type ATPase*
VRACs	*Volume-regulated anion channels*
whole-EL	*Whole-endolysosome*
WT	*Wild-type*

ABSTRACT

Impaired lysosomal ion homeostasis can result in a failure of lysosomes to degrade metabolites, export catabolites and traffic correctly within cells. These lysosomal dysfunctions can result in lysosomal storage diseases and neurodegenerative disorders. My thesis is focused on two newly discovered lysosomal ion channels and their contributions to regulating cellular homeostasis.

The first data chapter of this thesis reports the discovery and characterization of Lyso-VRACs (lysosomal volume-regulated anion channels), the first ionic-strength-sensitive ion channels of lysosomes. This work provides a molecular foundation upon which to explore the links between lysosome volume regulation, lysosome physiology and human diseases. We determined that these channels are encoded by LRRC8 family genes. Previously, it had been thought that the only site of action of LRRC8 proteins was on the plasma membrane, but these studies revealed an additional essential role played by intracellular LRRC8 proteins in lysosome physiology. We have discovered essential roles of lysosomes in intracellular water homeostasis, and provide compelling evidence that in individual cells, lysosomes sequester, then extrude toxic levels of intracellular water to help alleviate the water crisis in cells under hypo-osmotic stress, comparable with the "charging" and "discharging" phases of the bladder organ in animals. Thus, lysosomes not only function as the cell's stomach for nutrient processing, but also behave as the cell's "bladder" for osmoregulation.

The second data chapter of this thesis reports the discovery and characterization of the first proton-selective channel of lysosomes. TMEM175, which was previously reported to act as a constitutively-active potassium selective channel, instead acts as a proton selective channel when

mammalian lysosomes are studied at their normal pH. By exploring the cellular effects of alterations in TMEM175 activity, I discovered that proton-mediated functions of TMEM175 are essential for lysosomal homeostasis. When TMEM175 is genetically deleted, lysosomes are hyper-acidic, and their protein degradative activity is impaired. When TMEM175 is overexpressed, lysosomes are hypo-acidic. Optimization of lysosomal hyper-acidification pharmacologically or genetically restored degradative activity in lysosomes toward normal.

These discoveries about the roles of LRRC8 and TEM175 proteins within lysosomes suggest important roles for these proteins at the level of the physiology and pathophysiology of the whole animal. The role we have demonstrated for Lyso-VRACs in cellular water balance may open a new chapter in understanding the secretion of "watery" body fluids, like saliva, tears, sweat, breast milk, bile acids, and vaginal secretions. Furthermore, the role we have demonstrated for TMEM175 suggests an explanation for why recent Genome Wide Associated Studies have identified TMEM175 as one of the most prominent genetic risk factors for Parkinson's Disease, and suggest that manipulation of the activity of TMEM175 may have therapeutic applications not only for Parkinson's Disease but also for many other diseases that have alterations in intracellular pH.

CHAPTER I

Introduction

I-1 Overview of lysosomes

1.1 Basic properties of lysosomes

The lysosome, a membrane-bound organelle, has been classically identified as a terminal degradative center. The degradative function is dependent on a variety of lysosomal hydrolases and needs an acidic lysosomal luminal pH (~ 4.6), which is maintained by a proton-importing V-type ATPase (V-ATPase) (Mindell, 2012). Macromolecule substrates are obtained through endocytosis, phagocytosis or autophagy. By breaking down macromolecules in lysosomes, including proteins, polysaccharides, and complex lipids, their respective constituents such as amino acids (AAs), monosaccharides, and free fatty acids are available for metabolic reutilization (Xu and Ren, 2015). In recent studies, the lysosome has been demonstrated to be a crucial effector in many cellular processes, including metabolic signaling, plasma membrane repair, cell migration, tumor invasion and metastasis, and apoptotic cell death (Pu et al., 2016). Additionally, defects in lysosomes may lead to lysosomal storage disorders (LSDs) and neurodegenerative disorders such as Parkinson's disease (Zhang et al., 2009; Xu and Ren, 2015). In this part of the Introduction, I will discuss lysosomal contents and function, specifically on lysosomal ion channels and transporters, lysosomal acidic environment, lysosomal exocytosis, and lysosome-related diseases.

1.1.2 Lysosome membrane proteins and enzymes

Two major types of proteins are essential for maintaining the function of lysosomes: lysosomal hydrolases and lysosomal membrane proteins (LMPs). There are more than 60 different hydrolases in lysosomes including lipases, proteases, and glycosidases (Xu and Ren, 2015). Substrates delivered by endocytosis and autophagy are degraded by specific lysosomal hydrolases and the lysosomal catabolites these enzymes produce are exported from the lysosomes and then reutilized for energy homeostasis or synthesis into new macromolecules. (Pisoni and Thoene, 1991; Xu and Ren, 2015). Besides cargo degradation, lysosomal hydrolases also participate in regulating cell homeostasis. One example is that lysosomal cathepsin release induces apoptosis through activating subsequent caspases as a result of lysosomal membrane permeabilization (Conus and Simon, 2008). This lysosomal apoptotic pathway plays an important role in the pathogenesis of neurodegeneration and auto-immune disease.

There are more than 50 lysosomal membrane proteins with identified functions and approximately 300 more whose role is yet unclear (Xu and Ren, 2015). While lysosomal membrane lipids form a physical barrier between the luminal acidic environment and the cytosol, lysosomal membrane proteins participate in a wide range of cellular events including lysosomal biogenesis, acidification, phagocytosis, autophagy, membrane integrity, transport of ions and catabolites, regulation of fusion and fission events, cell death, virus infection and membrane repair (Schwake et al., 2013).

The most abundant lysosome membrane proteins are two highly glycosylated lysosome-associated membrane proteins (LAMP1 and LAMP2). Because of its high level of expression, LAMP1 is the most commonly used marker of lysosomes. In LAMP1 knock-out cells, lysosomal properties including enzyme activities, pH and osmotic stability remain normal, and LAMP1

knock-out mice are still viable and fertile with a mild regional astrogliosis and impaired immunoreactivity against cathepsin D in the brain (Andrejewski et al., 1999). Moreover, the glycosylation of LAMP1 has been shown to regulate lysosomal exocytosis (Kima et al., 2000). Knocking out LAMP2 causes vacuolar myopathy in cardiac and skeletal muscles (Danon disease) (Nishino et al., 2000; Tanaka et al., 2000). Double knock-out of LAMP1 and LAMP2 causes lysosomal cholesterol and autophagosome accumulation, as a result of the malfunction of autophagosome-lysosome fusion (Tanaka et al., 2000; Eskelinen et al., 2004). Knocking out both LAMP1 and LAMP2 also impairs phagosome-lysosome fusion and reduces pathogen killing ability (Huynh et al., 2007; Beertsen et al., 2008). It is also likely that LAMPs play a role in lysosome motility and positioning based on knock-out cells exhibiting peripheral localization of lysosomes (Huynh et al., 2007). Knocking down LAMPs increases the sensitivity of cells to lysosomal cell death as a result of triggering lysosomal membrane permeabilization, which indicates LAMPs are necessary to support lysosomal membrane integrity (Fehrenbacher et al., 2008).

Some lysosomal membrane proteins (ion channels and transporters) are used for maintaining luminal ionic homeostasis or for signaling, by moving metabolites and ions into or out of this organelle. Ion channels allow materials to move through the membrane within a continuous water-filled passageway open to the bathing solutions on both sides of the membrane. Materials move in the direction controlled by their electrochemical gradient. Transport through these channels is controlled by gates that can open and close, and by specific amino acids in the channel lining that restrict which materials can move. Transporters do not provide a continuous pathway. Rather at any instant in time they are open only to the bathing solution on one side of the membrane. In response to binding of the molecules they transport (or sometimes an external energy

source) they undergo a series of conformational changes so that the transported materials that initially faced one side of the membrane eventually become exposed to the other side. When external energy is coupled to the conformation changes, materials can be moved against their electrochemical gradient.

Although more work needs to be done to identify the full lysosomal proteome, by using the lysosomal patch clamp technique, many interesting recent findings have been made concerning lysosomal ion channels and transporters. For example, lysosomal Ca^{2+} release is important for lysosome trafficking and lysosome signaling such as lysosome biogenesis, lysosome fusion, and lysosomal exocytosis. Transient receptor mucolipin 1 (MCOLN1) has been found to be the main lysosomal Ca^{2+} channel regulating Ca^{2+} release from the lumen (Morgan, 2011; Xu and Ren, 2015). Besides, transmembrane protein 175 (TMEM175) and the big-conductance Ca^{2+}-activated potassium channel (BK) are thought to be the major as K^+ selective channels used to maintain lysosome potential and membrane stability (Cang et al., 2015; Cao et al., 2015). Moreover, lysosomal acidic pH (~4.6) is essential for proper activity of enzymes and lysosomal trafficking, and the acidic environment is maintained by proton pump vacuolar-ATPase (V-ATPase) and other transporters and channels (Graves et al., 2008; Ishida et al., 2013; Mindell, 2012), which will be further discussed in section 1.3.

1.1.3 Lysosome exocytosis

Lysosome exocytosis, the fusion between the lysosome membrane and the plasma membrane is an essential lysosome trafficking event. Lysosome exocytosis was first found in fibroblasts and now has been observed in all cell types tested (Rodriguez et al., 1997; Samie and Xu, 2014). Upon stimulation, lysosomes move from perinuclear and cytosolic regions to dock and

fuse with the plasma membrane, followed by lysosomal content release into the extracellular space. Therefore, lysosome exocytosis can be measured by the presence of the lysosomal membrane protein LAMP1 on the plasma membrane by imaging or by the secretion of lysosomal enzymes into the extracellular space using enzyme activity kits (Samie and Xu, 2014).

The purposes of lysosome exocytosis are to provide either lysosomal membrane or contents. Lysosome exocytosis helps repair damaged plasma membranes, a process that requires donating lysosomal membranes to the plasma membrane. Therefore, induced lysosomal exocytosis may work as a therapeutic way to treat Duchenne muscular dystrophy by repairing the damaged sarcolemma (Yu et al., 2020). Lysosome exocytosis also contributes to secretion and transmitter release. For example, microglia migration is mediated by releasing ATP through lysosomal exocytosis (Dou et al., 2012). In summary, lysosomal exocytosis contributes to multiple biological processes and related pathologies.

1.2 Creating and maintaining the lysosome acidic environment

1.2.1 V-ATPase

The V-ATPase was discovered as an electrogenic proton pump in plants and bacteria in the early 1980s (Churchill et al., 1983; Churchill and Sze, 1983; Lichko and Okorokov, 1984). It was then found to be ubiquitously expressed in various eukaryotes including animals, and in multiple locations including lysosomes, endoplasmic reticulum, Golgi bodies, secretory granules and in some cases the plasma membrane (Finbow and Harrison, 1997). In order to achieve digestive function and the active transport of metabolites, transmitters, and ions, lysosomes rely on a highly acidic luminal pH (~4.6) due to a 50-5,000 fold proton gradient between the vesicular lumen and the cytoplasm. This acidic environment and proton gradient are maintained

by a V-ATPase which pumps protons against the electrochemical gradient into the lysosome lumen by consuming metabolic energy released by ATP hydrolysis (Ohkuma et al., 1982; Mindell, 2012; Xu and Ren, 2015). The proton gradients created directly and indirectly by ATP hydrolysis generate a lysosomal voltage difference about -20 to -40 mV (20 to 40 mV more negative in the cytosol compared with the lysosomal lumen), which can be dissipated by either anion influx or cation efflux (Steinberg et al., 2010).

Moving only protons would create a macroscopic charge imbalance, so movement of a negatively charged counterion must be coordinated to allow efficient proton pumping. One counterion is chloride. Cl^- influx through ClC-7, a 2 Cl^-/1H^+ electrogenic antiporter on lysosomal membranes may help accumulate Cl^- inside the lumen by transporting two Cl^- into the cytosol for one H^+ into the lysosomal lumen； however， how much it is involved remains unclear (Graves et al., 2008; Jentsch and Pusch, 2018).

A second way to maintain macroscopic charge balance when protons are brought into the lumen by the V-ATPase is for a cation to leave. There is data supporting the idea that K^+ efflux through a cation channel or transporter participates in maintaining charge balance, but the underlying molecular pathway remains in question (Cang et al., 2014). In a word, the V-ATPase and the counterion transporter(s) are considered as two important factors that are likely to maintain the stable lysosome pH, however the specific mechanism is still uncertain.

When bafilomycin A1, a specific potent inhibitor of V-ATPase, is applied, there is rapid organelle alkalization, suggesting the presence of unidentified proton “leak” channels on the membranes of intracellular acidic compartments (Bowman et al., 1988; Christensen et al., 2002). Two families of proton channels have been identified in mammals, OTOPs and HV1, but neither has endosomal or lysosomal expression and their action is restricted to specific cell types such as

sour taste receptor cells and neutrophils (Morgan et al., 2009; Tu et al., 2018). An additional family of proton channels related in structure to voltage gated K^+ channels play an important role in sperm functions in fish (Vílchez et al., 2016), but to date no members of this family are found in mammals. Therefore, whether there is a proton leak channel on lysosomes and how it contributes to lysosome pH homeostasis needs further investigation. This issue is the focus of Chapter III.

1.2.2 Lysosomal enzyme activity and pH

Enzyme activity is most rapid at a specific pH and the optimal pH for lysosomal enzymes is highly acidic. Thus abnormal lysosomal pH impairs lysosomal degradation (Xu and Ren, 2015). For example, cysteine cathepsins including cathepsin B and L, which play an important role in protein turnover, are synthesized as zymogens when they are delivered to late endosomes and then activated by other proteases or autocatalytically within lysosomes. For procathepsins B and L activation is due to a pH-dependent cleavage that reveals the active site. This activation is 22-fold faster at pH 4.0 than at pH 6.0, with an optimal pH around 4.5 (Quraishi et al., 1999; Pungerčar et al., 2009). In conclusion the appropriate acidic lysosomal pH is required for normal enzymatic activity.

1.3 Lysosomal channel and transporters

1.3.1 Overview of lysosomal channels

Ion selectivity of a channel depends on its pore or pore-associated subunits (Hille, 1978). Ion selectivity is usually assessed using electrophysiogical methods to measure changes in reversal potential as one ion is substituted while all others are left unchanged. The alternative approach of measuring the absolute permeability of any particular type of ion through a channel (P) is

technically challenging, typically requiring radioactive flux measurements from intact cells that are only interpretable when just a single type of channels is open during the measurement period, a situation that is rare in intact cells. However, as long as there is a way to selectively activate the channels of interest, simple electrophysiological experiments allow one to easily calculate the relative permeability of two ions, as the effect of all other channels present can be subtracted away. The biophysical basis for making these types of measurements is explained in detail in a book by Bertil Hille (2001) and the next few paragraphs summarize information present in chapter 14 of his book.

In electrophysiological measurements, the reversal potential for an open channel, V_{rev}, is the membrane potential at which the current is 0. For a channel through which only one type of ion can pass, V_{rev} is the Nernst equilibrium potential

$$\text{Vrev} = \frac{RT}{zF} * ln \frac{[X]_e}{[X]_i}$$

in which, R, T, z, F and $[X^+]_{i/e}$ are the gas constant, absolute temperature, the valence, Faraday's constant and the internal or external X concentration respectively. At V_{rev}, there is no net movement of the permeant ion across the membrane. However, ion substitution experiments have demonstrated that most channels are permeable to more than one ion.

When two or more permeant ions are present, at V_{rev}, some ions move inward and others outward with their summed current coming to zero. Basic biophysical principles allow one to derive equations for unidirectional flux of an ion based on its concentration, the membrane potential, and the absolute permeability of the channel for that ion. The unidirectional influxes and effluxes of all permeant ions present can then be combined to produce the Goldman–Hodgkin–Katz voltage and current equations, which have only permeability ratios, not absolute permeability. These equations can be rearranged in a number of ways. For example, if only two permeant

monovalent cations are present, the relative permeability of the two at the reversal potential can be calculated as follows:

$$\frac{P_X}{P_Y} = \frac{[Y^+]_e - [Y^+]_i e^{(FV_{rev}/RT)}}{[X^+]_i e^{(FV_{rev}/RT)} - [X^+]_e}$$

in which $[X^+]_{i/e}$, $[Y^+]_{i/e}$, F, V_{rev}, R, and T, are respectively internal or external X^+ and Y^+ concentrations, Faraday's constant, the reversal potential, the gas constant and the absolute temperature. As the relative value of permeability is a ratio, it is unit-less. Somewhat more complex equations can be derived if some of the permeant ions are cations and others anions or if one of the permeant cations is divalent.

Control of ion concentrations initially present on both sides of the membrane is easy in patch-clamp experiments (whole cell, excised patch or whole endolysosome), and so the experimental analysis can be simplified if conditions are set up so that cation X is present only on one side of the membrane and cation Y on this other. In this bi-ionic case, the GHK equation can be simplified to:

$$\frac{P_X}{P_Y} = e^{(FV_{rev}/RT)} \qquad or \qquad V_{rev} = \frac{RT}{F} * \ln\left(\frac{P_X}{P_Y}\right)$$

If the reversal potential is 0, then $P_X/P_Y = 1$ (meaning that the permeability of X^+ is equal to Y^+). In this case the GHK current equation shows that the current-voltage (I-V) curve will be linear and cross the x-axis at 0 mV (i.e. the reversal potential = 0 mV). Furthermore, if one replaced all of X with Y, nothing would change because the channel is incapable of telling the difference between the two ions. If the permeability of X^+ is greater than Y^+, then the reversal potential will be positive to 0 mV by an amount that depends on the natural log of the ratio and the I-V curve is predicted to display inward rectification (this means that at equal positive and negative potential differences

from the reversal potential, the absolute value of the inward current is larger than the outward current). The opposite will be true if the permeability of X^+ is less than Y^+.

Once a patch clamp configuration is achieved, it becomes difficult to change the solution exposed to the inside of the pipette, but easy to change the external solution, When ion X replaces ion Y, the change in reversal potential is a function of $\frac{P_X}{P_Y}$

$$\Delta V_{rev} = V_{rev,\ X} - V_{rev,\ Y} = \frac{RT}{F} * \ln\left(\frac{P_X * [X_{external}]}{P_Y * [Y_{exteral}]}\right)$$

In chapter 2 and 3, relative permeability for a series of ions is estimated by changing only the bath solution, while the pipette solution was kept constant. The shift in reversal potential was then used to solve for $\frac{P_X}{P_Y}$.

Various ion channels and transporters on the lysosomal membranes mediate the movement of Ca^{2+}, Na^+, K^+, Cl^-, and H^+ (Xiong and Zhu, 2016). Lysosomal Ca^{2+} efflux is thought to be important for signal transduction and vesicle trafficking, and it is thought to be largely regulated by transient receptor potential mucolipins (TRPMLs) (Cheng et al., 2010; Dong et al., 2010a; Dong et al., 2010b; Morgan et al., 2011). Lysosomal Na^+ is the most abundant cation and sodium permeable channels act to regulate lysosomal membrane potential (Wang et al., 2012). Two-pore channels (TPC1 and TPC2) have also been shown to act as Na^+ channels (Mackenzie and Erickson, 2004; Wang et al., 2012; Wang et al., 2015). Na^+ movement is also coupled with amino acid transporters of the SLC38 family for sodium-amino acid co-transporter

It has been reported that K^+ depolarizes or reverses lysosomal membrane potential and regulates lysosomal Ca^{2+} signaling, implying that there must be lysosomal K^+ channels (Christensen et al., 2002). One such K^+ channel belongs to the big-conductance Ca^{2+}-activated

potassium channel (BK) (Wang et al., 2017). A second channel that can conduct potassium is transmembrane protein 175 (TMEM175) (Cang et al., 2015) but our results reported in Chapter III call this into question.

Cl^- imported by CLC7 transporter is required for regulating lysosomal membrane potential and lysosomal acidification for H^+ pumping by providing counterions (Graves et al., 2008). In chapter II our results identify a chloride selective channel of lysosomes, Lyso-VRACs.

Besides allowing Na^+, K^+ and Ca^{2+} fluxes, MCOLN1/TRPML1 allows movement of the heavy metals Fe^{2+} and Zn^{2+}. Heavy metal release of Fe^{2+} mediated by TRPML1 is required for reactive oxygen species production (Dong et al., 2008; Dixon et al., 2012). Lysosomal Zn^{2+} is released by TRPML1, and ZIP3 and ZIP8 transporters localized to the lysosome have been shown to export Zn^{2+} out of the lysosome as well (Dong et al., 2008; Jeong and Eide, 2013). Lysosomal Zn^{2+} may be required for the activity of hydrolases as a coenzyme, and high lysosomal Zn^{2+} impairs cathepsin activity (Lockwood, 2013).

Although there are remarkable findings regarding ion channels and transporters on lysosomes, many other lysosomal channels remain unidentified. Thus, it is still largely unclear how lysosomal ion homeostasis is maintained. For example, whether there is a lysosomal channel taking up Cl^- and whether there is a proton leak channel are still unclear. Therefore, identifying lysosomal channels is an interesting aspect to explore and will greatly enhance our understanding of regulation of the lysosomal ion homeostasis.

1.4 Lysosome function and disease

1.4.1 Lysosomal storage diseases

Impairments in macromolecule degradation, catabolite export, or trafficking can all lead to lysosomal storage diseases (LSDs) (Vitner et al., 2010). So far, more than 50 lysosomal storage diseases have been identified that are caused by mutations in lysosomal enzymes or impaired lysosomal membrane proteins (Parkinson-Lawrence et al., 2010; Schulze, 2011). For example, ML4 disease is caused by defects of TRPML1; Pompe disease is caused by mutations in acid α-glucosidase (GAA); NPC disease is caused by mutations in the cholesterol transporter NPC1, which leads to accumulation of cholesterol and sphingomyelin (Shea and Raben, 2009; Parenti et al., 2015). Even though each LSD is rare, the frequency of LSDs in total reaches 1 in 8000 live births. The clinical manifestation of LSDs is usually associated with skeletomuscular (dysostosis multiplex, osteonecrosis, joint limitations), visceral (hepatosplenomegaly) and extremely variable neurological abnormalities. Other organs, including skin (hypohidrosis, angiokeratoma), kidney, blood system, heart (cardiomegaly, arrhythmias and cardiac failure), respiratory tracts and lungs, stomach and intestines, can also be affected by LSDs (Parenti et al., 2015).

Multiple therapeutic methods that have been proposed and tested for treating LSDs including substrate reduction therapy, enzyme replacement therapy, and gene therapy. Substrate reduction therapy needs a special diet or specific drugs to disrupt a biosynthesis step essential for producing the substrate. For example, miglustat (Actelion Pharmaceuticals, San Francisco, CA), has been approved for clinical use for type 1 Gaucher disease by inhibiting the enzyme glucosylceramide synthase for the synthesis of glucosylceramide, so significant residual enzyme activity can break down glucosylceramide more efficiently to allow clearance of from glucosylceramide accumulating lysosomes (Platt et al., 2007). Enzyme replacement therapy is

designed to inject a working protein to replace the defective enzyme, for example glucocerebrosidase has been approved for treating Gaucher's disease patients mainly by targeting affected spleen and liver cells. However, the drawback of this method is that many LSDs have effects on the brain and because of the blood brain barrier, systemically injected recombinant protein is unable to reach therapeutic concentrations (Brady, 2006). Gene therapy is another strategy by transducing the defective enzyme gene. The most common recent approaches use adeno-associated viral vectors (AAVs) for *in vivo* gene therapy, and lentiviruses for *ex vivo* gene therapy. For example, AAVs for Pompe disease, Gaucher disease, and Fabry disease have been nominated as orphan drugs and are still in clinical trials. In conclusion, all treatments currently in use or in development for LSDs have limitations or need further investigation (Rastall and Amalfitano, 2015; Parenti et al., 2015).

1.4.2 Neurodegenerative diseases

Recent studies have found connections between lysosome dysfunction and several neurodegenerative diseases (Kovacs, 2017) and some LSD related genes have been identified as risk factors for neurodegenerative diseases. For example, patients with mutations in α-glucocerebrosidase, which causes Gaucher disease, have a higher probability of developing Parkinson's Disease (PD) (Sidransky et al., 2009). Amyloid beta peptides, which are highly expressed in Alzheimer's disease (AD), are also found aggregated in NPC cells (Nixon, 2004). Such correlations result in lysosomes having been proposed as a new target for treating neurodegenerative diseases (Lie and Nixon, 2018). For example, genetic and pharmacological ways to regulate the autophagic-lysosomal pathway have been proven to treat aggregated α-

synuclein in a mouse model of Parkinson's Disease, which will be discussed in more detail later in this Introduction (Decressac et al., 2013).

I-2 Volume regulated anion channels (VRACs)

Chapter II will present results indicating that lysosomes contribute to cytosolic water homeostasis in response to physiological stresses by using ionic strength-sensitive ion channels formed from LRRC8 proteins on lysosomal membranes (Lyso-VRACs) acting in parallel with plasma membrane VRAC channels. Therefore, in this section I have summarized the key information known about cell volume regulation and VRAC previous to our studies.

2.1 Cell volume is essential to maintain normal cell homeostasis

Maintaining appropriate cell volume is essential for cell survival (Lang et al., 1998). Excessive changes of cell volume cause alterations in the integrity of the cell membrane and organelle architecture (Lang, 2007). Moreover, cell volume changes have been proposed to be a signaling event for fundamental cellular processes including cell proliferation and migration, as well as hormone and neurotransmitter release. During cell proliferation, cells need to increase their volume during the late stages of mitosis to make two daughter cells of sufficient size to survive and grow. During migration, both normally and during metastasis in cancer, cells need to adjust their volume and shape to invade the extracellular space. During hormone and neurotransmitter release, cell swelling caused by hypo-osmotic stresses induces a quick release of enzymes and peptide hormones in different cell types such as endocrine cells, neurons and exocrine pancreatic cells (Strbák and Greer, 2000; Dubois and Rouzaire-Dubois, 2012). Thus, even a small change of

the amount of cellular water has a profound influence on cellular performance and protein function (Al-Habori et al., 2001).

2.2 Regulated cell volume decrease under hypotonic conditions

Water channels permit the movement of water across cell membranes. The driving force is the osmotic gradient (Borgnia et al.,1999). When using an external medium with osmolarity lower than the intracellular osmolarity (hypotonic stress), water enters the cell following the osmotic gradient, which results in cell swelling. When using an external medium with osmolarity higher than the intracellular osmolarity (hypertonic stress), water moves out of the cell which causes cell shrinkage. In mammals, organismal level mechanisms regulating salt and water balance ensure that most cell types probably never encounter large osmotic gradients like those frequently encountered by the cells lining the digestive tract and the collecting tubules of the kidney (Bourque, 2008). Nonetheless, cells from most tissues of mammals display rapid adaptations to both hypotonic and hypertonic challenges (Delpire and Gagnon, 2018; Hoffmann et al., 2009).

There are two phases of cell volume changes after a hypotonic stress. In the first phase, water quickly flows across the plasma membrane following the osmotic gradient. In the second one, the cell goes through volume regulation to counteract the initial cell volume increase, a process referred to as regulatory volume decrease (RVD) (Lang, 2007; Hoffmann et al., 2009). There are multiple mechanisms which have been proposed to be involved in RVD. For example, swelling-activated K^+ channels, organic osmolyte selective channels and K^+-Cl^- cotransporters were all considered to play a role (Lang, 2007). However, the cellular and molecular basis of intracellular osmoregulatory mechanisms still needed further understanding and studies over the last 10 years have focused on volume-regulated anion channels (VRACs).

2.3 Milestones in understanding the role of VRACs

The first VRAC currents were recorded from human lymphocytes and epithelial cells in response to decreased extracellular osmolality (Cahalan and Lewis, 1988; Hazama and Okada, 1988). Later on, VRAC currents were found in various mammalian cell types (Nilius et al., 1997). The role of VRACs in cell volume regulation and mediating Cl^- efflux has been extensively reviewed (Hoffmann et al., 2009; Jentsch, 2016). Moreover, VRACs have been shown to have a variety of other critical roles in physiological and cellular processes including regulation of membrane potential, cell proliferation, apoptosis, salt and fluid secretion, glutamate release (Pedersen et al., 2016). Over the years, many proposed molecular mechanisms to account for VRAC currents were proposed but the situation began to be resolved when a member of the LRRC8 (leucine-rich repeat containing protein 8) family was demonstrated to be as essential components of VRAC channels (Qiu et al., 2014).

2.4 Channel structure of VRAC

Through a genome-wide small interfering RNA screen, the transmembrane protein, leucine-rich repeat containing 8A (LRRC8A), was identified as an essential component of VRAC in mammalian cells and given the name Stim1 (Qiu et al., 2014). Mammals have 5 members of this gene family (LRRC8A to LRRC8E) and studies deleting and then re-expressing the various *LRRC8* genes indicate that detectable levels of VRAC channel function on the plasma membrane requires LRRC8A and at least one other subunit (Voss et al., 2014). The properties of the channels vary depending on whether the partner is LRRC8B, C, D or E. LRRC8A expressed alone at very high, and probably unphysiological, levels can form functional channels (Voss et al., 2014; Qiu et al., 2014; Syeda et al., 2016) and a cryo-EM structure of homomeric LRRC8A (Kefauver et al.,

2018) indicated that these proteins form hexamers (**Fig 1.1)**. Immunofluorescence studies have shown LRRC8A is present not only on plasma membranes but also in what appear to be puncta within the cytoplasm, suggesting VRAC may also localize on intracellular organelles (Voss et al., 2014).

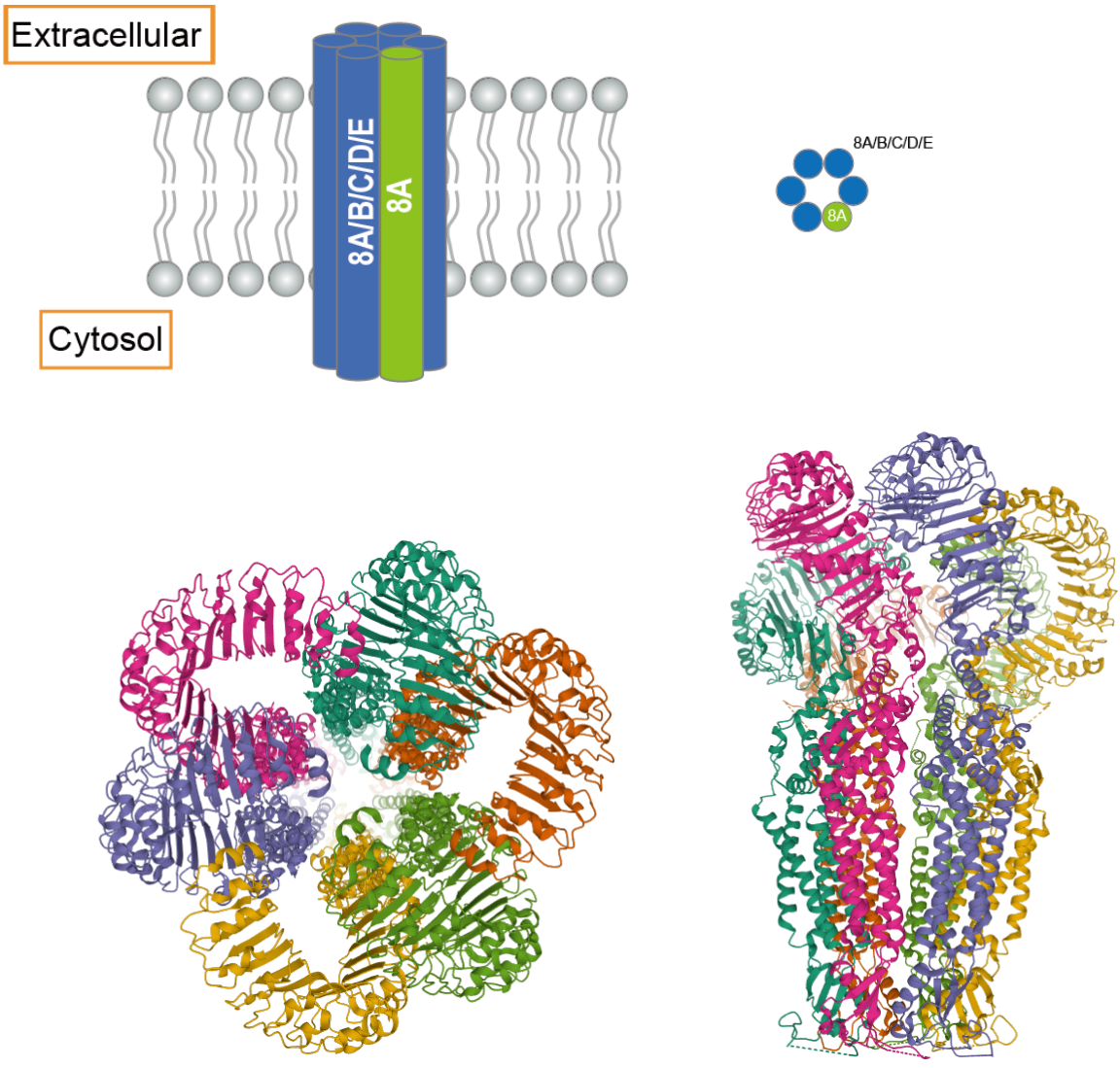


Figure 1.1 VRAC channel structure. The upper panel is the cartoon showing VRAC is a hexamer which is formed by at least one LRRC8A subunit. The lower panel is the Cryo-EM structure of VRAC from PDB (Entry 6DJB) in a top view and a side view.

2.5 Permeability and gating properties of VRAC

Based on shifts in reversal potential, it was concluded that VRAC channels are more permeable to Cl^- than to any other ion normally present, but that they actually have a greater relative permeability to iodide (I^-) than to chloride (Cl^-) and are also permeable to organic osmolytes present in the cytosol such as taurine (Jackson et al., 1993). Ion selectivity of VRAC has a permeability sequence of characteristic $I^- > NO_3^- > Cl^- >> Glc^-$ (gluconate) (Voss et al., 2014). Studies have proven that VRAC anion selectivity particularly I^- versus Cl^- can be significantly changed by point mutations in LRRC8A, providing strong evidence that LRRC8A is an essential VRAC component (Qiu et al., 2014).

The activation mechanism of the plasma membrane osmotic sensitive channel VRAC is controversial. VRAC was initially identified based on activation in intact cells by extracellular hypotonicity, but low ionic strength (Γ), in the absence of an osmotic gradient, can also activate VRAC and it has been claimed that a sensor for low Γ is an integral part of purified LRRC8A-containing complexes (Voss et al., 2014; Qiu et al., 2014; Syeda et al., 2016; Deneka et al., 2018).

Pharmacological studies indicate that ethacrynic acid derivative, 4-(2-butyl-6,7-dichloro-2-cyclopentyl-indan-1-on-5-yl) oxobutyric acid (DCPIB) is an antagonist of VRAC, and it has recently been demonstrated by cryo-EM that DCPIB binds to a site exposed on the luminal surface and is held within the binding site by a negatively charged carboxyl group (Kern et al., 2019). NS3728, a blocker of several types of Cl^- channels with a very different chemical structure than DCPIB (acidic diaryl ureas) is negatively charged and membrane impermeable, and has also been found to be a potent VRAC inhibitor (Kern et al., 2019). Interestingly, VRAC inhibitors may have a therapeutic potential for cancer treatment possibly because of the need for regulating cell volume during cell proliferation and migration (Chou et al., 1995; Shen et al., 2000). However, further

understanding of VRACs is needed to guide the use of agents that act on them for therapeutic contributions in other pathologies such as stroke and ischemia (Syeda et al., 2016).

To date, the focus of studies on the roles of VRACs is on channels in the plasma membrane. In chapter II I describe our studies showing a critical role for VRACs within lysosomes.

I-3 TMEM175 as a lysosomal potassium channel

Chapter III will present the unexpected discovery that TMEM175, a channel previously identified as a lysosomal potassium channel, instead acts as a proton channel under the conditions found in normal lysosomes. Therefore, in this section I have summarized the key information known about TMEM175 previous to our studies.

3.1 Milestones in understanding the role of TMEM175

Inspection of sequences revealed by the Human Genome project led to the name TMEM175 being assigned by HUGO Gene Nomenclature Committee to an open reading frame that based on its predicted domain structure was a putative membrane protein. The first hint of the potential role of TMEM175 was when the protein encoded by this gene was detected in purified lysosomal membrane extracts by mass spectrometry (Schröder et al., 2007), a discovery that was subsequently replicated (Chapel et al., 2013). Interest in TMEM175 was greatly increased when two meta-analyses of Genome-wide Association Studies (GWASs) suggested that TMEM175-linked polymorphisms are highly associated with susceptibility to Parkinson's Disease (Yang et al., 2013, Nalls et al., 2014). The next year, a major paper provided the first functional evidence for the role of TMEM175, reporting that it is a lysosomal ion channel and that under the conditions used, the channel was potassium selective (Cang et al 2015). Over the past five years these

important early findings have been extended in many ways that will be explored in detail in the next few sections.

3.1.1 Phylogenetic distribution of TMEM175

As various genomes began to be annotated and compared, a family of related proteins was initially given the family designation of Domain of Unknown Function (DUF) 1211. Some genome and protein databases continue to use this designation, while others now refer to the family as TMEM175. To date there are no other transmembrane proteins that have features similar enough to be considered as distant paralogs of the DUF1211/TMEM175 family. As of October 2020, information in the PFAM database and the InterPro database indicate that DUF1211 related proteins exist in unicellular organisms and multicellular organisms including archaea, bacteria, and eukaryotes (see representative species in **Table1.1**). There are no known TMEM175 sequences in budding yeast or any other fungi. There also are no homologs found in some commonly studied model animals (*C. elegans* and *D. melanogaster*) but there is a detectable sequence in at least one nematode species (*Diploscapter pachys*) as well as in Porifera (sponges), Cnidaria (anemones and corals) and Annelida (segmented worms) so it seems most likely that the TMEM175 homolog was lost in some invertebrate lineages. TMEM175 is found in all vertebrates that have been studied, as well as the non-vertebrate Chordata (Amphioxus and Ciona). The TMEM175 amino acid sequence is highly conserved between humans and mice (81% identity).

Table1.1 Conserved TMEM175 in representative species in three domains of life (from Pfam database DUF1211 website https://pfam.xfam.org/family/PF06736#tabview=tab7)

Domain	Representative species
Eukaryotes (Total:139)	Homo sapiens (human) NM_001297428.2, Mus musculus (house mouse) NM_028223.3, Rattus norvegicus (rat) NM_001013991.1, Danio rerio (zebrafish) NM_001100075.1, Gallus gallus (chicken) NM_001006582.1, Alligator mississippiensis (American alligator) XP_006259322.3, Zootoca vivipara (common lizard) XM_035141125.1
Archaea (Total:47)	Methanobacterium lacus CP002551.1, Natrialba magadii CP001932.1, Halobonum sp CP058529, Methanobacterium formicicum NZ_LN734822.1
Bacteria (Total:1119)	Chamaesiphon minutus CP003600.1, Chitinophaga costaii QCYL01000010.1, Mucilaginibacter rubeus CP043450.1, Lacticaseibacillus paracasei NC_021721.1, Stenotrophomonas panacihumi WP_057648038.1

3.1.2 Expression pattern of TMEM175

Based on expressed-sequence-tag and RNA-sequencing databases TMEM175 is expressed in all human tissues and organs that have been studied, including the heart and the brain as well as in many cultured cell lines (Cang et al., 2015). Consistent with the RNA expression and proteomic studies suggesting lysosomal localization, TMEM175 fluorescently tagged at its N terminus or C terminus with GFP or YFP is found to co-localize with endosomal and lysosomal markers (Cang et al., 2015). Because at the acidic pH of the lysosomal lumen GFP and YFP would lose fluorescence, the detection of strong YFP and GFP signals strongly suggested that both the N and

C termini of TMEM175 are on the cytosolic side. This inference was confirmed by recent cryo-electron microscopic (cryo-EM) structures (see below).

3.2 Permeability and gating properties of TMEM175

Potassium is the most abundant ion in the intracellular fluid. Through a candidate gene screening of human lysosomal proteins of unknown functions which contain at least one transmembrane domain, Cang et al. (2015) found that TMEM175 was the only one of the sixteen proteins tested that led to a large increase in "leak" currents (defined as currents that showed little if any voltage dependent activation or inactivation) when whole endosome and lysosome patch clamp recordings were made on HEK293 cells. The basal conditions they used had the identical high [K^+] solution on both sides of the membrane, and based on ion substitution experiments they concluded that TMEM175 was a K^+ selective channel. For example, similar to many canonical K^+ channels, when they replaced bath K^+ with Rb^+, the current increased, suggesting hTMEM175 is Rb^+ permeable; but when they replaced bath K^+ with NMDG, the outward current was abolished, indicating hTMEM175 is NMDG impermeable. However, unlike canonical K^+ channels which are highly selective for K^+ over Na^+ and impermeable to Cs^+, the permeability of TMEM175 to cations corresponded to a lyotropic sequence, with Ca^{2+} being least permeable and Na^+, K^+ and Cs^+ being most permeable (P_K/P_{Ca} = 141.6 ± 27.7, n = 9; P_K/P_{Na} = 36.0 ± 4.4, n = 11; P_K/P_{Cs} = 0.51 ± 0.03, n = 9) (Cang et al., 2015). TMEM175 also showed different pharmacological properties from canonical K^+ channels. Zn^{2+} (IC50, 38.4 μM) and 4-aminopyridine (IC50, 35.0 μM) blocked TMEM175 activity while other common K^+ channel inhibitors including Cs^+, Ba^+, tetraethylammonium, and quinine were not able to inhibit TMEM175. Subsequent studies have confirmed that some of the bacterial TEME175 family members can also act as K^+ channels

(Brunner et al., 2020; Oh et al., 2020). It is noteworthy that all these studies were carried out at a neutral pH on both sides of the membrane, quite different from the situation in lysosomes, where the cytosol is at a near neutral pH (approximately 7.2), but the lumen is very acidic (approximately pH 4.5).

3.3 TMEM175 channel structure

By hydrophobicity analysis, the structure of hTMEM 175 (and all other animal TMEMs) is predicted to have two similar repeats of a motif with a six-transmembrane-spanning (2 × 6TM) topology (**Fig. 1.2**). The InterPro website assigns the identifier PR010617 refers to these 6TM domain motifs (http://www.ebi.ac.uk/interpro/entry/InterPro/IPR010617/domain_architecture) and reports that the TMEM175 sequences of most prokaryotes (over 9,000 entries) are predicted to contain only a single 6-TM domain (1 × 6TM). However, there are a few prokaryote sequences that have a 2 × 6TM organization including examples from both bacteria (*Lactobacillus siliginis* A0A0R2L6U6) and archea (*Methanobrevibacter olleyae*, A0A126QYI9). InterPro also reports that besides these two most common organizations there are 14 additional classes of prokaryote proteins that have a PR010617 domain and some other known domain, but there are only 1 or 2 examples for each. TMEM175 has substantial amino acid similarity between prokaryotes and humans especially in the first two TMs with 39% identity and 56% similarity in repeat II (Cang et al, 2015).

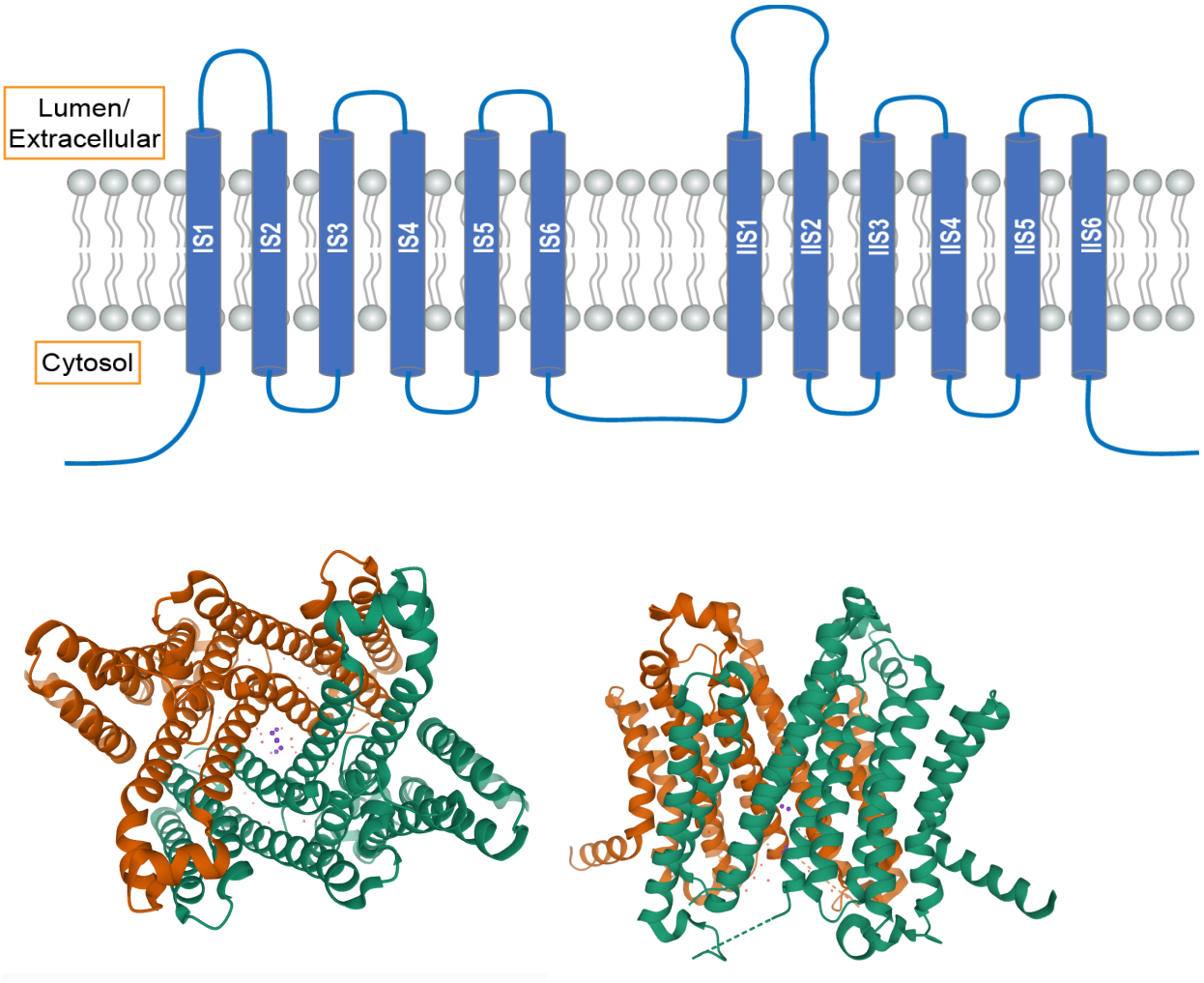


Figure 1.2 hTMEM175 channel structure. The upper panel is the cartoon showing the two-repeat six-transmembrane-spanning (2 × 6TM) topology of hTMEM175. The lower panel is the Cryo-EM structure of hTMEM175 from PDB (Entry 6WCA) in a top view and a side view.

The first member of the TMEM175 family to have its structure characterized in detail was a prokaryotic TMEM175 channel from *Chamaesiphon minutus* (CmTMEM175) for which a crystal structure of was determined and refined to 3.3 Å (Lee et al., 2017). This structure not only supported the topology predictions but also revealed a tetrameric fold different from classical K^+ channels and not known to be present in any other protein yet to be characterized. As a non-

canonical potassium channel, there is no pore helix and TVGYG selectivity filter, and all transmembrane helices are tightly packed within each subunit without any domain swapping. Two additional structures were reported in 2020, and provided important information about the structural basis for selectivity and gating mechanisms of TMEM175. One study presented another bacterial crystal structure, a closed TMEM175 channel from *Marivirga tractuosa* (MtTMEM175) at a resolution of 2.4 A˚ (Brunner et al., 2020). They interpret the pore of MtTMEM175 as having several functional layers. The other study (Oh et al., 2020) reports a cryo-EM structure of hTMEM175 in open and closed conformations at a resolution up to 2.6 A˚. It shows that hTMEM175 has a homodimeric architecture with a central ion-conduction pore lined by the side chains of the pore-lining helices.

These structural studies also report mutagenesis experiments to identify the specific residues are important for K^+ selectivity and gating. Whole-cell patch clamp studies of a MtTMEM175 threonine mutant at a position that is conserved in hTMEM175 demonstrated that this highly conserved layer with threonine residues in the pore and contributes to K^+ selectivity of the MtTMEM175 channel. An additional layer comprising two serines further increases K^+ selectivity in hTMEM175 (make clear whether this is in the Bruner paper or another paper. Whole-cell patch clamp of isoleucine mutants of hTMEM175, isoleucine side chains are essential to establish a selectivity filter. The homologous residues in CmTMEM175 (Ile23) or human TMEM175 (Ile46 and Ile271) was defined as the central factor in selectivity (Lee et al., 2017). Consistently, the cryo-EM structure study of human TMEM175 also determined Ile46 and Ile271 as the ion selectivity filter. They also proposed these two residues formed the channel gate (Oh et al., 2020). Because there was no potent agonist identified, this claim about gating properties remains an open question. In contrast with the two studies mentioned above, the crystal structure

study of MtTMEM175 claims that homologous residues Thr38 in MtTMEM175 or Thr49 and Thr274 in hTMEM175 convey K^+ selectivity (Brunner et al., 2020). Therefore, it is still controversial that what residues play a central role in selectivity or gating.

Taken together, studies of the structure and function of TMEM 175 from both bacteria and humans give important insights into the molecular mechanisms of gating and ion selectivity but linking this information to the normal role of TMEM175 in cells still needs more additional study.

3.4 TMEM175-linked pathology

Parkinson's disease was first diagnosed in the early nineteenth century and is the second most common neurodegenerative disease affecting older adults, while not common in young people under 40 (Sherer et al., 2012; Chou et al., 2013). Classic symptoms of PD patients including resting tremor, rigidity, bradykinesia, and stooping posture. Many patients also display other symptoms like neurobehavioral disorders, cognitive impairment, and autonomic dysfunction (Beitz, 2014). A key feature of the neuropathology of Parkinson's is degeneration of dopaminergic (DA) neurons in the substantia nigra of the midbrain. At autopsy, the brains of Parkinson's patients typically show accumulation of α-synuclein in neuronal Lewy Bodies.

So far, PD is linked to risk factors such as aging, family history and environmental chemicals but the cause remains unknown and no treatment has been proven to cease or even slow the pathogenic process, although l-DOPA can ameliorate the symptoms as long as some DA neurons remain. Hence, establishing animal and cellular models is necessary to screen and test for new therapies (Savitt et al., 2006). Genetic manipulation is a powerful approach to develop these models (**Table 1.2)**. One example is transgenic overexpression of mutant autosomal-dominant genes such as leucine rich repeat kinase 2 (LRRK2) in mouse lines, which shares some pathogenic

mechanisms with PD, for example α-synuclein inclusions. Also, autosomal-recessive genes such as *Parkin, DJ-1*, phosphatase and tensin homolog (PTEN)-induced novel kinase 1 (*PINK1*) can be knocked out or knocked down in mice, which leads to mitochondrial dysfunction and neurodegeneration (Dawson et al., 2010). Other mutations like glucocerebrosidase (GBA) mouse lines have been created through crossing α-synuclein A53T mutation mice with mice carrying one of the most common GBA mutations, L444P, which have reduced lysosomal α-synuclein degradation and consequent α-synuclein aggregation (Fishbein et al., 2014). Thus, many different organisms and cellular models have been very valuable to understand the pathogenic mechanisms of PD.

Table 1.2 Animal models of PD

model type	genotype	phenotype
Autosomal Dominant Models	Mutant α-synuclein (A53T, A30P, E46K)	α-synuclein aggregation and fibrillization
	Mutant LRRK2, GBA	Pathologic kinase activity impaired
Autosomal Recessive Models	Loss of function of PINK1	kinase activity impaired
	Loss of function of parkin	parkin's ubiquitin E3 ligase activity impaired
	Loss of function of DJ-1	chaperone activity and peroxidase activity impaired

Genome-wide association (GWA) studies have provided new evidence to show associations between PD and risk loci. GWA studies have been used to discover regions of the

genome that may contain common genetic variants to demonstrate susceptibility for various traits and diseases (Yang et al., 2013). By analyzing all existing European ancestry PD patients identified as exonic variants, twenty-six loci have been identified as having a significant linkage to the development of PD based on a widely-accepted genome-wide p-value threshold. Among these risk factors, TMEM175 has been identified as a highly significant risk locus linked to PD (Yang et al., 2013; Nalls et al., 2014). Genotyping results from PD patients have shown the TMEM175 variant rs34311866, a missense mutation, has significantly decreased age at onset in PD (Lill et al., 2015). Also, a recent study shows that by knocking down 7 risk loci as candidates for PD based on a highly significant peak of GWAS, only TMEM175 knockdown can consistently influence accumulation of phosphorylated α-synuclein in rat primary hippocampal neurons. They also did the further investigation of the lead single nucleotide polymorphism (SNP) rs34311866. With a methionine to threonine conversion in the 10th transmembrane domain of TMEM175 in exon 11 (p.M393T), this missense variant has intermediate effects between WT and TMEM 175 knockout SH-SY5Y cells. The mutants were characterized by unstable lysosomal pH in response to starvation, damage of autophagy substrates clearance, and increased accumulation of p-α-syn. This result indicates that potentially manipulation of TMEM175 activity may influence α-synuclein biology and may work as a therapeutic way to treat PD (Jinn et al., 2019).

There is evidence that suggests that intact TMEM175 is required to degrade intracellular and extracellular α-synuclein through the autophagy lysosomal pathway (ALP) (Stefanis et al., 2019; Poehler et al., 2014). ALP consists of two parallel autophagic pathways, chaperone-mediated autophagy and macroautophagy (Xilouri et al., 2011). In the lysosome, specific cathepsins including cathepsins B, D and L, are essential to degrade α-synuclein. Cathepsin B and cathepsin L degrade α-synuclein within its central and amyloidogenic region. Once difference is

that cathepsin D needs anionic lipids to cleave that same region. Moreover, cathepsin L is capable of digesting α-synuclein amyloid fibrils (McGlinchey et al., 2015). ALP relys on optimal lysosomal pH because activity of cysteine cathepsins is lysosomal pH dependent to degrade α-synuclein. Lysosomal pH and as a result the activity of cysteine cathepsins can be affected by TMEM175, but the underlying mechanism is not fully understood (Jinn et al., 2017). A further study shows that lack of TMEM175 has been proved to impair autophagy-mediated degradation of α-synuclein as a result of unstable lysosomal pH. Also, the effect of the p.M393T mutation, which has defects in maintaining lysosomal pH stability, is recognized as partial loss-of-function mutation based on autophagy control is less severe than that of TMEM175 KO in the SH-SY5Y neuroblastoma cell line (Jinn et al., 2019).

Taken together, a deeper understanding of how TMEM175 regulates lysosomal pH is essential to reveal the specific role of TMEM175 in α-synuclein degradation and perhaps to help develop potential therapeutic methods of PD based on this knowledge.

CHAPTER II [1]

LRRC8 Family Proteins Within Lysosomes Regulate Cellular Osmoregulation and Enhance Cell Survival to Hypotonic Stress

II-1 Abstract

LRRC8 family proteins on the plasma membrane play a critical role in cellular osmoregulation by forming volume regulated anion channels (VRACs) necessary to prevent necrotic cell death. We demonstrate that intracellular LRRC8 proteins acting within lysosomes also play an essential role in cellular osmoregulation. LRRC8 proteins on lysosome membranes generate large Lysosomal Volume-Regulated Anion Channel (Lyso-VRAC) currents in response to low cytoplasmic ionic strength conditions. When a double leucine $L^{706}L^{707}$ motif at the C-terminus of LRRC8A was mutated to alanines, normal plasma membrane VRAC currents were still observed, but Lyso-VRAC currents were absent. We used this targeting mutant, as well as pharmacological tools, to demonstrate that Lyso-VRAC currents are necessary for the formation of large lysosome-derived vacuoles, which store and then expel excess water to maintain cytosolic water homeostasis. Thus, Lyso-VRACs allow lysosomes of mammalian cells to act as the cell's "bladder". When Lyso-VRAC current was selectively eliminated, the extent of necrotic cell death to sustained stress was greatly increased, not only in response to hypo-osmotic stress, but also to hypoxic and hypothermic

[1]Materials presented in this chapter are adapted from a published paper (Li et al, 2020) entitled "LRRC8 family proteins within Lysosomes Regulate Cellular Osmoregulation and Enhance Cell Survival to Multiple Physiological Stresses" Ping Li was the first author, with Meiqin Hu and I listed as co-equal second authors. A detailed explanation of my contributions to the work in this chapter are in the Preface of this thesis (pages v-vi).

stresses. Thus Lyso-VRACs play an essential role in enabling cells to mount successful homeostatic responses to multiple stressors.

II-2 Introduction

A fundamental aspect of cell physiology is that when the extracellular osmolarity is raised or lowered from the normal level, water flows across the plasma membrane. This results in rapid changes in cell volume and would disrupt plasma membrane integrity and lead to cell death if compensatory mechanisms were not rapidly activated (Hoffmann et al., 2009; Delpire and Gagno, 2018). In mammals, organismal level mechanisms regulating salt and water balance ensure that most cell types probably never encounter large osmotic gradients like those frequently encountered by the cells lining the digestive tract and the collecting tubules of the kidney (Bourque, 2008), but nonetheless, cells from most or all tissues of mammals display rapid adaptations to both hypo- and hyper-osmotic challenges (Hoffmann et al., 2009; Delpire and Gagno, 2018).

Cellular osmoregulation is pivotal for maintaining intracellular water homeostasis, cell volume and membrane integrity under osmotic challenges (Kultz, 2001; Jentsch 2016). In circumstances of hyper-osmolarity, water leaves the cell, leading to an excess of plasma membrane which has to be internalized to allow cellular volume shrinkage (Gauthier et al., 2012). Hypo-osmolarity elicits a complementary process leading to cellular volume expansion. In response to hypo-osmotic stress, excess membrane lipids stored in protrusions and invaginations, such as microvilli and caveolae, are used to successfully deal with the immediate volume increase in animal cells (Raucher and Sheetz, 1999; Gauthier et al., 2012). If hypo-osmotic conditions persist after the folded area is used up, the insertion of intracellular membrane materials to the plasma membrane via

exocytosis is required for cell surface tension reduction (Groulx et al., 2006; Diz-Munoz et al., 2013). Additionally, in epithelial cells of the kidney, when luminal water in the collecting duct rushes through aquaporin channels on the apical membrane, intracellular giant vacuoles derived from endocytotic compartments are essential for cell osmoregulation (Bailey and Kirk, 1991; Snigirevskaya and Komissarchik, 2000). The intracellular membrane trafficking and cytoplasmic structure changes under osmotic stress suggest that a contribution of intracellular organelles to cellular osmoregulation may exist (Snigirevskaya and Komissarchik, 2000). The lysosome has been referred to as the "osmometer" of mammalian cells (Lloyd and Forster, 1986) because it responds to the osmotic pressure (Park et al., 1988), and lysosomes may be a source of intracellular lipids that are added to the plasma membrane under hypotonic condition (Groulx et al., 2006; Diz-Munoz et al., 2013). However, the cellular and molecular basis of intracellular osmoregulatory mechanisms are poorly understood.

Volume-Regulated Anion Channels (VRACs), which are composed of LRRC8 family proteins (LRRC8A-E) assembled as hexamers, have been demonstrated to play an essential role in cellular osmoregulation (Jentsch, 2016; Qiu Z, et al., 2014; Voss FK, et al., 2014; Deneka et al., 2018). Studies deleting and then re-expressing the various LRRC8 genes indicate that detectable levels of VRAC channel function on the plasma membrane requires LRRC8A (Swell1) and at least one other subunit, that the properties of the channels vary depending on whether the partner is LRRC8B, C, D or E, and that LRRC8A expressed alone at very high levels can form functional channels (Voss FK, et al., 2014; Qiu Z, et al., 2014; Syeda R, et al., 2016).

We used Stimulated Emission depletion (STED) microscopy and electrophysiological recordings from giant vacuoles to demonstrate that there is a substantial amount of expression of LRRC8 family members on lysosome membranes, and that these proteins form functional

Lysosomal Volume-Regulated Anion Channels (Lyso-VRACs). By genetically and pharmacologically selective manipulation of Lyso-VRAC activity, we demonstrate that both plasma membrane VRACs and Lyso-VRACs are required to prevent necrotic cell death following hypo-osmotic stress. Furthermore, Lyso-VRACs are also required to successfully respond to two other stresses that can lead to necrotic cell death.

II-3 Results

3.1 Lysosomes are highly osmosensitive organelles in many types of mammalian cells.

Our initial studies of lysosomal responses to a hypo-osmotic challenge focused on Cos1 cells (an epithelial cell line derived from the kidney of an African green monkey) because, in the kidney, the luminal osmolarity can range widely, from 50 milliosmoles (mOsm) to 1,200 mOsm, depending on the hydration state of the individual (Sands and Layton, 2014). Consistent with previous studies (Snigirevskaya and Komissarchik, 2000; Bailey and Kirk 1991; Kirk, 1988), Cos1 cells exposed to a physiologically relevant hypo-osmotic challenge (170 mOsm rather than the normal 300 mOsm) demonstrated extensive cytoplasmic vacuolation 30 min after the solution change (**Fig. 2.1a**). Similar responses in about the same proportion of cells were observed in Hap1 cells (a leukemia-derived cell line) and HeLa cells (a cervical epithelial-derived cell line). Thus cytoplasmic vacuolation in response to hypotonicity is not limited to those mammalian cell types most likely to encounter large osmotic gradients in an intact animal. In Hap1 and HeLa cells, the large cytoplasmic vacuoles observed under hypotonic stress contained markers for late endosomes and lysosomes, including lysosomal associated membrane protein 1 (LAMP1) (**Fig. 2.1b-c**), Rab7 (**Fig. 2.1d**), Dextran-Green (an endocytic marker that reaches lysosomes at steady state) (**Fig. 2.1e**), or LysoTracker (a lysosomal pH indicator) (**Fig. 2.1e**) (Xu and Ren, 2015; Li

et al., 2019). In contrast, most insult-induced vacuoles were not immune-positive for an early endosomal marker (EEA1) (**Fig. 2.1f**), nor for markers of endoplasmic reticulum (ER) or mitochondria, suggesting that late endosomes and lysosomes (referred to as lysosomes for simplicity hereafter) are likely the primary vacuolar membrane source.

A super resolution fluorescence imaging assay was used to quantify the volume of lysosomes and vacuoles in Hap1 cells as a function of osmotic strength (**Fig. 2.2 a**). The principle of the assay is that Dextran-Green is trapped in the lumen of lysosomes and endosomes following endocytosis and then a chase (Johnson et al., 2016; Freeman et al., 2020), and LAMP1-mCherry fluorescence allows one to identify lysosomes (Xu and Ren, 2015), so for each green object surrounded by red fluorescence, the length of the green region (or the distance between the two peaks of red fluorescence that surround it) is the diameter of the object. Thus, lysosomal volume can be estimated by treating each object as a sphere with Volume $= \frac{4}{3} * pi * (\frac{Distance}{2})^3$. At 300 mOsm, the diameter of all lysosomes was small, but, as the osmolarity was decreased from the control level to 220 or 170 mOsm, the diameter of some lysosomes enlarged to over 2 μm while others remained much smaller (**Fig. 2.2 a-b**). As compared to 300mOsm solution (mean volume 0.006 ± 0.003 μm^3), the average volume of lysosomes increased about fivefold at 220 mOsm (0.031 ± 0.011 μm^3) and more than 100-fold at 170 mOsm (0.705 ± 0.135 μm3) (**Fig. 2.2 c**). In contrast, early endosomes were not enlarged by exposure to the 170-mOsm solution (**Fig. 2.2 d**). Large vacuoles without green dextran labeling were occasionally observed (one example is present on the left side of the cell at 170 mOsm illustrated in **Fig. 2.2 a**), but these represented only 4.7% of all vacuoles. These vacuoles without green fluorescence appeared to have a rim of LAMP1 staining, but, without the Dextran-Green labeling to clearly define that the LAMP1 was on the vacuole membrane, it could not be confirmed that they were of lysosomal origin.

Nevertheless, we conclude that at least 95% and probably all giant cytoplasmic vacuoles of mammalian cells observed following hypo-osmotic challenge are enlarged lysosomes.

3.2 Lysosome-derived vacuoles express chloride channels gated by low ionic strength.

The plasma membranes of many mammalian cell types express ion channels that respond to changes in the osmotic strength of the bathing medium. Whole-endolysosome (whole-EL) patch-clamp recording (**Fig. 2.3 a**) was used to test whether osmolarity-sensitive ion channels were present on vacuolated lysosome membranes. Large vacuoles were produced by exposing Cos1 cells to 80 mOsm solution. Whole-EL recordings were then established in the same solution, and the current–voltage relation was determined by the responses to voltage ramps from -120 mV to +120 mV. Large outwardly rectifying currents were observed at positive membrane potentials and were greatly decreased by transferring to 320 mOsm, or exposure to DCPIB, a small molecule usually used as a pharmacological tool for ion channel studies, including VRAC (Minieri et al., 2013; Kern et al., 2019) (**Fig. 2.3 b**). Because the activation mechanism of the plasma membrane osmotic-sensitive channel VRAC is controversial, with both cytosolic low ionic strength (Deneka et al., 2018; Syeda R, et al., 2016; Nilius et al., 1998) and extracellular hypotonicity (Voss et al., 2014; Qiu et al., 2014) suggested to be the relevant signal, solutions of a variety of osmolarities and ionic strengths (Γ) in both the intracellular/cytosolic/bath and luminal/pipette solutions were tested. Reduced intracellular ionic strength (Γi) is likely to be the primary stimulus causing dose-dependent activation of current (**Fig. 2.3 c**). Recordings from vacuoles enlarged by chemical treatment with vacuolin-1 (Dong et al., 2008) (**Fig. 2.3 d**) also showed outwardly rectifying currents that were very small at Γi 140 (normal ionic strength) and greatly increased at Γi 40.

With the standard recording solutions, the ionic strength-sensitive current of the lysosome had a reversal potential (Erev) of −31.8 ± 1.6 mV（**Fig. 2.3 e**), close to the equilibrium potential for Cl^- (calculated Erev = −32.2 mV based on $[Cl^-]_{Lumen}$ = 140 mM and $[Cl^-]$Cytosol = 40 mM). Changing $[Cl^-]_{Lumen}$ resulted in Nernstian shifts in Erev (**Fig. 2.3 e**). We therefore refer to the channel carrying this current as the Lyso-VRAC. The compound known to inhibit PM-VRACs (DCPIB) (Kern et al., 2019) also inhibited Lyso-VRACs (**Fig. 2.3 b**). Lyso-VRAC currents were present in vacuoles from all cell types that we investigated, including Cos1, Hap1, Hap1-KI GFP, HEK293T, human breast cancer cells (MDA231), primary mouse embryonic fibroblasts (MEFs), and bone marrow macrophages (BMMs) (**Fig. 2.3 f**).

3.3 The Lyso-VRAC current is mediated by LRRC8 proteins

LRRC8A codes for an essential subunit of the plasma membrane VRAC (PM-VRAC). Because of the great similarity between the electrophysiological and pharmacological properties of Lyso-VRAC and PM-VRAC, we tested whether LRRC8A is also an essential subunit of Lyso-VRAC by making LRRC8A knockout (8A KO) cell lines in both Hap1 and HeLa cells using the CRISPR-Cas9 system (Komor et al., 2017). Γi 40 solutions failed to induce any current in 8A KO Hap1 cells (**Fig. 2.4 a**). PM-VRAC current was rescued by 8A-mCherry transfection (**Fig. 2.4 b**), but Lyso-VRAC was not (**Fig. 2.4 c**). Lyso-VRAC currents were restored in 8A KO Hap1 cells by co-expression of 8A-mCherry and 8E-GFP (**Fig. 2.4 d-e**).

To determine the intracellular localization of LRRC8 family proteins, the location of LRRC8A and LRRC8E was examined by using Western blots of proteins isolated from cell fractions enriched in lysosomes and imaging of fluorescent fusion proteins. To explore the

localization of LRRC8A at normal expression levels, knock-in Hap1 cells (GFP-KI) were generated so that expression of the fusion protein was controlled by the endogenous LRRC8A promoter. Western blot analysis of lysosomes isolated by gradient-based centrifugation or immunoisolation (Abu-Remaileh et al., 2017) demonstrated that these organelles were enriched for endogenous (**Fig. 2.5 a**).

When LRRC8A-GFP knock-in cells were exposed to solutions of normal osmotic strength (300 mOsm), there was fluorescence on the plasma membrane and brighter fluorescence localized to intracellular puncta which primarily colocalized with LAMP1 (**Fig. 2.5 b**) and barely any colocalization with early endosome markers (**Fig. 2.6 a**). Thus intracellular LRRC8A is associated mainly with lysosomes. In cells transiently transfected so that a fusion protein of LRRC8A-mCherry was expressed at high levels, imaging demonstrated abundant labeling on both the plasma membrane and on lysosomal membranes (**Fig. 2.6 b**). When wild-type (WT) LRRC8E fused to a fluorescent protein was overexpressed, very little fluorescence was localized to the lysosome (**Fig. 2.6 c**), with most fluorescence localized to the ER (**Fig. 2.6 d**). However, when both LRRC8A and LRRC8E fusion proteins were coexpressed at high levels, intracellular LRRC8E as well as intracellular LRRC8A localized mostly to lysosomes (**Fig. 2.6 e**). In these experiments, the colocalization of the two LRRC8 proteins was extensive. Unlike membrane proteins targeted to lysosomes for degradation, which are expected to be localized to intraluminal vesicles (Xu and Ren, 2015), after hypotonic challenge, almost all of the intracellular LRRC8A and LRRC8E signal was localized to the perimeter membranes of the lysosome-derived large vacuoles (**Fig. 2.6 f**). Thus, the distribution of LRRC8 proteins on vacuoles is consistent with the large Lyso-VRAC currents recorded from vacuole membranes.

3.4 Lyso-VRAC requires a double-leucine motif of LRRC8A.

Like many lysosomal membrane proteins that use an AP-2–dependent internalization route for lysosomal targeting (Xu and Ren, 2015), LRRC8A contains two double-leucine (LL) motifs near the intracellular C terminus. Mislocalization of other lysosomal membrane proteins with their LL domains deleted is known to be due to impaired internalization and also a secondary block of anterograde trafficking (Hunziker and Geuze, 1996). Mutation of the $L^{706}L^{707}$ motif to alanines (**Fig. 2.7 a**) was sufficient to abolish lysosomal localization of transfected LRRC8A, and the mutant protein was instead found on the plasma membrane and in the ER (**Fig. 2.6 g**). However, unlike coexpression with wild-type subunits, high level coexpression of $8A^{L706A, L707A}$-mCh and wild-type LRRC8E-GFP gave very little lysosomal expression of either (**Fig. 2.7 b**). Although the subunit stoichiometry of Lyso-VRAC in native lysosomes is not yet known, these results suggest that LRRC8A is required for other LRRC8 proteins to reach lysosomes.

Consistent with the imaging data, cotransfection of $8A^{L706A, L707A}$-mCherry and 8E-GFP failed to produce Lyso-VRAC in 8A KO Hap1 cells (**Fig. 2.7 c-d**). Therefore, lysosome-targeted LRRC8A and at least one of the other LRRC8 proteins are required for the Lyso-VRAC current. However, the PM-VRAC current was fully restored in 8A KO Hap1 cells by coexpression of 8E-GFP together with either LRRC8A or $8A^{L706A, L707A}$-mCherry (**Fig. 2.7 e-i**). Hence, there are distinct trafficking mechanisms that regulate the expression of Lyso-VRAC versus PM-VRAC, suggesting that the biological roles of Lyso-VRAC and PM-VRAC can be distinguished. In summary, 8A KO cells coexpressing $8A^{L706A, L707A}$-mCherry and 8E-GFP are essentially PM-VRAC (+) but Lyso-VRAC (−) cells.

3.5 Lyso-VRAC plays a critical role in lysosome vacuolation.

8A KO Hap1 and HeLa cells did not become vacuolated under hypo-osmotic challenge (**Fig. 2.8 a**), nor did BMM cells from *ebo/ebo* mice, which have a frameshift mutation (Platt et al., 2017) in exon 3 of the LRRC8A gene (**Fig. 2.8 b**), but lysosomal vacuolation remained normal when several other lysosomal channels were knocked out (**Fig. 2.8 a**).

The ability to selectively rescue VRAC expression in 8A KO cells only on the plasma membrane (by coexpressing $8A^{L706A, L707A}$ and 8E) or on the plasma membrane and in lysosomes (by coexpressing WT 8A and 8E) allowed us to test the relative biological importance of PM-VRAC and Lyso-VRAC. In response to a hypotonic challenge, cells expressing VRAC only on the plasma membrane were incapable of expanding the volume of their lysosomes (**Fig. 2.8 c**) and incapable of forming giant vacuoles (**Fig. 2.8 d**). In contrast, expressing VRAC on both the plasma membrane and lysosome membranes completely restored the ability to expand the volume of lysosomes and nearly completely restored the ability to form giant vacuoles.

In DCPIB-treated WT cells, no lysosomal volume increase or vacuolation in response to hypo-osmotic challenge was observed (**Fig. 2.8 e-f**). Thus, channel function of VRAC somewhere in the cell is essential for lysosome vacuolation under hypo-osmotic challenge. The critical location was revealed by use of the VRAC inhibitor NS3728, which is negatively charged (Hélix et al., 2003) and membrane impermeable (Klausen et al., 2007). NS3728 can completely inhibit PM-VRAC but is not able to inhibit Lyso-VRAC. A likely reason for the failure of NS3728 to inhibit Lyso-VRAC in intact cells but potently inhibit PM-VRAC is that the NS3728 binding site is on the luminal surface, which is facing extracellular for PM-VRAC (Klausen et al., 2007), but is hidden behind two membranes for Lyso-VRAC (see Discussion). NS3728 was therefore a powerful pharmacological tool to create PM-VRAC (–) but Lyso-VRAC (+) cells for further

dissection of the role of Lyso-VRAC in lysosome vacuolation. In Hap1 cells treated with NS3728 (30 μM for 2 h), lysosome vacuolation was not diminished (**Fig. 2.8 e**) so PM-VRAC, which is blocked by NS3728 is not required for this process. We infer that DCPIB must be blocking vacuolation by acting on Lyso-VRAC so activation of Lyso-VRAC is necessary for lysosome vacuolation under hypo-osmotic stress.

3.6 Lysosomes maintain intracellular water homeostasis

Under hypo-osmotic challenge, H_2O influx mediated by aquaporins on the plasma membrane has been reported to reduce the osmolarity and ionic strength of the cytosol (King et al., 2004). Exposure to 50 μM Hg^{2+}, which blocks aquaporin activity, eliminated hypotonicity-induced lysosomal vacuolation in Hap1 cells (**Fig. 2.9 a**). Therefore, low expression or activity of aquaporin on a subset of cells might explain why some cells failed to become vacuolated in response to hypotonicity over the time course of our other experiments. Furthermore, high expression of aquaporin should rapidly bring the intracellular ionic strength into the range that activates Lyso-VRAC. A fluorescence assay was used to investigate water flow across the lysosomal membrane. Lysosomes within intact cells were loaded with Lucifer yellow dextran (LY-Dextran), which displays enhanced fluorescence in the presence of deuterated water (D_2O) (Chaurra et al., 2011). Hypo-osmotic challenge with D_2O quickly augmented the fluorescence intensity (**Fig. 2.9 b**), indicating that there is substantial water flux into the lumen of lysosomes from the cytosol soon after water penetration across the plasma membrane.

As a consequence of the water influx across the plasma membrane during hypotonic challenge, cell volume initially increases dramatically (**Fig. 2.9 c-d**). Based on published calibration curves for the assay used (Zhou et al., 2020; Capó-Aponte et al., 2005), the increase

to 125% of the basal fluorescence at the peak of the response indicates that the cell volume increased nearly threefold and so presumably dropped the intracellular ionic strength from Γ140 to about one-third its normal level, which can activate substantial Lyso-VRAC current (**Fig. 2.3 d**). In WT HeLa and Hap1 cells, volume began to return toward normal after about 15 to 20 min. This regulatory volume decrease (RVD) was prevented in WT cells by DCPIB (**Fig. 2.9 c**), which blocks both PM-VRAC and Lyso-VRAC, and was absent in HeLa and Hap1 8A KO cells that lack both PM-VRAC and Lyso-VRAC (**Fig. 2.9 c-e**). RVD was largely restored in 8A KO cells by coexpressing LRRC8A and LRRC8E, which rescues both PM-VRAC and Lyso-VRAC (**Fig. 2.9 d**). A treatment that rescued only PM-VRAC in 8A KO cells (the combination of $8A^{L706A, L707A}$ and 8E) did not restore RVD (**Fig. 2.9 d**), indicating that vacuolar LRRC8 proteins are necessary for RVD. Conversely, NS3728 treatment, which blocks only PM-VRAC, also prevented RVD (**Fig. 2.9 e**), indicating that plasma membrane LRRC8s are also necessary for RVD. Taken together, these experiments thus demonstrate a dual requirement for both PM-VRAC and Lyso-VRAC. RVD could also be suppressed in WT cells by two V-ATPase inhibitors (Baf-A1 and Concanamycin A) (**Fig. 2.9 c and e**).

Water entering lysosomes and enlarging them into vacuoles might help restore the normal ionic strength and osmolarity of the cytosol but would not relieve the plasma membrane tension stress. Previous studies had demonstrated that intracellular membrane exocytosis occurs in response to hypo-osmotic stress (Diz-Muñoz, et al., 2013; Groulx et al., 2006). By making time-lapse video observations of Cos1 cells expressing fluorescent LAMP1, we observed that lysosome-derived giant vacuoles underwent exocytosis (**Fig. 2.9 f**). Another consequence of lysosome exocytosis was a greatly increased abundance of LAMP1 on the plasma membrane (**Fig. 2.9 f**). Thus, just as the mammalian bladder fills with wastes from the kidney and then discharges

the waste and any excess water to the outside of the animal, lysosomes serve as the cell's "bladder," sequestering intracellular excess water through vacuolation and then expelling the potentially toxic level of water through exocytosis, which also relieves the plasma membrane tension stress.

3.7 Lyso-VRACs protect cells from necrotic cell death in response to hypo-osmotic stress

Vacuolization followed by exocytosis and RVD occurs within an hour of exposure to hypotonic stress. However, when cells encountered a sustained stress, substantial necrotic cell death resulted, whether assessed by propidium iodide (PI) staining or by lactate dehydrogenase (LDH) release into the medium. The imaging-based assay (**Fig. 2.10 a**) also showed that becoming vacuolated is highly correlated with survival. Under the tested conditions (80 mOsm solution for 1 h), only 0.4% of the cells that were vacuolated died (i.e., became propidium iodide-positive), but 46.9% of the nonvacuolated cells died (more than 600 cells were randomly selected for analysis). Lyso-VRAC plays an important role in survival under these conditions because the survival index calculated from LDH activity release was much lower in LRRC8A KO cells, and survival was restored to close to WT levels when 8A KO cells were cotransfected with 8A plus 8E, but not with $8A^{L706A,\ L707A}$ plus 8E (**Fig. 2.10 b**). However, NS3728, which does not inhibit Lyso-VRAC but does inhibit PM-VRAC, results in a level of cell death to 80 mOsm solution similar to the amount observed in the LRRC8A KO (**Fig. 2.10 c**) so VRACs are needed at both locations to stave off cell death to this intensity of hypo-osmotic stress.

Acute treatment with 5 μM Baf-A1 prevented vacuolation in response to hypo-osmotic stress, but prolonged treatment with Baf-A1 had no effect on Hap1 cell survival when these cells were maintained under control osmotic conditions (**Fig. 2.10 d-e**). However, Baf-A1 greatly increased the extent of necrotic cell death caused by hypo-osmotic stress (**Fig. 2.10 f**). The

necrotic cell death induced by hypotonicity requires functional synaptotagmin-VII to protect against the stress. The evidence for this conclusion is that transfection with a dominant negative Synt-VII construct, which has no effect on the survival of cells under normal conditions, leads to cell death as severe as the 8A KO when cells are subjected to hypotonic stress (**Fig. 2.10 g**). This requirement for Synt-VII is likely because it is required for lysosome exocytosis (Xu and Ren, 2015).

II-4 Discussion

In an intact animal, the bladder stores and expels urine. We provide compelling evidence that, in individual cells, lysosomes play a critical role in alleviating the intracellular water crisis caused by hypotonic stress by acting as the cell's "bladder." Lysosomes sequester water, an action that will help to restore the optimal physiological concentrations of proteins and metabolites. Lysosome-derived vacuoles then fuse with the plasma membrane, an action that by expelling water helps restore the cell volume to its original size. According to the "square-cube law," volume increases in proportion to the cube of the diameter, but surface area only increases in proportion to the square of the diameter. Thus, by placing the amount of membrane surface area that is present in a very large number of lysosomes into a much smaller number of large vacuoles, a huge increase in luminal volume becomes available for water storage. Lysosomal exocytosis also delivers more materials to the plasma membrane, both lipids and lysosome resident proteins. This will substantially relieve membrane tension stress and allow larger PM-VRAC currents than the channels originally located there could produce (**Fig. 2.11 a**).

We demonstrated that Lyso-VRAC, but not PM-VRAC, is essential for lysosomal vacuolation, but both are required to ultimately allow the cell to survive. It is not yet clear why

VRACs at two locations are necessary for successful RVD and cell survival, but one appealing idea is that the processes they regulate are in series so, if either fails, osmoregulation fails. Testing this idea requires the ability to have temporal control over when each VRAC is active, but at present this is only possible for PM-VRAC.

It is well known that lysosomes are the cell's center for degrading macromolecules. The amino acids and sugars produced by this catabolism contribute to luminal osmolarity, and lysosomal degradation itself is a water-consuming process (Xu and Ren, 2015). Thus, lysosomes are an excellent location to regulate intracellular water homeostasis and maintain osmotic homeostasis. The "bladder" function of lysosomes may therefore be fundamental and critical for cell survival under various physiological and pathological osmotic perturbations. The osmoregulatory role of lysosomes also could provide protection from cell damage in patients with hyponatremia, nephrotic syndrome, and liver cirrhosis (Shah and Magdiga, 2019). In addition to the hypotonic challenges present in the digestive tract and the collecting tubules of the kidney of adult animals, there are developmental challenges. The yolk sac and amniotic and allantoic fluid are all hypo-osmotic to the developing fetus and may take on a level as low as 30 mOsm (Goldstein et al., 1980). Thus powerful osmoregulatory mechanisms are required to allow normal embryonic development (Baggott, 2009). A role for Lyso-VRAC in this osmoregulatory behavior might account for some of the development deficiencies of LRRC8A KO animals (Yamada et al., 2016; Kumar et al., 2014). Therefore, our identification of Lyso-VRAC provides a molecular foundation upon which to explore new links between lysosome function, normal human physiology, and disease pathologies.

II-5 Methods

Primary cell cultures

Mouse embryonic fibroblasts (MEFs) were isolated from P1 mouse (C57BL/6) skin and cultured in DMEM with 20% FBS. Bone marrow macrophages (BMMs) were isolated and cultured in Dulbecco's Modified Eagle Medium (DMEM, Thermo Fisher Scientific) with 10% (v/v) fetal bovine serum (FBS; Atlantic Biologicals) with 20 ng/mL granulocyte macrophage colony-stimulating factor (Sigma Aldrich, Cat. G5035) and 1× antibiotic-antimycotic (Thermo Fisher Scientific, Cat. A5955). To obtain BMMs, *ebo/ ebo* mice which have a frameshift mutation in LRRC8A (Platt et al., 2017) were genotyped by polymerase chain reaction (PCR; forward primer, 5'-GCC AGC GCC TCA CCA AGA AC-3'; and reverse primer, 5'-CGG GAT GGT CAC GTC GGG T-3'). Both sexes of mice were used under an approved animal protocol following the Institutional Animal Care Guidelines at the University of Michigan.

Mammalian cell lines

Hap1 cells (Horizon Company) were cultured in Iscove's Modified Dulbecco's Medium (IMDM, Thermo Fisher Scientific) with 10% FBS and 1× penicillin- streptomycin-glutamine (Thermo Fisher Scientific, Cat. 10378016). They were transfected with the Neon^{TM} transfection system (Neon) or CalPhos mammalian transfection (Takara, Cat. 631312) kit. Cos1, HeLa, and MDA231 cells were purchased from American Type Culture Collection (ATCC) and cultured in DMEM with 10% FBS. HEK293T cells (ATCC) were cultured in DMEM/F12 (Thermo Fisher Scientific) with 10% FBS. Cos1, HeLa, and HEK293T cells were transfected with Lipofectamine 2000 (Invitrogen). All cells were used at low passages with further authentication for mycoplasma contamination.

Reagents

Oregon Green™ 488-dextran was purchased from Thermo Fisher Scientific (cat. O6798). Propidium iodide (cat. P4864), $HgCl_2$ (cat. 215465), NS3728 (cat. SML1964), and carbenoxolone disodium salt (cat. C4790) were purchased from Sigma-Aldrich. Other reagents used in the study included: LysoTrackerTM Red DND-99 (Thermo Fisher Scientific, cat. L7528); DCPIB (Tocris Bioscience, cat. 1540); Baflomycin-A1 (LC laboratories, cat. B- 1080); Wortmannin (Tocris Bioscience, cat. 1232); Latrunculin B (Tocris Bioscience, cat. 3974); R(+)-IAA94 (Cayman Chemical, cat. 17877); Vacuolin-1 (Millipore Sigma, cat. 673000); GPN (Santa Cruz, cat. Sc-252858); Calcein-AM (Thermo Fisher Scientific, cat. C1430); D_2O (Cambridge Isotope Laboratories, Inc., cat. DLM-7005); Lucifer yellow dextran (Thermo Fisher Scientific, cat. D1825); Rhodamine dextran (Thermo Fisher Scientific, cat. D1824).

CRISPR mediated knock in (KI) and knock out (KO) cell line

We used a CRISPR- Cas9 system (Komor et al., 2017) to generate LRRC8A KO HeLa cells, TPC1&2 double KO, TMEM175 KO, CLC7 KO by the non-homologous end joining repair method. The guide sequences were designed with a CRISPR design tool (http://crispr.mit.edu/) and cloned in the pSpCas9 (BB)- 2A-Puro vector (PX459; from Addgene). For LRRC8A KO, guide RNA (gRNA) targeted the sequence AAG TAG CGG AGC TCG TCA C [CGG]. For TMEM175 KO Hap1 cell line, the sequence CGC GTG GAA GCC TTC AGC GA [CGG] was targeted. For TPC1&2 DKO Hap1 cell line, the TPC1 sequence CTT GCA GTA CTT CAG CAC CC [TGG] and the TPC2 CCC CAG CGT CGG GCT GCT GC [TGG] were targeted. For the CLC7 KO Hap1 cell line, the sequence GAC GAG TAG ATC AGC ACG A [AGG] was targeted. LRRC8A-GFP KI was introduced by homology directed repair-mediated gene editing. The

sequence ACA AGG AGC AGG CCT GAG CG [AGG] near the stop codon was targeted. To construct a homology directed repair donor for LRRC8A GFP-KI, a 1,159-bp segment upstream (LRRC8A_L) and a 1,052-bp segment downstream (LRRC8A_R) of the stop codon were amplified as the homology arms. The EGFP cassette with a stop codon was amplified from pEGFP-C3 and inserted between LRRC8A_L and LRRC8A_R. Five glycine residues were inserted between LRRC8A-L and EGFP. The donor DNA (LRRC8A_L-5XGly-EGFP-LRRC8A_R) sandwiched by the 23-nuceotide LRRC8A gRNA target sequence was used to replace the CMV-EGFP cassette in the pEGFP-C3 by subcloning (ClonExpress II One Step Cloning Kit, Vazyme). The resulting donor plasmid was co-transfected with PX459 and gRNA to insert a GFP tag at the C terminus of LRRC8A. Hap1 and HeLa cells were transfected by a calcium phosphate method and with Lipofectamine 2000 (Sigma), respectively. LRRC8A-single gRNA-transfected cells were selected in the presence of puromycin for 48~72h. After single- cell clones were established, their genomic DNAs were sequenced to confirm the intended genetic disruptions. For Hap1 clones, a near-haploid cell line, genetic editing was confirmed by sequencing of PCR products. For HeLa clones, the PCR product was inserted into a pMDTM19-T vector by TA cloning (pMD^{TM}19-T Vector Cloning Kit, Takara). The primers are listed below

	Primer 1	Primer 2
8A KO	AAGGGCTGATAAGTGGGCTGC	ATACTTGATGCCTGTGGGGCC
8A GFP-KI	CACACCCACCTCACTCTCAC	CCACTCTGCTGAAGTCCAGG
TPC1 KO	ATGGCCCAGACATGTGACTC	TGCCTGTCTCCATCCTCTCA
TPC2 KO	TGAGCTGAGCATGAGGCAAG	AAAGGACAAGTGGCCCTGAG
175 KO	CCGAGGCCCGTGTGCGTGGT	GGGCAGGTGACGCGGGGTCC
CLC7 KO	GACGAGTAGATCAGCACGA	TCGTGCTGATCTACTCGTC

Cytoplasmic vacuolization assays

Hap1 and HeLa cells (40~70% confluence) were seeded onto poly-L-Lysine coated coverslips in 24-well plates and challenged with 170 mOsm or 80mOsm solution (IMDM diluted with distilled H_2O in a 1:1 or 1:4 ratio). In control experiments, mannitol (135mM) was added to the 170 mOsm solution to make a solution isotonic with IMDM (300mOsm). Hypoxic treatment was performed on Hap1 cells using an air-tight hypoxia chamber (Billups-Rothenberg Inc., Del Mar, CA) saturated with 5%O_2 + 5%CO_2 + 90%N_2; 5%O_2 was achieved by flushing the hypoxia chamber with an O_2-CO_2-N_2 mixture at no more than 2 psi for 10 min. The flushing was repeated after half the incubation time, then the hypoxia chamber was placed in the incubator (37°C) for 6h. For hypothermia experiments, HeLa cells were seeded onto poly-L-Lysine coated coverslips in 24-well plates and challenged with 4°C in refrigerator for 18h in HEPES-buffered culture medium. The cell vacuolation images were collected using an Olympus IX81 or the spinning-disk confocal microscope (Olympus IX-83) with fluorescence. Images are randomly captured, and vacuoles with the diameter larger than 0.4 μm were counted.

Confocal imaging

Non-super-resolution fluorescence imaging and time-lapse imaging were conducted using an Olympus spinning-disk confocal microscope (IX-83) equipped with a temperature controller that maintained the temperature at 37°C. For time-lapse imaging, cells were perfused with isotonic Tris-based saline (iso-TBS; 300 mOsm) for 10 min during baseline stabilization. Iso-TBS consisted of (in mM): 137 NaCl, 7.37 KCl, 1.26 $CaCl_2$, 0.8 $MgCl_2$, 5.6 glucose, 20 Tris-HCl, and 4 $NaHCO_3$ (pH adjusted to 7.20 with Tris base). Cells were then challenged with 170 mOsm Hypo-

TBS. The 170 mOsm Hypo-TBS contained (in mM): 45.7 NaCl, 1.79 KCl, 0.42 $CaCl_2$, 0.27 $MgCl_2$, 1.87 glucose, 20 Tris-HCl, and 4 $NaHCO_3$ (pH adjusted to 7.20 with Tris base).

For pre-loading of lysosomes with fluorescent molecules by endocytosis, cells were exposed to Dextran-Green (5 μM), Lucifer yellow-Dextran (25 μM) and/or Rhodamine- Dextran (25 μM) for 24 h (the pulse), then washed with medium without label for 18h (the chase); then incubated with LysoTrackerTM (50 nM), and propidium iodide (10 μM) for 30 min just before imaging. In some experiments, cells were pretreated with 100 μM DCPIB, 200 μM GPN, or 5 μM Baf-A1 in IMDM for the time indicated in Results before hypo- osmotic challenges.

Super-resolution microscopy

Stimulated emission depletion (STED) imaging was performed with the STED module of a Leica TCS SP8 STED 100× microscope (Leica Microsystems). The 775-nm, 660-nm, 592-nm and 405-nm depletion lasers were used for mCherry, GFP, and V500 streptavidin (BD Horizon, Cat. 561419), respectively. Images were de-convolved with Huygens Professional Software (Scientific Volume Imaging). In the X-Y plain, features as small as 0.1μm could be clearly resolved and measured.

Immunohistochemistry

Cells were fixed with 4% (v/v) paraformaldehyde or with iced 100% methanol for 15 min and then permeabilized with 0.3% Triton-X100 (Thermo Fisher Scientific) in phosphate buffered saline (PBS) with 1% (w/v) BSA. After blocking with PBS + 1% BSA for 1 h, samples were incubated with primary antibodies overnight and then secondary antibodies for 1 h. After 10 min of DAPI counterstaining, coverslips were mounted with Fluoromount-G (Southern Biotechnology

Associates, Inc.). The antibodies used were: anti-LAMP1 (DSHB, cat. H4A3; methanol fixation), anti-EEA1 (Santa Cruz, Cat. sc-137130, PFA fixation), and anti-mTORC1 (Cell signaling, cat. 2983s, methanol fixation). Images were analyzed with MetaMorph Advanced imaging acquisition software v.7.7.8.0 (Molecular Devices) and Image J (NIH).

Electrophysiology

All electrophysiology experiments were conducted at room temperature (21~23^{o}C) with a 1M KCl Agar Bridge connecting the recording chamber to a ground wire. All bath solutions were applied through a perfusion system, in which solutions were exchanged completely within a few seconds. Data was collected via an Axopatch 200B patch clamp amplifier, Digidata 1332, and pClamp 10.2 software (Axon Instruments). Currents were digitized at 10 kHz and filtered at 2 kHz. A ramp protocol for measuring the current- voltage relation was applied every 5 s after membrane rupture, and consisted of a holding potential of 0 mV, then a 20 ms step to -120 mV followed by a 200 ms ramp from -120 to +120 mV and then a return to the holding potential. All traces were analyzed with pClamp 10.2 and Origin 8.0 (OriginLab, Northampton, MA).

Whole-endolysosomal recordings

We employed a modified patch-clamp method to record endosomal and lysosomal channels (Chen CC, et al., 2017; Dong XP, et al., 2008). Lysosomes were enlarged with either incubation for 1 h in a low-osmolarity solution (80 mOsm) made by mixing the control cytosolic/internal recording solution in a 1:4 ratio with distilled water, or by treatment with 1 μM vacuolin-1 for ~12h. Early endosomes were enlarged with wortmannin (200 nM) and latrunculin B (10 nM) for 20~60 min (Chen CC, et al., 2017). The plasma membrane was ruptured with a fine

glass pipette and then the enlarged endolysosomes were captured by gentle suction from a second glass recording pipette. After a giga-seal was reached, a break-in step protocol with a few hundred mVs lasting 1~4 ms was applied to break the vacuolar membrane. The whole-EL configuration was verified by the re- appearance of capacitance transients after break-in.

Unless other stated, the luminal/pipette solution contained (in mM): 140 CsCl, 1 $MgCl_2$, 1.9 $CaCl_2$, 5 EGTA, and 10 HEPES (pH adjusted to 7.2 with CsOH). The cytosolic/internal solution contained (in mM): 140 K-gluconate, 4 NaCl, 1 EGTA, 2 $MgCl_2$, 0.39 $CaCl_2$, and 20 HEPES (pH adjusted with KOH to 7.2; free $[Ca^{2+}]_i$ ~ 100 nM calculated by MaxChelator software). The 40 mM low ionic strength cytosolic solutions (Γi 40) contained (in mM): 40 CsCl, 180 mannitol, and 10 HEPES (pH 7.20; overall osmolarity = 290 mOsm). Other low Γi solutions were prepared by mixing the Γi 40 solutions with different concentrations of Cs-methanesulfonate. Alternatively, the low Γi solutions contained (in mM): 20 CsCl, 10 HEPES, and various concentrations of mannitol and Cs-methanesulfonate. For Cl^- permeability measurement, the concentrations of CsCl and mannitol in the pipette solutions were (in mM, respectively): 20 and 210; 40 and 180; 90 and 110; and 180 and 0. Patch pipette electrodes had a resistance of 8~12 mΩ. Recordings with a membrane resistance > 3 GΩ were accepted.

Liquid junction potentials were measured for all solutions and adjusted. The molar ionic strength, Γ, of solutions was calculated as:

$$\Gamma = \frac{1}{2}\sum_{i=1}^{n} C_i Z_i^2$$

where *Ci*, *Zi*, and n represent the molar ion concentration, ion charge number, and total number of ion species, respectively.

Whole-cell electrophysiology

Whole-cell VRAC currents were measured using a Γi40 pipette/cytosolic solution that contained (in mM): 40 CsCl, 180 mannitol, and 10 HEPES (pH adjusted to 7.2 with CsOH; overall osmolarity = 290 mOsm). The bath/extracellular solution contained (in mM): 140 CsCl, 1 $MgCl_2$, 1.9 $CaCl_2$, and 10 HEPES (pH 7.2 adjusted with CsOH). VRAC current was activated 3~5 min after establishment of whole-cell recording mode. Patch pipettes had a resistance of 2~4mΩ. Whole-cell currents were digitized at 10 kHz and filtered at 2 kHz

Cytosol volume measurement

Volume increase was measured with a Calcein-AM-based fluorescence imaging (Voss FK, et al. 2014; Capo-Aponte et al., 2005; Hamann et al., 2002). Cells were seeded onto 96-well plates (30,000 cells/well), and incubated with 10 μM Calcein-AM (Thermo Fisher Scientific) in IMDM for 2 h. After replacing the medium with 100 μL of isotonic solution (in mM: 145 NaCl, 5 KCl, 1 $MgCl_2$, 2 $CaCl_2$, 10 glucose, and 10 HEPES; pH 7.40 and 320 mOsm), the fluorescence intensity (at $\lambda_{excitation}$ = 485 nm, $\lambda_{emission}$= 535 nm) was collected for 10 min by a TECAN infinite F200 PRO plate reader. Upon baseline stabilization, the solution was replaced with 100 μL of hypotonic solution (in mM: 41.43 NaCl, 1.43 KCl, 0.29 $MgCl_2$, 0.58 $CaCl_2$, 2.86 glucose, 2.86 HEPES, pH 7.40, and 110 mOsm), and fluorescence intensity was monitored for ≥ 90min. The Calcein-AM fluorescence was normalized to the original fluorescence under isotonic solution (Capo-Aponte et al., 2005).

Lysosomal water flux assay

Lucifer yellow dextran (25 μM) and Rhodamine dextran (25 μM) were loaded in Cos1 cells for 24 h, and the cells were then washed for 18 h in medium without dextrans (Chaurra et al., 2011). Prior to the start of imaging, cells were treated with 170 mOsm HypoTBS saline for 30 min. The isotonic and hypotonic solutions were Iso-TBS and Hypo-TBS. For the 170 mOsm (D_2O) solution, H_2O was completely replaced with D_2O (Cambridge Isotope Laboratories, Inc., cat. DLM-7005). 450 mOsm (H_2O) solution was composed of an isotonic solution supplemented with 150mM sucrose.

LDH cell membrane integrity measurement assay

Cell membrane integrity was measured with extracellular lactate dehydrogenase activity that released from the broken Hap1 and HeLa cells. Cells were cultured in 96-well plates with/out hypotonicity. Afterwards, the culture medium was collected and centrifuged at 600 ×g. The cleared medium was then transferred into optically clear 96-well plates. The LDH reaction mix was added into each well. After 30 min reaction at room temperature, the absorbance at 450 nm was measured using a TECAN infinite M200 PRO plate reader. The LDH activity was normalized to the activity with total cell lysis produced by the lysis solution provided in the LDH cytotoxicity kits (Abcam, cat. ab 65393).

Molecular biology and Biochemistry

Site directed mutants were generated with a QuickChange Lightning site-directed mutagenesis kit (Agilent) and confirmed by DNA sequencing. Standard procedures were used for western blot analyses with lysis buffer containing 1% NP-40, 0.1% SDS, 0.5% Na-deoxycholate,

20mM NaF, 1mM Na_3VO_4, 2mM EGTA, 150mM NaCl and 50mM Tris-HCl (pH 7.4) supplemented with Phosphatase inhibitor cocktail I (Sigma, cat. P0044) and Protease inhibitor cocktail (Sigma, cat. P8340).

Lysosome isolation by subcellular fractionation

Iodixanol gradient ultracentrifugation was performed to separate lysosomes from other organelles as described previously (Wang X, et al., 2012). Briefly, cells were harvested in a HM buffer (0.25M sucrose, 1mM EDTA, and 10mM HEPES, pH7.0) and then processed with a Dounce homogenizer. Cell lysates were centrifuged at 1,000 ×g at 4°C for 10min to remove nuclei and intact cells. Supernatants were collected, separated through a Percoll density gradient, and centrifuged at 100,000 ×g at 4°C for 1 h in a Thermo Sorvall WX 80 centrifuge and a Fiberlite F65L-6×13.5 rotor. Post-nuclear supernatants were added to Percoll density gradients [(bottom to top) 0.5mL of 2.5M sucrose and 6mL of 18% Percoll solution (1.8mL Percoll, 0.2mL 2.5M sucrose, and 8.0mL HM buffer)]. The heavy lysosome-containing membrane fractions of the Percoll density gradient were collected with care and further separated through a discontinuous iodixanol gradient at 200,000 ×g for 2.5h at 4°C. The iodixanol gradient was prepared with 0.5mL of 2.5M sucrose and 6mL of HM buffer-diluted iodixanol solutions with discontinuous concentrations of 27%, 22.5%, 19%, 16%, 12% and 8%, together with 1mL of the heavy membrane fractions from bottom to top. The final iodixanol gradient was divided carefully into several 0.5-mL fractions. The fractions containing purified lysosomes were determined by western blotting and used for subsequent analyses. Antibodies against the follow targets were used: LAMP1 (DSHB, cat. H4A3), EEA1 (Abcam, cat. ab2900), Cathepsin D (Abcam, cat. ab72915), Complex II (Thermo Fisher

Scientific, cat. 459200), GM130 (Abcam, ab52649), GFP (Thermo Fisher Scientific, cat. A6455 and LRRC8A (custom generated by R.S. (Kang et al., 2018).

Lysosomal immuno-isolation and immunoprecipitation

HEK293T cells were rinsed, collected, spun down, and re-suspended in 1 mL of K-PBS buffer (136mM KCl and 10mM KH_2PO_4, pH adjusted to 7.25 with KOH) in the presence of protease inhibitors. Cells were processed with a Dounce homogenizer and then spun down at 1,000 ×g at 4°C for 10min to generate post-nuclear supernatants. Supernatants, which contained lysosomes and other organelles, were incubated with anti-LAMP1 (Abcam, cat. 24170; cytosolic epitope) and 50 μL protein-G Surebeads™ (Bio-rad, 1614821) overnight at 4°C. Bound fractions were eluted by K-PBS buffer for 3 times and total lysosomal proteins were extracted by appropriate amount of lysis buffer plus 1/4 volumes of LDS buffer (Thermo Fisher Scientific, NP0008, supplemented with 2-mercaptoethanol) under 75°C for 10min for denaturation. Samples were then subjected to western blotting analysis with anti-Cathepsin D (Abcam, cat. ab72915), anti-Complex II (Thermo Fisher Scientific, cat. 459200), and anti-GFP (Thermo Fisher Scientific, cat. A6455) antibodies

Statistical analysis

Statistical comparisons were performed with one-way analyses of variance (ANOVAs) with Bonferroni's *post hoc* analysis or with paired and unpaired Student's t-tests where appropriate. Average data are presented as means ± standard errors of the mean (SEMs), with the sample size (N) and the statistical test used indicated in the accompanying text or figure legend. Significance is indicated as N.S (not significant) or *P < .05, **P < .01, ***P < .001.

II-6 Figures

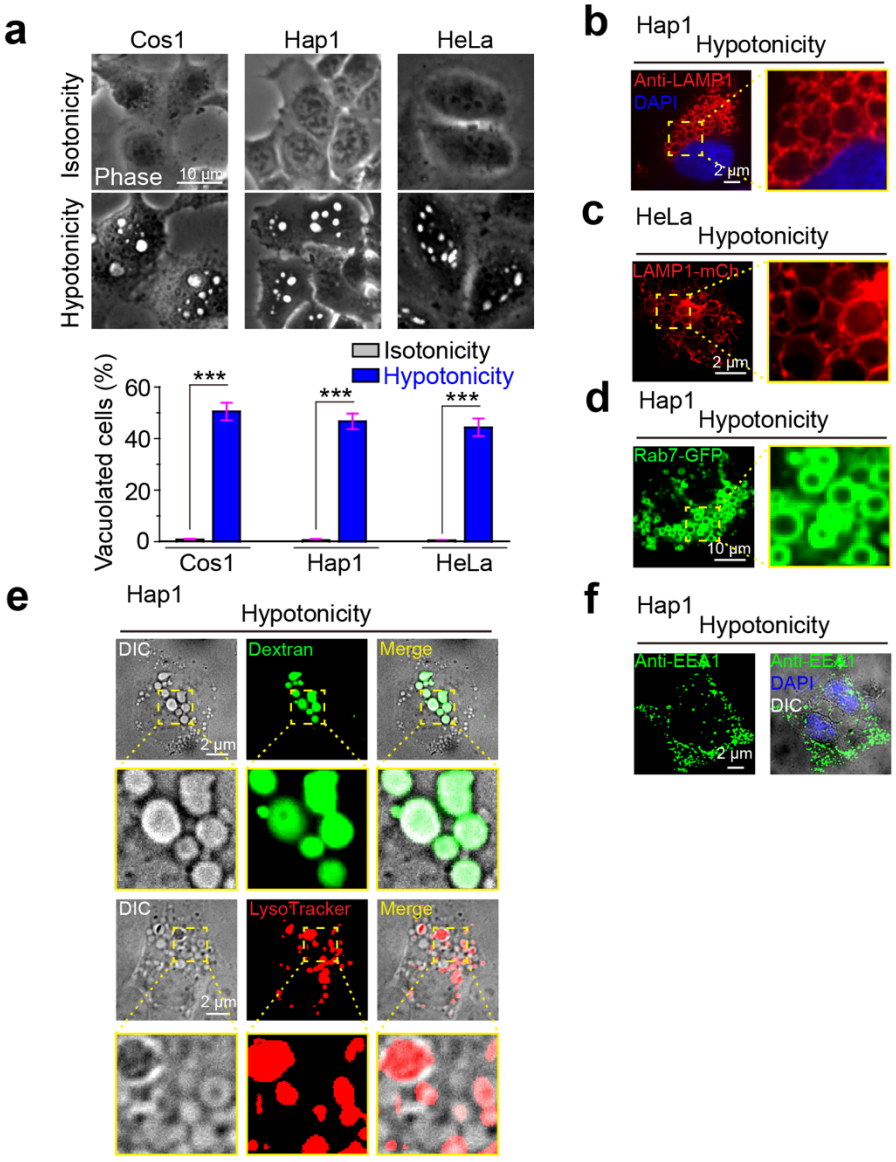


Figure 2.1 Vacuoles are derived from late endosomes and lysosomes under hypotonicity.

(a) Responses of Cos1, Hap1 and HeLa cells to a hypotonic challenge. 30 minutes prior to data collection, the complete medium was replaced with fresh complete medium (Isotonicity-300 mOsm) or the test medium (Hypotonicity-170 mOsm). The photomicrographs show phase contrast images with examples of the vacuoles (bright white spots) commonly observed in cells exposed to hypotonic solutions. *** is $p < 0.001$. **(b-d)** Representative images of vacuolated Hap1 cells after 0.5 h of 170 mOsm treatment. Cells were stained with LAMP1 antibody (b), or transfected prior to hypotonic

treatment with either LAMP1-mCherry (c) or Rab7-GFP (d). In the left panel, the nucleus was counterstained with DAPI (blue). Zoomed-in images of the boxed regions are shown to the right of each image. **(e)** Oregon Green^{TM}488-dextran (upper panels) and LysoTracker^{TM} (lower panels) staining of vacuolated Hap1 cells after 0.5 h of 170 mOsm treatment. Zoomed-in images of the boxed regions are shown below each low power image. **(f)** EEA1 staining (green) of Hap1 cells after 0.5 h of 170 mOsm treatment. Nuclei were counterstained with DAPI (blue).

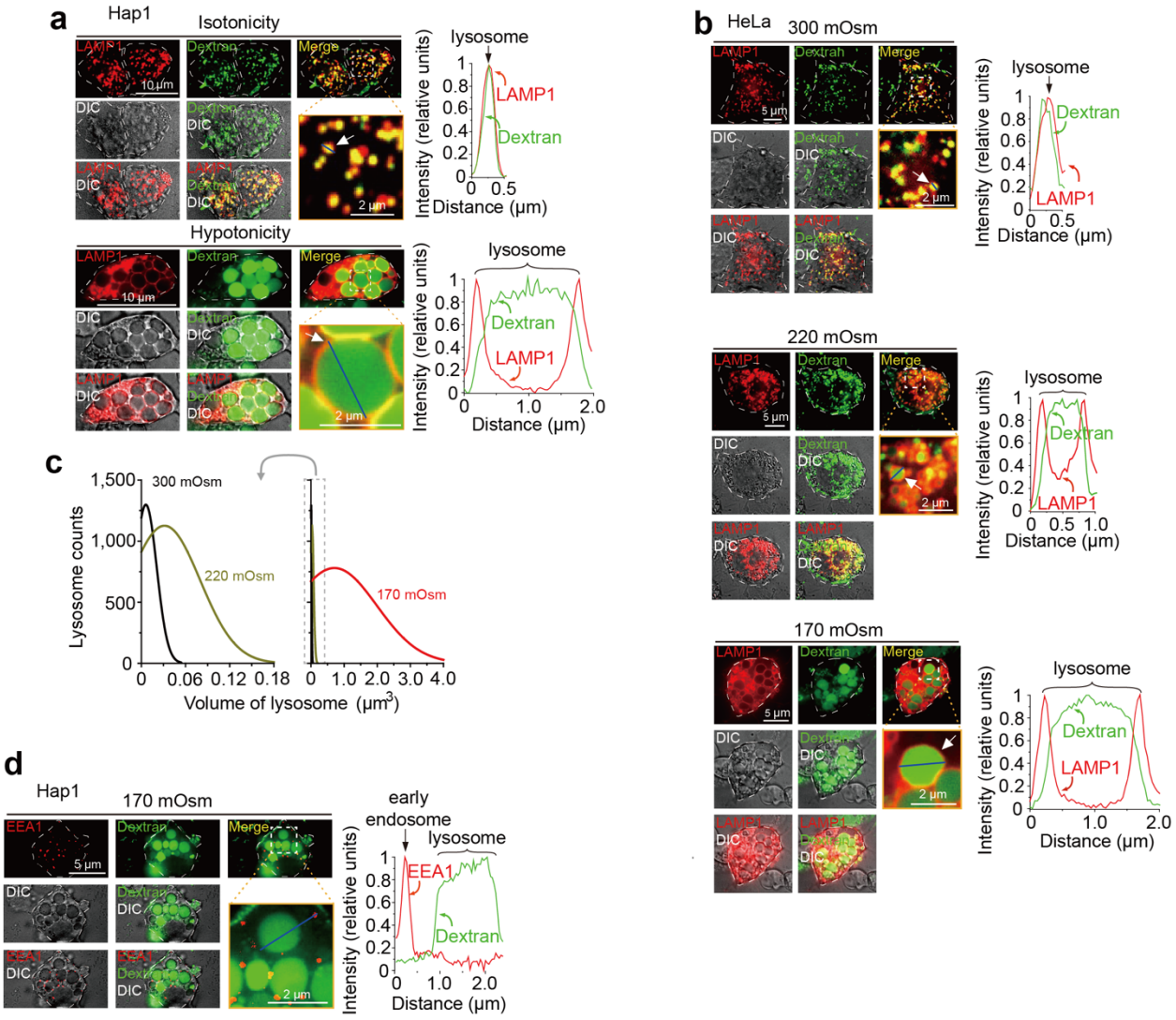


Figure 2.2 Lysosomes are highly osmosensitive organelles.

(**a**) Each group of images shows cells studied after 0.5 h in either 300mOsm (upper panels) or 170mOsm (lower panels) medium. The red signal is LAMP1-mCherry driven by transient transfection, and the green signal is Oregon Green^{TM}488-dextran loaded into the cell by endocytosis. The graph to the right of each panel shows the fluorescence intensity of a line scan (blue line on the blown up image) through the double labelled object indicated by the white arrow. (**b**) Data similar to those shown in (a), but for HeLa cells rather than Hap1 cells. (**c**) The distribution of lysosome volume as described in Results from line scan data like those shown in (b). The data collected at 300mOsm and 220mOsm are presented in both panels to emphasize the change in the x axis scale

for the data collected at 170 mOsm. Mean values for each condition are given in Results. Data were collected from 6 independent experiments. (**d**) Data similar to those shown in (a), but for cells transfected with EEA1-mCherry rather than LAMP1-mCherry.

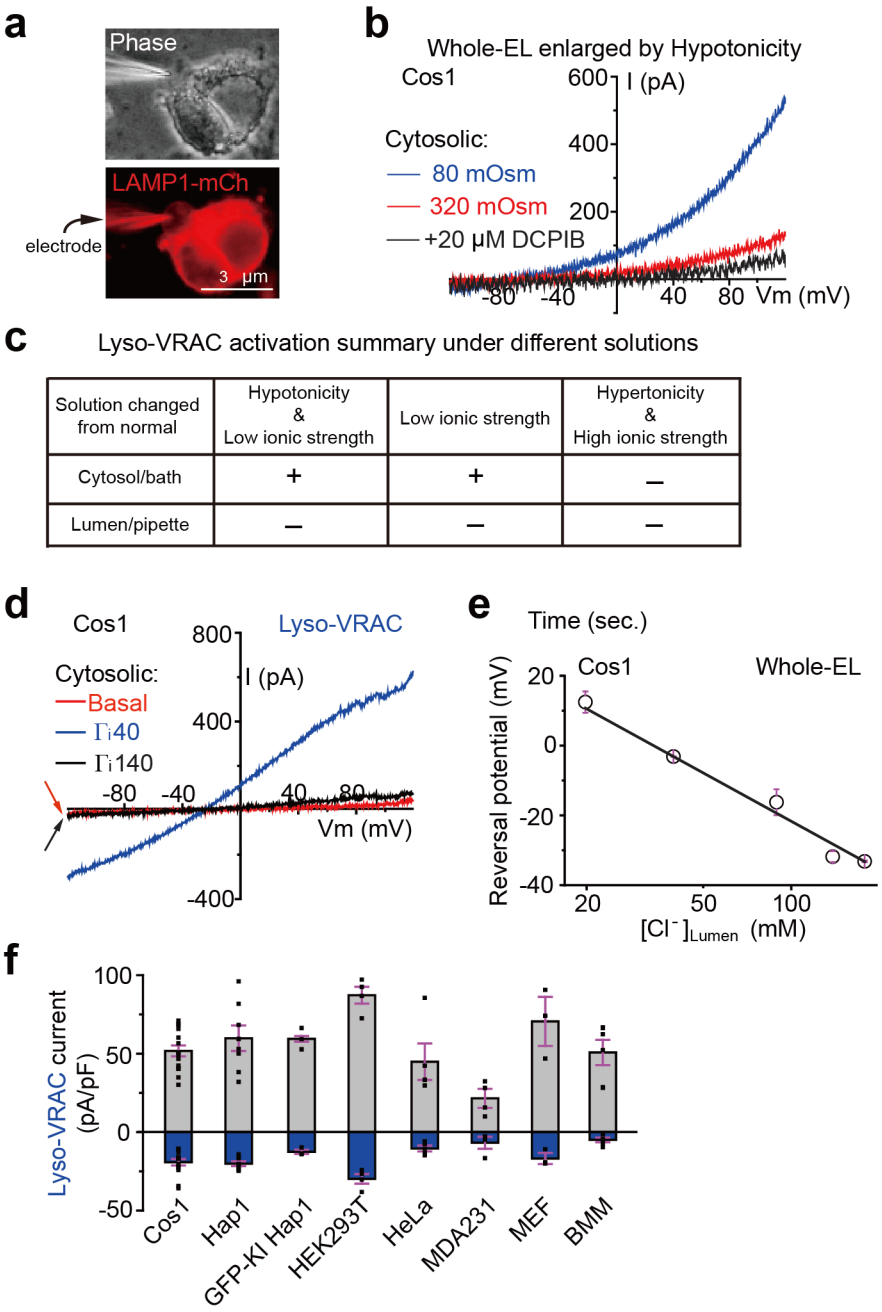


Figure 2.3 Lysosome-derived vacuoles express chloride channels gated by low ionic strength

(**a**) Images demonstrating the whole-endolysosome (whole-EL) patch-clamp configuration being achieved on a vacuolated lysosome that had been induced by hypotonic (80 mOsm) challenge. Note that approximately half the cell had been torn away to make the vacuole accessible for recording. (**b**) Representative currents on a vacuole of a Cos1 cell induced by exposure to 80 mOsm solution. The

difference between the currents in 320 mOsm cytosolic solution and 80 mOsm cytosolic solution is defined as Lyso-VRAC. The currents were elicited by 200-ms ramps from −120 mV to +120 mV. Vm represents membrane potential. (**c**) Summary of the changes in osmolarity and ionic strength conditions that were tested for their ability to activate Lyso-VRAC. A plus sign indicates that a solution that changed these properties induced a Lyso-VRAC of at least 100 pA at +120 mV. (**d**) Representative I-V traces from vacuoles of Cos1 cells treated with vacuolin in response to various cytosol-side solutions (Basal, 140 mM K-Gluconate, 290 mOsm; Γi 40, 40 mM CsCl, 290 mOsm; Γi 140, 140 mM CsCl, 290 mOsm). (**e**) Reversal potential of the Lyso-VRAC current was dependent on $[Cl^-]_{Lumen}$. The slope of the line fit to the data was −46.1 ± 0.5 mV per 10-fold concentration change. (**f**) Lyso-VRAC induced by Γi 40 in additional cell types. In addition to Cos1, HeLa, and Hap1 cells, the cell types shown are Hap1 cells in which the endogenous LRRC8A gene was replaced with a sequence encoding an LRRC8A-GFP fusion protein (GFP-KI Hap1), HEK293T, human breast cancer cells (MDA231), mouse embryonic fibroblasts (MEF), and WT mouse bone marrow macrophages (BMM). For all panels showing averaged data, n>6 and Student's *t* tests were used to determine statistical significance.

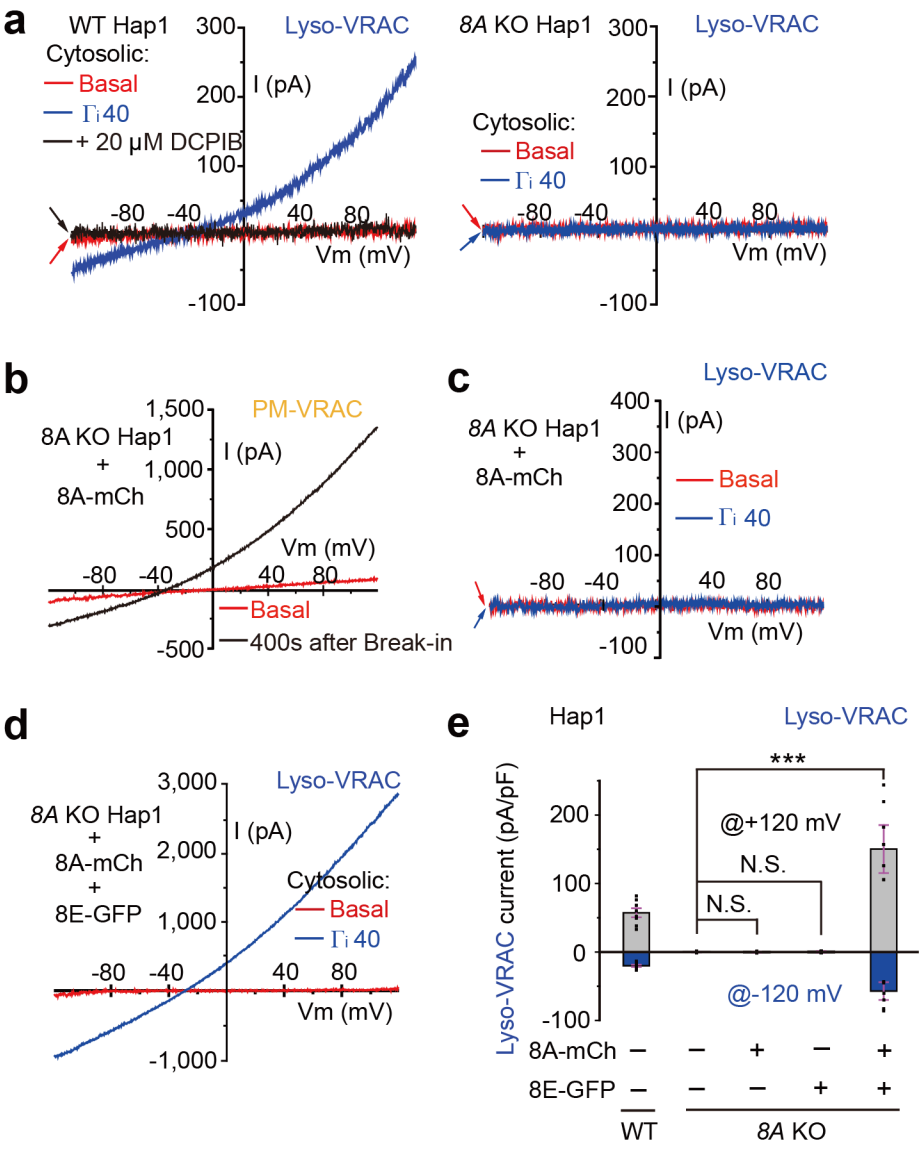


Figure 2.4 LRRC8A is required for Lyso-VRAC currents.

(**a**) $I_{Lyso\text{-}VRAC}$ from endolysosomes enlarged with vacuolin-1 in WT and 8A KO Hap1 cells with basal and low ionic strength bath solutions. $[Cl^-]_{Pipette/Lumen}$ = 140mM, and $[Cl^-]$ = 40mM for Γi 40. DCPIB was applied in the Γi 40 solution. (**b**) Representative traces of $I_{PM\text{-}VRAC}$ in WT and 8A KO Hap1 cells. (**c**) Representative trace of $I_{Lyso\text{-}VRAC}$ in 8A KO Hap1 cells overexpressing 8A-mCherry. (**d**) $I_{Lyso\text{-}VRAC}$ in 8A KO Hap1 cells dually transfected with LRRC8A-mCherry and LRRC8E-GFP. (**e**) Current density of $I_{Lyso\text{-}VRAC}$ in WT and in 8A KO Hap1 with or without

overexpressed LRRC8 proteins. Current densities at ±120 mV are shown. Data for each condition were assessed for significance using Student's *t* test and were collected from six or more independent experiments. *** is $p < 0.001$, N.S. is > 0.05.

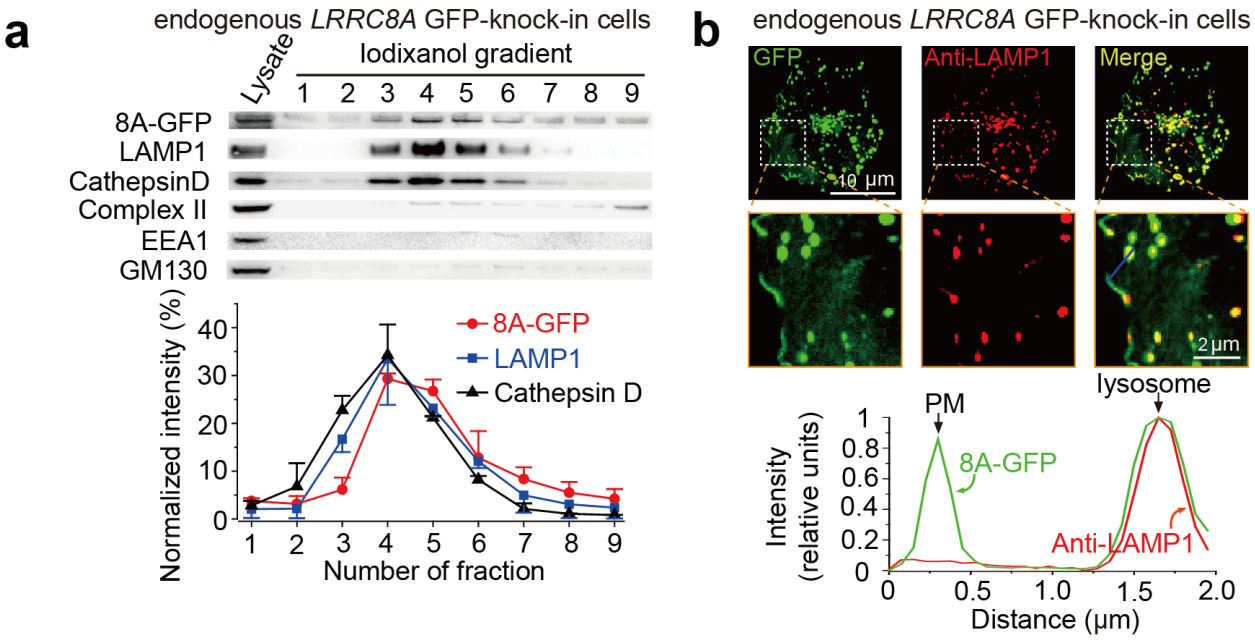


Figure 2.5 LRRC8A is localized on lysosomes.

(**a**) Subcellular fractionation analysis of LRRC8A-GFP expression in various organelle fractions of LRRC8A-GFP–knock-in Hap1 cells. The organelle-specific markers identified in these Western blots were as follows: Lysosomes, LAMP1 and Cathepsin D; Mitochondria, Complex II; Early Endosomes, EEA1; and the Golgi apparatus, GM130. Similar data were collected from three independent experiments, and the graph shows the means ± SEMs. (**b**) The expression pattern of LRRC8A-GFP when this coding sequence was knocked into the endogenous location of LRRC8A in Hap1 cells. Lysosomes were labeled by immunostaining for LAMP1 (red). The boxed regions in the Upper images are shown at higher magnification in the Lower images. The graph below each group of images is a line scan through the plasma membrane and lysosome shown in the boxed region indicating the intensity of 8A-GFP (green lines) and Anti-LAMP1 (red lines) along the blue line.

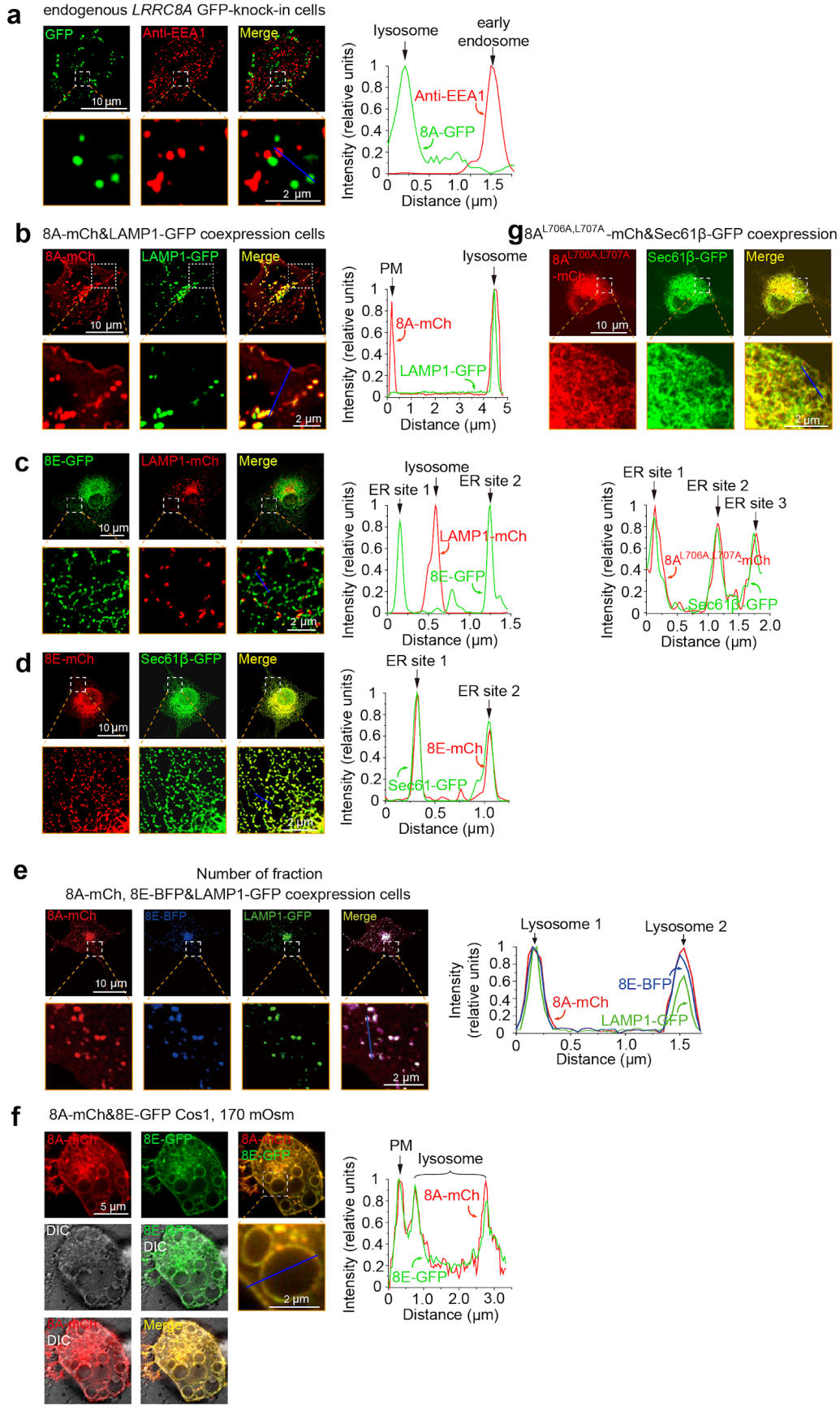

a
endogenous LRRC8A GFP-knock-in cells
GFP
Anti-EEA1
Merge
10 μm
2 μm
lysosome
early endosome
Anti-EEA1
8A-GFP
Intensity (relative units)
Distance (μm)
b
8A-mCh&LAMP1-GFP coexpression cells
8A-mCh
LAMP1-GFP
Merge
PM
lysosome
g
8A L706A,L707A -mCh&Sec61β-GFP coexpression
Sec61β-GFP
c
8E-GFP
LAMP1-mCh
ER site 1
ER site 2
ER site 3
d
8E-mCh
Sec61β-GFP
Sec61-GFP
e
Number of fraction
8A-mCh, 8E-BFP&LAMP1-GFP coexpression cells
8E-BFP
Lysosome 1
Lysosome 2
f
8A-mCh&8E-GFP Cos1, 170 mOsm
DIC
5 μm

Figure 2.6 Intracellular LRRC8 proteins are localized on the perimeter membrane of lysosomes.

(**a**) Analysis of the lack of co-localization between the early endosome marker EEA1 (red, detected by immunostaining) and LRRC8A-GFP (green) driven by knocking GFP into the endogenous LRRC8A gene of Hap1 cells. The lower panel shows the boxed regions at higher power. The graph to the right shows the intensity of fluorescence along the blue line shown in the high magnification merged image. (**b**) Analysis of the extent of the co-localization of 8A-mCherry (red) and LAMP1-GFP (green) in transfected Cos1 cells. (**c**) Analysis of the lack of co-localization between the 8E-GFP (green) and LAMP1-mCherry (red) both transfected into Cos1 cells. (**d**) Analysis of the extent of co-localization between the ER marker Sec61β-GFP (green) and 8E-mCherry (red) both transfected into Cos1 cells. (**e**) Images and line scan analysis showing the co-localization of 8A-mCherry (red), 8E-BFP (blue), and LAMP1-GFP (green) in transfected Cos1 cells. (**f**) The expression pattern of 8A-mCherry (red) and 8E-GFP (green) on both the plasma membrane and the vacuolated lysosome membranes in Cos1 cells after a hypotonic challenge (170mOsm for 0.5 h). (**g**) Analysis of the extent of co-localization between the ER marker Sec61β-GFP (green) and $8A^{L706A,\ L707A}$-mCherry (red) both transfected into Cos1 cells.

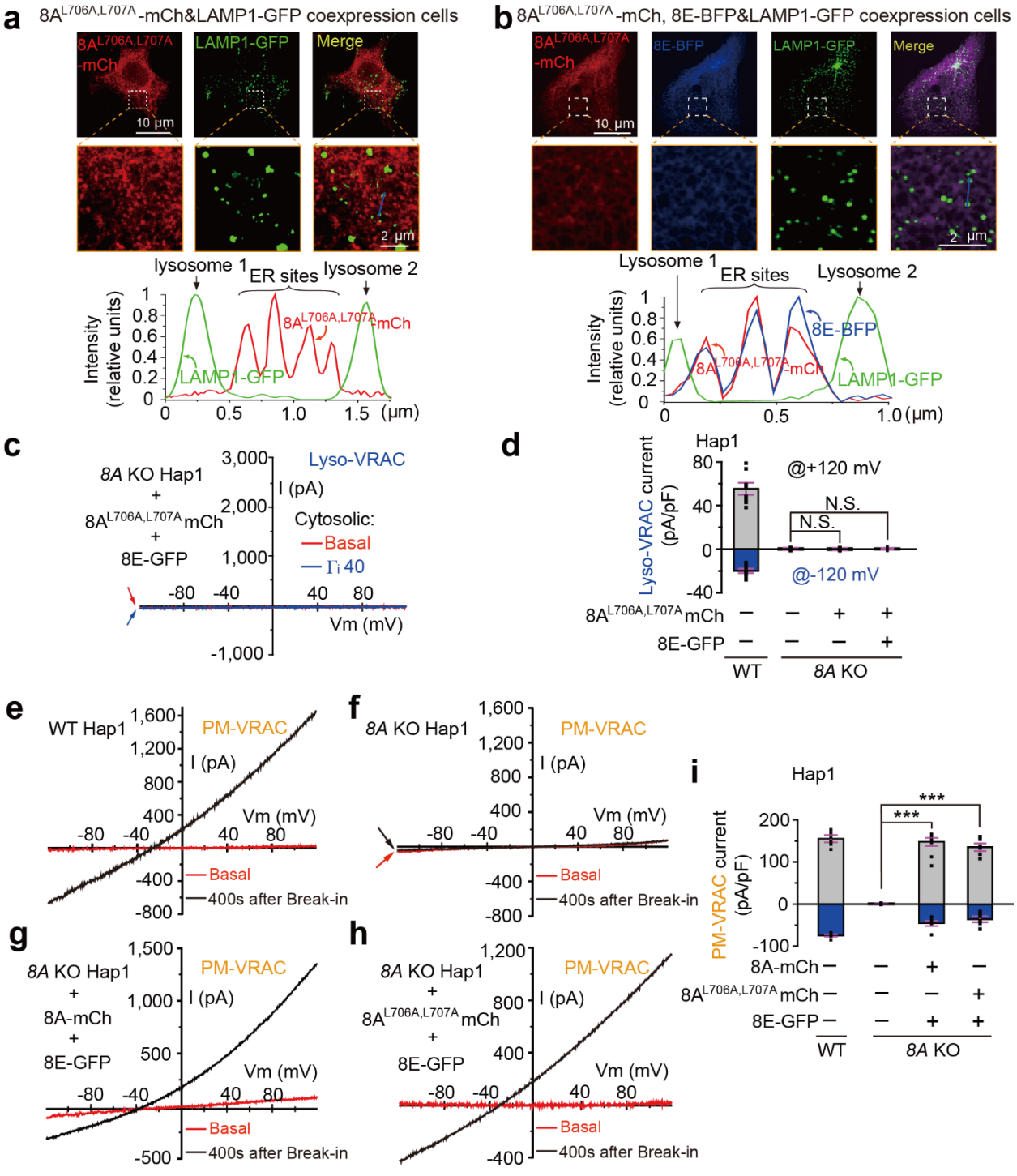


Figure 2.7 A double-leucine motif is required for lysosomal localization of LRRC8A to mediate Lyso-VRAC.

(**a**) Images and line scan analysis showing the lack of colocalization of $8A^{L706A, L707A}$-mCherry (red) and LAMP1-GFP (green) in transfected Cos1 cells. See Figure 2.6 f for evidence that the $8A^{L706A, L707A}$-mCherry staining is in the ER. (**b**) Images and line scan analysis showing that $8A^{L706A, L707A}$-mCherry (red) and 8E-BFP (blue) localized to a different organelle than LAMP1-GFP (green) in transfected Cos1 cells. (**c**) Representative traces of $I_{Lyso\text{-}VRA}$C in 8A KO Hap1 cells dually transfected with $8A^{L706A, L707A}$-mCherry and 8E-GFP. (**d**) Current density of $I_{Lyso\text{-}VRAC}$ in WT and in 8A KO Hap1 with or without overexpressed $8A^{L706A, L707A}$-mCherry and 8E-GFP. Data for each condition in this panel and in I were assessed for significance using Student's *t* test and were collected from six or more independent experiments. (**e and f**) Whole cell recordings to test for plasma membrane VRAC (PM-VRAC) currents in WT and 8A KO Hap1 cells. These experiments used Γi 40 ($[Cl^-]$ = 40 mM) as the cytosolic/pipette solution and Γi 140 ($[Cl^-]$ = 140 mM) as the extracellular/bath solution. The responses are shown at 0 (red) and 400 s (black) after break-in. (**g**) Experiment similar to E except that the 8A KO Hap1 cells were cotransfected with 8A-mCherry and 8E-GFP. (**h**) Experiment similar to E except that the 8A KO Hap1 cells were transfected with $8A^{L706A, L707A}$-mCherry and 8E-GFP. (**i**) Current density of $I_{PM\text{-}VRAC}$ in WT and 8A KO Hap1 cells with or without LRRC8 proteins overexpressed. **** is $p < 0.001$, N.S. is > 0.05.

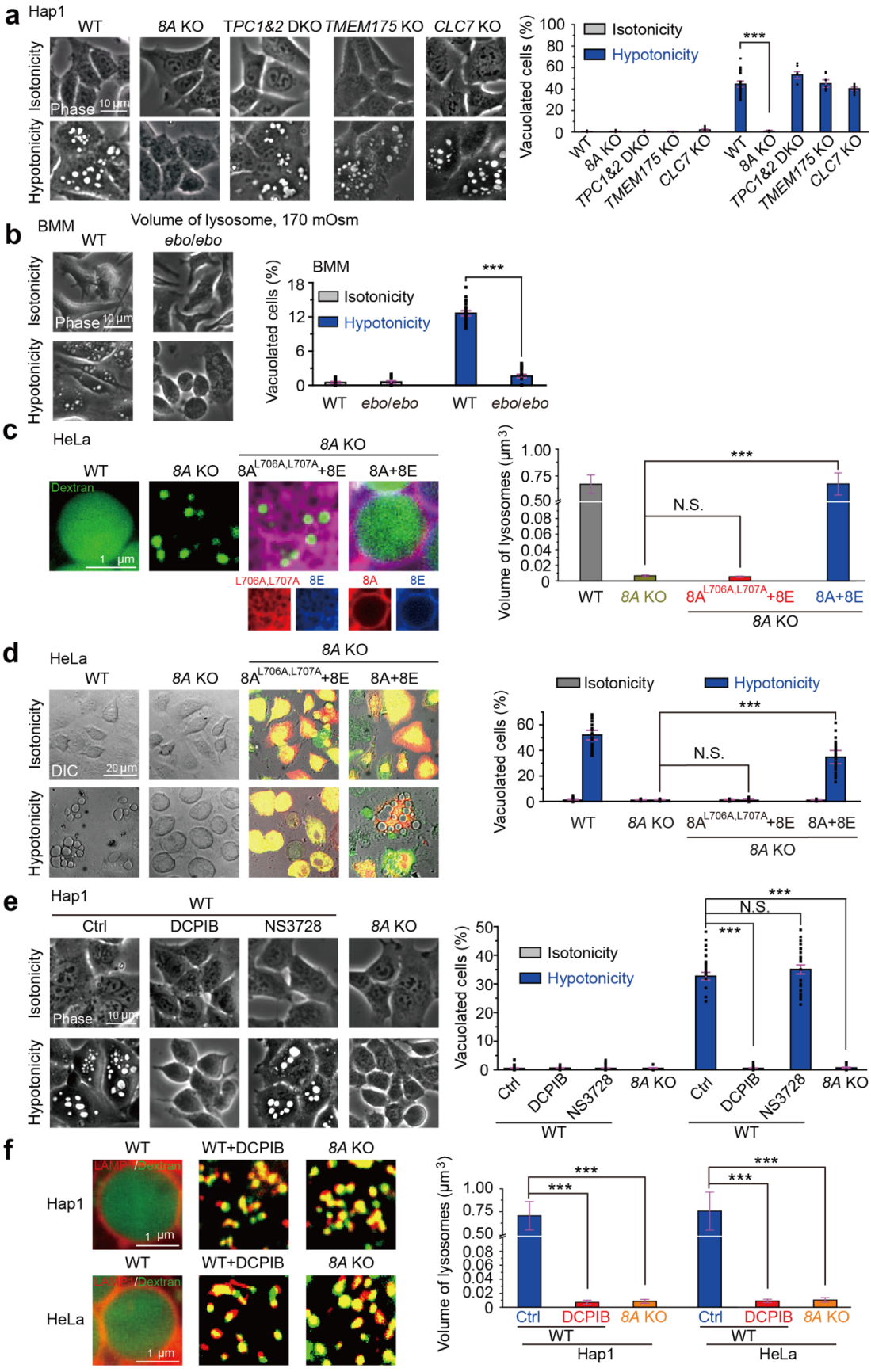

a
Hap1
WT
8A KO
TPC1&2 DKO
TMEM175 KO
CLC7 KO
Isotonicity
Hypotonicity
Phase
10 μm
Vacuolated cells (%)
Isotonicity
Hypotonicity
***
b
BMM
Volume of lysosome, 170 mOsm
ebo/ebo
c
HeLa
8A KO
8A^L706A,L707A+8E
8A+8E
Dextran
1 μm
L706A,L707A
8E
8A
Volume of lysosomes (μm3)
N.S.
d
DIC
20 μm
e
Hap1
Ctrl
DCPIB
NS3728
f
LAMP1/Dextran

Figure 2.8 Lyso-VRAC is required for hypotonicity-induced lysosomal vacuolation.

(**a**) Hypotonicity-induced cytoplasmic vacuolation in WT, 8A KO, TPC1&2 double KO (DKO), TMEM175 KO, and CLC7 KO Hap1 cells. Quantitative analysis is to the Right. (**b**) Representative images (left panel) and quantitative analysis (right panel) of lysosome vacuolation under hypotonic treatment (1h in 170mOsm) in WT and *ebo/ebo* BMMs. (**c and d**) Sample images (Left) and quantitative analysis (Right) of lysosomal volume expansion (**c**) and lysosome vacuolation (**d**) under hypotonic stress in 8A KO HeLa cells that were dually transfected with 8E-BFP + 8A-mCherry or $8A^{L706A,\ L707A}$-mCherry. (**e**) Differential effects of NS3728 (30 μM; membrane-impermeable) and DCPIB (100 μM, membrane-permeable) VRAC inhibitors on hypotonicity-induced vacuolation in WT and 8A KO Hap1 cells. (**f**) Effect of 100 μM DCPIB and LRRC8A knock out on lysosomal volume. In all bar graphs, data points were collected from more than six independent experiments, and Student's *t* test was used to determine significance. *** is $p < 0.001$, N.S. is > 0.05.

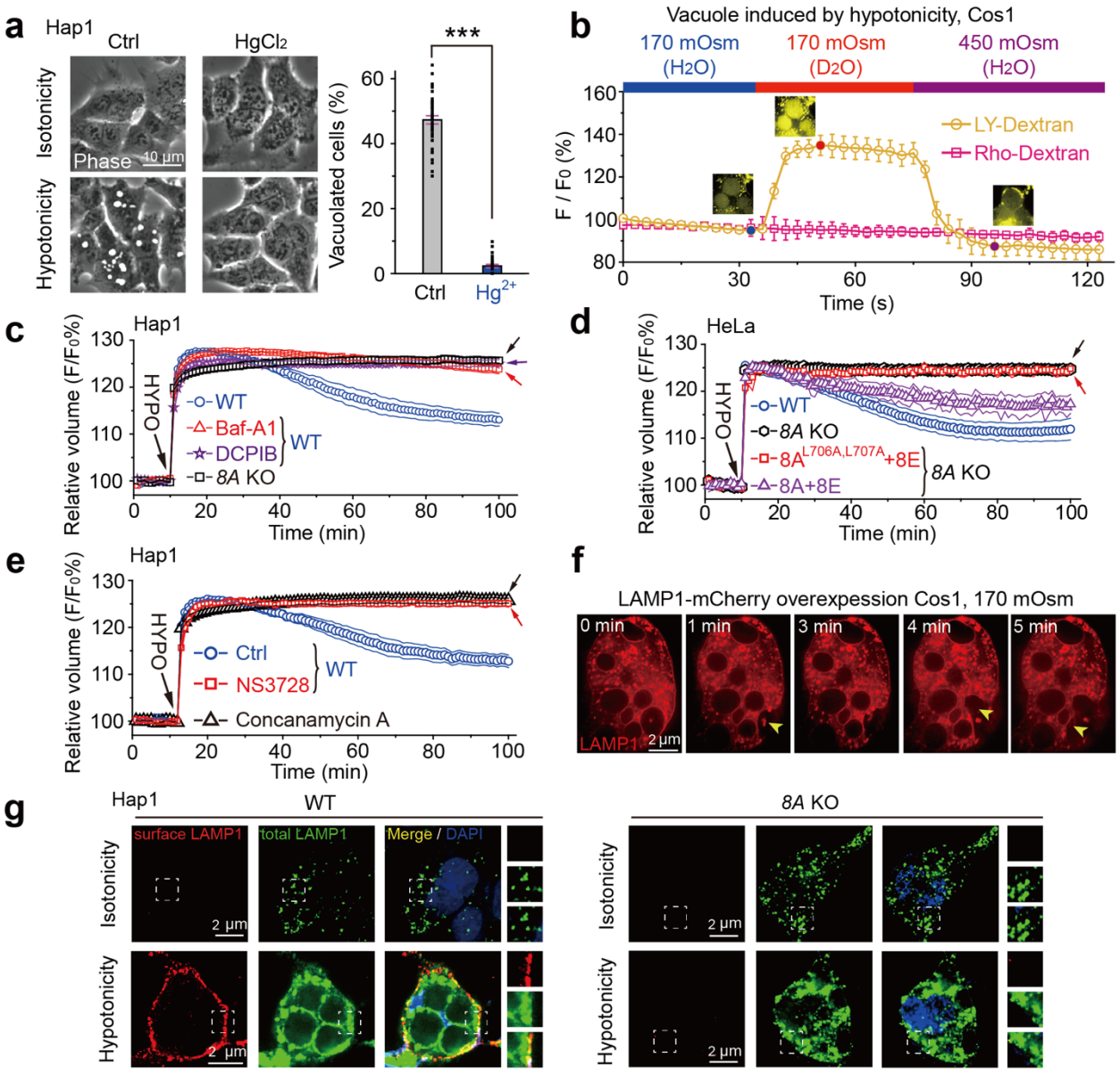


Figure 2.9 Lysosomes store and expel intracellular water to regulate cytosolic RVD.

(**a**) Representative images (Left) and quantitation (Right) of effects of 50 μM $HgCl_2$ (an aquaporin inhibitor) on lysosome vacuolation induced by hypotonicity. *** is $p < 0.001$. (**b**) Fluorescence of Lucifer yellow dextran (LY-Dx, yellow) and Rhodamine dextran (Rho-Dx, red) in response to D_2O- or H_2O-containing hypotonic (170 mOsm) solutions in Cos1 cells. LY-Dextran and Rho-Dextran were preloaded into lysosomes of Cos1 cells by endocytosis. (**c–e**) Time course of

regulatory cytosol volume decrease (RVD) in response to 110-mOsm solutions estimated by measuring the fluorescence intensity of Calcein-AM (Hamann et al., 2002). The concentrations of drugs used were 5 μM Baf-A1, 100 μM DCPIB, 30 μM NS3728, and 20 μM Concanamycin A. (**f**) Snapshots of a Cos1 cell transfected with LAMP1-mCherry from a time-lapse series. Time 0 is defined as 78 min after the onset of the cell being placed in 170 mOsm medium to induce production of large vacuoles. Exocytosis events are indicated with yellow arrowheads at 1, 4, and 5 min. (**g**) Effects of hypotonic treatment (0.5 h) on LAMP1 surface staining in WT (Left) and 8A KO (Right) Hap1 cells. Cells were immunostained using an anti-LAMP1 antibody that recognized an extracellular/luminal epitope under conditions that first stained only plasma membrane LAMP1 (non-permeabilized cells, red) and then total LAMP1 (permeabilized cells, green). Nuclei were counterstained with DAPI (blue). Zoomed-in images of the boxed regions are shown in Right. In **b**–**e**, data points were collected from six independent experiments.

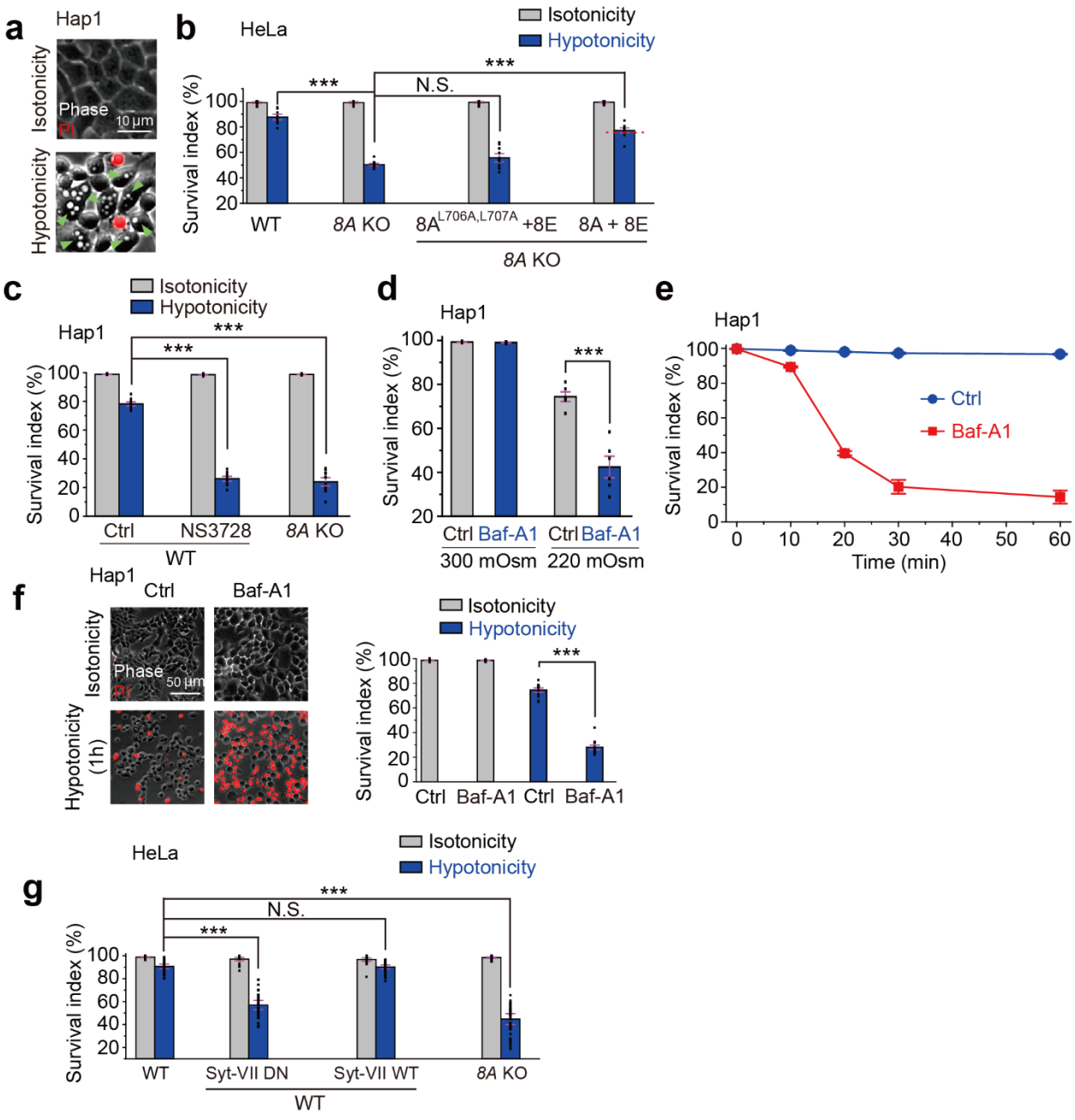


Figure 2.10 Lyso-VRACs protect cells from necrotic cell death in response to hypo-osmotic stress.

(**a**) Effects of 1 h hour of treatment with hypotonicity (80 mOsm B), on cell survival of Hap1 or HeLa cells. Representative images of cells stained with propidium iodide (red) to identify necrotic cells, viewed with phase contest microscopy. Cells with vacuoles are indicated with green

arrowheads. (**b**) Cell survival assayed by measuring extracellular LDH activity for samples from the indicated cell type. LDH activity for each group of cells was normalized as the percentage of the LDH activity released from the same number of cells by treatment with distilled water (which caused all cells to die). The survival index was then calculated as 100%-relative LDH activity. (**c**) Effect of 30 μM NS3728 on hypotonicity induced necrotic cell death. LDH activity was collected from the indicated cell type after exposure to 80 mOsm medium or control medium (300 mOsm) for 2 h. (**d, e**) Effect of 5μM Baf-A1 on survival from hypotonic stress assessed using the LDH release assay. In panel d, the medium from the cells shown in was collected after 1h in the indicated osmotic strength solution. In panel e, the cells were subjected to a stronger stress (80 mOsm) and data were collected at the indicated time points. (**f**) Effect of Baf-A1 on necrotic cell death under three different types of stress measured with two different assays. (**g**) Survival of the indicated cell types was assessed with the LDH activity assay. Some of the wild type cells were transfected with a plasmid driving expression of wild type Synaptotagmin VII or with a plasmid driving expression of mutant Synaptotagmin VII that is known to act as a dominant negative (Syt-VII-DN). *** is $p < 0.001$, N.S. is > 0.05.

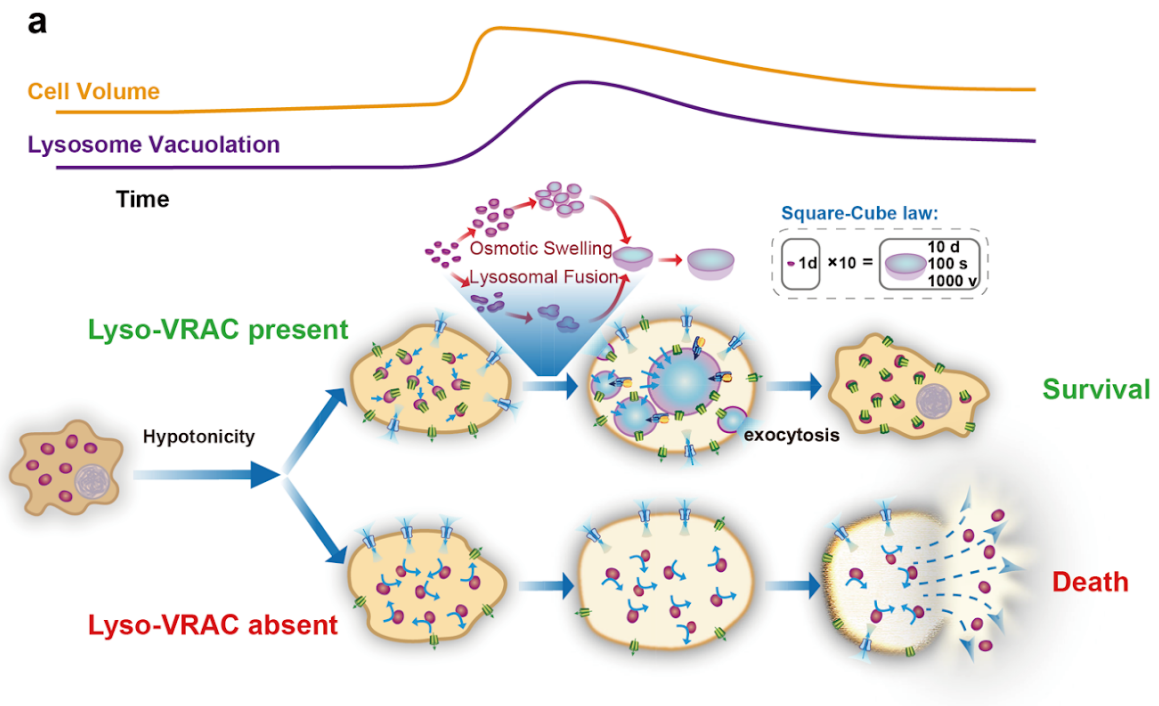


Figure 2.11. Working model for how Lyso-VRAC-mediated lysosome osmoregulation behavior is protective for cell survival.

Hypotonicity results in water influx through aquaporin channels on the plasma membrane (cyan), and the cell volume increases almost instantly (the yellow curve on the top). This decreases cytosolic ionic strength, normally activating VRAC channels (green) formed from LRRC8 proteins on both the plasma membrane (PM-VRAC) and in lysosomes (Lyso-VRAC). The activation of Lyso-VRAC (but not PM-VRAC) triggers lysosomal vacuolation (the purple curve on the top) through lysosomal osmotic swelling and/or homotypic fusion, creating large-volume compartments for intracellular water storage. Lysosome vacuolation decreases the cytosol volume of cells, helping to maintain the physiological concentrations of proteins and metabolites. Exocytosis of water-filled vacuoles substantially reduces the cell volume by dumping excess water into the extracellular environment, and reduces plasma membrane tension stress by delivering more intracellular lipids to the cell surface (Survival, upper scenario). When Lyso-VRAC is absent,

giant vacuoles do not form, the plasma membrane breaks and cells die, even if PM-VRAC currents are normal (Death, lower scenario).

CHAPTER III[2]

TMEM175 Encodes a Proton-Activated, Proton Channel of Lysosomes

III-1 Abstract

The acidic environment within lysosomes is maintained within a narrow pH range optimal for digesting macromolecules so that critical metabolic building blocks can be reused. This pH homeostasis is a consequence of proton influx produced by a V-type H^+ ATPase and rapid proton efflux through unidentified "leak" pathways (Casey et al., 2010; Mindell, 2012; Xu and Ren, 2015). By performing a candidate expression screen, we discovered that the TMEM175 gene encodes a proton-activated, proton-selective channel that is required for lysosomal H^+ "leak" currents. A potent agonist was identified that activates TMEM175 and triggers lysosomal proton release. Cells lacking TMEM175 exhibit lysosomal hyper-acidification and impaired proteolytic degradation, both of which can be restored by lysosomal pH optimization. Variants of TMEM175 are associated with susceptibility to Parkinson's disease (PD), so our studies not only reveal an essential H^+ dissipating pathway of lysosomes but also provide a new conceptual framework for mechanistically understanding the disease association.

[2]Materials presented in this chapter are adapted from a manuscript in preparation entitled "TMEM175 encodes a proton-activated, proton channel of lysosomes". Meiqin Hu is the first listed author but Ping Li and I are indicated as equal co-first authors with him. A list of all the authors whose names will be on this paper, and a detailed explanation of my contributions to the work in this chapter are in the Preface of this thesis (Pages v-vi).

III-2 Introduction

Endosomes and lysosomes require a V-type H^+ ATPase (V-ATPase) to establish and maintain 50-fold to 5,000-fold proton concentration gradients across their membranes. This gradient is then used to drive the active transport of metabolites, transmitters, and ions between the vesicular lumen and the cytoplasm (Mindell, 2012; Xu and Ren, 2015; Xiong and Zhu, 2016). Moreover, crucial cellular processes depend on the acidic luminal pH inside lysosomes. For example, substrate degradation in the lysosome and transport of digested materials requires an optimal luminal pH. Abnormal lysosomal pH is believed to impair lysosomal degradation, positioning, catabolite transport, nutrient sensing and channel activity (Kim et al., 2008; Xu and Ren, 2015; Ballabio and Bonifacino, 2019).

Inhibition of the V-ATPase by bafilomycin A1 quickly leads to lysosomal alkalinization, suggesting that there are unidentified channels on the lysosomal membrane that allow rapid proton efflux during this process (Christensen et al., 2002). Two families of mammalian proton channels have been identified. The protein H_V1 which has a transmembrane motif homologous to the voltage sensors of voltage-gated Na, K and Ca channels but lacks a canonical pore domain is sufficient for expression of voltage-sensitive proton-selective ion channel activity (Sasaki et al., 2006; Ramsey et al., 2006) and the protein Otopetrin1 (OTOP1) was identified by a genetic screen from mouse taste receptor cells, protein to also form a proton-selective ion channel (Tu et al., 2018).). However, each of these channels is only expressed in specific cell types and neither of them shows discernible lysosomal membrane localization. In the current study, by expression-based screening of a library of putative lysosomal membrane proteins, we discovered that TMEM175 is a ubiquitously expressed, proton selective channel of endosomes and lysosomes.

III-3 Results

3.1 A proton "leak" channel exists in endosomes and lysosomes

To facilitate the detection of lysosomal proton currents, patch clamp recordings (**Fig. 3.1 a)** (Dong et al., 2008; Chen et al., 2017) from isolated, chemically enlarged endolysosomes (LELs) were made using solutions in which the large ions N-methyl-D-glucamine ($NMDG^+$) and methanesulfonic acid (MSA^-) replaced the normal physiological cations and anions (Na^+, K^+, Ca^{2+}, Mg^{2+} and Cl^-), and a proton gradient between the cytosolic and luminal sides was established using appropriate pH buffers. When luminal pH (pH_L) was set to 3.5 with a cytosolic pH (pH_C) of 7.2, detectable inward leak currents at -120 mV were found in LELs and in these LELs the leak current reversed at about +120 mV (**Fig. 3.1b-c**). When both sides were equally acidic (pH_L/pH_C of 3.5/3.5) the reversal potential (E_{rev}) shifted to near 0 mV (**Fig. 3.1b**), consistent with the absence of proton gradient across the membrane. No measurable current was seen at all potentials with pH_L and pH_C both set to 7.2 (**Fig. 3.1c**). Hereafter, we refer to the channel carrying H^+ "leak" current as the lysosomal proton activated, proton permeant channel (LyPAP).

3.2 Lysosomal membrane protein TMEM175 is required for LyPAP currents

An expression screening approach was used to identify candidates that may mediate LyPAP. The candidate library (See **Methods** for genes screened) was established based on lists of putative lysosomal membrane proteins from lysosome proteomic studies (Schroder et al., 2010; Wyant, G. A. et al. 2018) excluding well-studied TPRML, TPC and CLCN family members (Xiong and Zhu, 2016; Zhang et al., 2018). To make recognizing a positive hit easier, the screening was conducted with pH_L set to 4.6, which only allows small endogenous LyPAP currents (**Fig 3.1 c**) The only positive hit was TMEM175, for which the average LyPAP currents at -120 mV were more than 10 times larger than

those from control (un-transfected) cells or cells transfected with the other candidates (**Fig. 3.2 a**). Like endogenous LyPAP currents, E_{rev} of the currents from TMEM175-transfected cells shifted from > +80mV to 0 mV when pH_C was changed from 7.2 to 4.6 (equaling pH_L) (**Fig. 3.2 b**).

TMEM175 knockout (KO) HAP1 cells were generated using Crispr-Cas9 (Ran et al., 2013). LyPAP currents were absent in endolysosomes from KO cells but routinely observed in endolysosomes from unmodified wild-type (WT) HAP1 cells, and from KO cells re-expressing human TMEM175 (**Fig. 3.2 c-f**). Thus, TMEM175 is both necessary and sufficient for LyPAP currents in endolysosomes.

To observe endogenous localization of TMEM175, we generated HA-tagged TMEM175 knock-in HAP1 cells since a suitable antibody for immunodetection of endogenous levels of TMEM175 protein was unavailable. Consistent with a previous report that TMEM175 is present in endolysosomes (Cang et al., 2015), in the knock-in cells, most HA-tag positive puncta were observed to overlap with markers for late endosome and lysosomes (LAMP1) (**Fig. 3.2 g**).

3.3 TMEM175 acts as a proton-activated, proton-selective channel.

TMEM175 was previously reported to be a K^+ permeable channel, but those experiments were done under neutral conditions, which are physiological for channels in the plasma membrane but non-physiological for endolysosomal channels (Cang et al, 2015). To assess the selectivity of TMEM175 for protons, we performed a series of experiments in the whole-cell recording configuration. The reason for choosing this recording configuration is that the extracellular face of TMEM175 present on the plasma membrane is topologically equivalent to its luminal face in endolysosome membranes (Lee et al., 2017), so this configuration allowed us to keep the cytosolic pH (pH_C) constant while the extracellular pH (referred to as $pH_{E/L}$) was easily switched with a

perfusion system to mimic changes in the luminal pH of endolysosomes. We set pH_C to 5.0 (to make the outward currents much larger than that at pH_C 7.2) and measured E_{rev} as a function of the proton gradient ($\Delta pH = pH_{E/L}-pH_C$). Under these conditions, E_{rev} closely followed the Nernst equation for a proton-selective ion channel (53 mV/ΔpH) (**Fig. 3.3 a-b**). Under normal physiological conditions for endolysosomes, where the luminal side is highly acidic and the cytosolic side is slightly alkaline with a high concentration of potassium, protons were much more permeable than potassium. For example, at $pH_{E/L}$ = 5.0 and pH_C = 7.2 the cytosolic side [K^+] concentration was 14,000 times higher than the extracellular/luminal side [H^+], but E_{rev} was quite positive, indicating that H^+ is much more permeable than K^+ through TMEM175 (**Fig. 3.3 c**). With 140 mM potassium present in the cytosol solution, E_{rev} shifted at the rate of approximately 53 mV/pH unit and therefore the relative permeability was estimated to be P_H/P_K = 48,000 ± 2,000. Similar experiments with 140 mM cytosolic sodium gave P_H/P_{Na} > 200,000 (**Fig. 3.3 c-d**). Experiments done by my collaborator Meiqin Hu that are not included in this thesis demonstrate that not only is TMEM175 proton permeable, but it is also activated by protons from the luminal side, but not from the cytosolic side.

The high H^+ selectivity indicated by our electrophysiological measurements predicts that H^+ flow through TMEM175 on the plasma membrane would rapidly alter cytosolic pH if an inward H^+ gradient was present. This was tested by using fluorescent intracellular pH indicators in sham cells and cells overexpressing TMEM175. Similar results were obtained whether the indicator was pHluorin (**Fig. 3.3 e-j**) or pHrodo Red (**Fig. 3.3 k**). A typical experiment began with a coverslip of cells bathed in the imaging solution (in Fig. 3.2 e TMA-MSA) at pH 7.2. The pH was then changed to 4.6 to establish an inwardly directed pH gradient, then switched back to the pH 7.2 to determine whether the response was transient or sustained. After 5 minutes, the cell was acidified

with acetic acid and then alkalized with ammonium chloride to determine the maximal and minimal possible fluorescence for the cell, which were used for normalizing the data. Data were then analyzed quantitatively (**Fig. 3.2 f**). For most of the cations ($NMDG^+$, TMA^+, K^+, Ca^{2+}, or Mg^{2+}) and anions (MSA^- or Cl^-) we tested (**Fig. 3.3 g-k***)*, exposure to $pH_{E/L}$ 4.6 elicited rapidly rising, substantial, sustained reductions in intracellular pH in TMEM175 positive cells, but only slow onset, small, rapidly recovering changes in sham cells (likely due to an endogenous plasma membrane H^+ leak pathway (Decoursey et al., 2003). In contrast, when the extracellular solution contained Na^+ (**Fig 3.3 h, j and k**) there was substantial recovery of fluorescence over 5 minutes, suggesting that a Na^+ dependent transport protein is able to restore cytosolic pH towards normal once the proton entry through TMEM175 has ceased.

3.4 Activation of TMEM175 induces lysosome H^+ release.

The synthetic small-molecule chemical, DCPIB, previously known to be a membrane permeable inhibitor of volume-regulated anion channels (VRAC) (Decher et al., 2001), was identified as a potent activator of TMEM175 (**Fig. 3.4 a-b**). The effect of DCPIB on TMEM175 whole-LEL H^+ currents was concentration dependent **(Fig. 3.4 c-d)**. The endogenous chemical arachidonic acid also activated TMEM175 currents (data not shown). Thus TMEM175 can be activated by ligand binding, and is not simply a constitutively active "leak" channel (Cang et al, 2015).

When HEK293T cells expressing pHluorin were imaged with a pH 7.2 bathing solution, application of DCPIB induced substantial fluorescence reductions in cells co-transfected with TMEM175, but much smaller reductions in sham cells **(Fig. 3.4 e-g)**. As there was only very low $[H^+]$ in the extracellular solution under these conditions, this result suggested DCPIB activated

TMEM175 channels on lysosomes, leading to lysosomal H^+ release into the cytosol. This was confirmed by pre-treating cells with GPN (glycyl-L-phenylalanine 2-naphthylamide) to dissipate the H^+ gradient across the lysosomes (Jadot et al., 1984). Under this condition, there were only small reductions similar to the changes observed in sham cells.

3.5 A single pore mutation in TMEM175 selectively eliminates its H^+ permeability without altering the K^+ permeability.

To identify residues potentially involved with luminal pH activation or H^+ selectivity of TMEM175, we mutated residues with side chains capable of H^+ binding (approximate pKa: D=3.9, E=4.3 and H=6.0) (Edsall and Wyman, 1958) in the pore region and luminal loops (**Fig. 3.5 a**). The cytosol solution used in these whole-cell recordings (K-Mes with pH_C = 7.2) allowed us to isolate either inward H^+ currents or outward K^+ currents. In contrast to WT TMEM175, D41A showed no indication of inward H^+ currents at $pH_{E/L}$ 4.6, but retained normal outward K^+ currents activated by DCPIB at $pH_{E/L}$ of 7.2 (**Fig. 3.5 b-d**), and thus is a selective H^+ conductance deficient mutant of TMEM175. None of the other mutants we studied showed a selective loss of H^+ permeation nor showed the converse phenotype (normal H^+ permeation but no K^+ permeation), but F39V showed no current under either condition. Intracellular pH imaging confirmed the incapacity of D41A to mediate significant H^+ flux, although this mutant was still correctly localized to lysosomes (**Fig. 3.5 e-h**).

3.6 H^+ conductance through TMEM175 is required for lysosomal pH homeostasis.

Lysosomal pH likely reflects a balance between proton import by the V-ATPase, which can be blocked with Bafilomycin-A1 (Baf-A1) (Bowman et al., 1988), and proton efflux through

TMEM175. By assaying luminal pH with Oregon Green^{TM} 488 Dextran or with LysoTracker Red DND-99 (LysoTracker), we found that in wild type cells a low concentration (1 nM) of Baf-A1 resulted in significant alkalinization of cells but that TMEM175 KO HeLa cells displayed significant lysosomal hyperacidity which could be brought back toward normal by this concentration of Baf-A1 (**Fig. 3.6 a-c**). Control experiments showed that knock-out of TMEM175 did not cause a change in lysosome levels as assayed by LAMP1 expression (**Fig. 3.6 d-e**). Conversely, two HEK293T cell lines stably overexpressing TMEM175 showed significant lysosomal hypoacidity likely due to faster proton leaking from lysosomes (**Fig. 3.6 f-g**). LysoTracker fluorescence also showed that re-expression of the D41A mutant, which does not allow proton permeation, had no effect on the hyperacidity of KO cells, but re-expression of WT TMEM175 was capable of increasing lysosomal pH (**Fig. 3.6 h-i**). The above findings indicate that the K^+ conductance of TMEM175 is not sufficient for lysosomal pH homeostasis and that the H^+ conductance is required.

3.7 TMEM175 is required for normal lysosome hydrolase activity.

Many lysosomal hydrolases, such as cathepsin B and cathepsin D, have a narrow optimal pH range for activation (Mindell, 2012; Yoshida et al., 2015) We detected the fluorescence of Magic Red, a substrate for cathepsin B, and demonstrated that cathepsin B activity was impaired in KO cells compared with WT cells and that 1 nM Baf-A1, the concentration that normalized the lysosomal pH of KO cells, brought cathepsin-B activity back to the normal level (**Fig. 3.7 a-b**).

III-4 Discussion

In this chapter, novel roles of TMEM175 in regulating lysosomal pH were elucidated. Lysosomal hyper-acidification or hypo-acidification impairs nutrient recycling, waste clearance and the efflux of digested nutrients because a broad range of enzymes only digest substrates in a narrow optimum pH range. Thus all these processes require a reliable H^+ gradient across the lysosomal membrane (Mindell, 2012). Furthermore, the lysosomal membrane hosts several H^+ coupled transporters, which get their energy from the lysosomal H^+ gradient. For example, CLCN7, by acting as an electrogenic 2 Cl^-/1 H^+ exchanger (Graves et al., 2008) provides negative charges to help balance out the net positive charge entry produced by the V-ATPase. However, lysosomes lacking CLCN7 appear to have a normal pH (Kasper et al., 2005; Steinberg et al., 2010), so other pathways must be required for pH homeostasis. An unidentified H^+ leak channel was therefore previously predicted to be on the lysosome membrane (Casey et al., 2010; Xu and Ren et al., 2015). We identified TMEM175 as an H^+ selective channel and showed it is required for maintaining lysosomal pH homeostasis.

TMEM175 was previously reported to be a lysosomal K^+ selective channel (Cang et al., 2015). That study characterized TMEM175 with solutions near pH 7 on both sides of the membrane, however, under normal physiological conditions the lumen of lysosomes is highly acidic. When we studied TMEM175 with a pH gradient normal for lysosomes, H^+ dependent currents flowed in the direction predicted by the H^+ electrochemical gradient and the shifts in the reversal potential indicated that the relative permeability of potassium was very low compared to the H^+ permeability, with P_H/P_K near 50,000. Our results are compatible with the data in the previous report. When TMEM175 is on the plasma membrane, whether due to overexpression as in our experiments, or due to lysosomal exocytosis, because the normal cytosolic [K^+] is

approximately 2 million fold higher than the intracellular or extracellular [H^+], even with the huge P_H/P_K selectivity both calculations and our data indicate that plasma membrane TMEM175 would be carrying almost exclusively potassium. Conversely, with the physiological H^+ and K^+ gradients across lysosomes, TMEM175 will carry almost exclusively protons.

The pH dependence of the channel activation makes TMEM175 well suited to a role in pH homeostasis, as it will lower the H^+ leak whenever the organelle gets too alkaline, setting up a negative feedback loop. What is unique about this negative feedback loop is that the sensor and the response elements are integrated into one protein: a proton-activated proton-permeable channel. We also found that arachidonic acid may exert control over TMEM175 activity. The identification of endogenous and exogenous modulators will allow us to screen for more potent and selective modulators with similar chemical structures and could be very useful for cell biological investigations of the role of TMEM175 channels. Identification of modulators that act on the pH dependent activation mechanism would also be of great interest.

Compromised lysosome function due to abnormal lysosomal pH leads to a range of diseases, some of them severe or even fatal and so lysosomal pH manipulation or optimization has been adopted to treat patients with lysosomal hyper-acidification (Nicoli et al., 2019) (**Fig 3.8**). Our demonstration that pH optimization in TMEM175 knock out cells results in restoration of normal cathepsin B activity provides the proof of concept that modulation of TMEM175 activity in the lysosome could be a new approach for developing therapies for neurodegenerative diseases and lysosomal storage diseases.

III-5 Methods

Mammalian cell lines

COS1, HEK293T and HeLa cells were cultured in high glucose DMEM (Gibco) with 10% fetal bovine serum (FBS, 100-106, Gemini Bio-Products). HAP1 cells were maintained in IMDM (Gibco) with 10% FBS. Cells were transfected with Lipofectamine 2000 (Invitrogen). Generation of TMEM175 knockout and HA-tagged knock-in cells TMEM175 knockout (KO) HAP1, HeLa and TMEM175-HA knock-in (KI) HAP1 cell lines were engineered by Crispr-Cas9 system (Ran et al., 2013). The guide RNA (gRNA) targeting exon 10 (5'-CGCGTGGAAGCCTTCAGCGA-3') was designed to generate KO cell lines which undergo a frameshift near IIS1. For HA tagged KI cells, a 2.2 kb human genomic DNA region spanning exon 11 with ~1.4 kb intron sequence was PCR amplified and inserted into a backbone vector. Flag (DYKDDDDK) and HA tags (YPYDVPDYA) linked by five (5) glycines were then inserted at the end of the Open Reading Frame (ORF) using site-directed mutagenesis to generate the template plasmid. The gRNA targeting the intron downstream of exon 11 (5'-TGTCCTCCCTGGTCCATCTC-3') was designed to trigger homologous recombination. The gRNA was cloned into pSpCas9 (BB)-2A-puro vector (Addgene) and transfected into target cells alone (for KO) or together with the template plasmid (for KI) using Lipofectamine 2000 (Invitrogen). After puromycin (Millipore Sigma) selection for 48 hours, the remaining cells were trypsin-digested and limiting diluted into 96-well plates to obtain monoclonal cell populations. The frameshift in KO cells and the HA tag in-place insertion in KI cells were confirmed with PCR amplification and Sanger sequencing.

Generation of TMEM175 site-directed mutants

Site-directed mutagenesis was performed on the template of EGFP-TMEM175 (pEZ-M29, GeneCopoeia) or mCherry-TMEM175 (pEZ-M55, GeneCopoeia) using QuikChange II Site-Directed Mutagenesis Kit (200523, Agilent) or Gibson Assembly Cloning Kit (E5510S, New England Biolabs). The sequence of each mutant was confirmed by Sanger sequencing.

Candidate plasmid library

All cDNA in plasmids used for the candidate expression screen are from the human genes and the proteins were tagged with EGFP or mCherry. Among them, plasmids inserted with the cDNA for *C1orf85, CLCN4, SCARB2* and *SLC36A1* were purchased from Origene; plasmids inserted with the cDNA for CLN8, LMBRD1, MFSD12, MFSD6, OCA2, SLC15A3, SLC15A4, SLC17A5, SLC17A9, SLC35F6, SLC38A7, SLC38A9, SLC46A3, SLC48A1, SLC7A14, TMEM123, TMEM175, TMEM179B, TMEM184C, TMEM243, TMEM55B and TTYH2 were purchased from GeneCopoeia; the NHE6 (pEGFP-N3) plasmid was a gift from Dr. Rajini Rao (Johns Hopkins University School of Medicine).

Whole-cell patch clamp electrophysiology

Ionic currents were recorded in the whole-cell configuration under voltage-clamp using an Axopatch 200B amplifier equipped with a Digidata 1440A digitizer (Molecular Devices). Unless otherwise stated, both pipette (cytosolic) and bath (extracellular) solutions contained NMDG-MSA as the major ions. The pipette (cytosolic) solution usually contained (in mM): 150 NMDG and HEPES (pH 7.2 adjusted with MSA). The pipette solution was supplemented with essential Cl^- (2443 mM) needed to stably conduct electricity through Ag/AgCl electrode. To vary the pH of

the bath (extracellular) solution from 7.2-3.5, an appropriate pH buffer (20 mM HEPES, MES or citrate acid) near its pKa was used and supplemented with sufficient NMDG (120-150 mM) to bring the osmolarity to ~ 300 mOsm (pH adjusted with MSA). All bath solutions were applied via a perfusion system that allowed us to achieve complete solution exchange within a few seconds. The Cl^- free solution used extracellularly was essential to prevent activation of H^+-activated Cl^- currents (Yang et al., 2019). An agar bridge filled with 3M KCl was used for the reference electrode. Glass electrodes were pulled with the resistance 2-4 MΩ. A ramp protocol (-120 mV to +120 mV, 400 ms, holding at 0 mV) was used to record the currents at 2 seconds intervals. All experiments were conducted at room temperature (22–25°C).

The chord ion conductance was calculated using a revised Ohm's law-based equation:

$$G = \frac{I_m}{E_m - E_{ion}}$$

where G is the chord ion conductance, Im is the recording current, Em is the holding membrane potential, E_{ion} is the driving force established by a specific ion and calculated using the Goldman-Hodgkin-Katz voltage equation (Lewis, 1979).

Whole-endolysosome (Whole-LEL) patch clamp electrophysiology

Endolysosomal electrophysiology was performed in isolated enlarged endolysosomes using a modified patch-clamp method (Dong et al., 2008). Briefly, cells were treated with 1 mM vacuolin-1 (673000, Millipore Sigma), a lipid-soluble polycyclic triazine that can selectively increase the size of endosomes and lysosomes (endolysosome) (Huynh and Andrews, 2005) for at least 1h and up to 12h. Whole-endolysosome recordings were performed on manually isolated enlarged endolysosomes. In brief, a glass pipette was pressed against a cell and quickly pulled away to break the cell membrane. Enlarged endolysosomes were released out of the hole in the plasma membrane

and visualized under an inverted microscope (IX71, Olympus). If applicable, the fluorescence emission was confirmed on the membrane of isolated endolysosomes expressing fluorescent proteins. After formation of a gigaseal between the glass pipette and the isolated endolysosome, capacitance transients were compensated. Voltage steps of several hundred millivolt (mV) with a 1-10 millisecond (ms) duration were then applied to break through the vacuolar membrane. The whole-endolysosome configuration was verified by the re-appearance of capacitance transients after break-in.

Unless otherwise stated, both bath (cytosolic) and pipette (luminal) solutions contained NMDG-MSA as the major ions. The bath (cytosolic) solution contained (in mM): 150 NMDG and 20 HEPES (pH 7.2 adjusted with MSA) and pipette (luminal) solution at pH 4.6 contained (in mM): 150 NMDG and 20 MES (pH adjusted with MSA). The pipette (luminal) solution at pH 3.5 contained (in mM): 110 NMDG and 25 citrate acid (pH adjusted with MSA). The pipette solution was supplemented with essential Cl^- (2 mM) needed to stably conduct electricity through the Ag/AgCl reference electrode. An agar bridge filled with 3M KCl was used for the reference electrode. A ramp protocol (-120 mV to +120 mV, 400 ms, holding at 0 mV) was used to record the currents at 2 seconds intervals. Data were collected using an Axonpatch 200B amplifier, Digidata 1440A Digitizer, and Clampex 10.7 software (Molecular Devices). All experiments were performed at room temperature (22-25ºC), and all data were analyzed with Clampfit 10.7 (Molecular Devices), Origin 2018 (OriginLab) or Prism 8.4 (Graphpad).

Endolysosomal excised patch clamp electrophysiology

Endolysosomal lumen-side out recordings were performed on giant excised patches as previously described (Wang et al., 2017). In brief, after formation of a gigaseal between the glass

pipette and an isolated endolysosome, the glass pipette was pulled away to obtain a giant excised patch, in which the luminal side faced outside. Both pipette (cytosolic) and bath (luminal) solutions were the same ones used in the whole-cell recordings. An agar bridge filled with 3M KCl was used for the reference electrode. Glass electrodes were pulled with the resistance 1-2 MΩ. A ramp protocol (-120 mV to +120 mV, 400 ms, holding at 0 mV) was used to record the currents at 2 seconds intervals. Data were collected using an Axonpatch 200B amplifier, Digidata 1440A Digitizer, and Clampex 10.7 software (Molecular Devices). All experiments were performed at room temperature (22-25ºC).

Determination of relative permeability (P_H/P_X)

The permeability of TMEM175 for H^+ relative to other monovalent cations (K^+ or Na^+) was estimated based on the Goldman-Hodgkin-Katz current equations (Lewis, 1979) and the measured E_{rev} using bi-ionic conditions:

$$\frac{P_H}{P_X} = \frac{[X^+]_e - [X^+]_i e^{\frac{(FV}{RT)}}}{[H^+]_i e^{\frac{(FV}{RT)}} - [H^+]_e}$$

where R, T, F and V are the gas constant, absolute temperature, Faraday's constant and the reversal potential, respectively. Assumed ion activity coefficients are 1 for monovalent ions. The liquid junction potentials were measured and corrected as described (Neher, 1992). The pipette (cytosolic) solution was buffered with 20 mM HEPES (adjusted to pH 7.2) and also contained either 150 mM Na-MSA or 140 mM K-MSA and 10 mM tetraethylammonium (TEA^+) chloride (used to block the endogenous basal outward K^+ current in HEK293T cells). The pipette solution containing Na^+ was supplemented with Cl^- (2 mM) in order to stably conduct electricity through the Ag/AgCl electrode. An agar bridge filled with 3M KCl was used for the reference electrode. The reversal potential was

determined using a ramp protocol (-120 mV to +120 mV, 400 ms, holding at 0 mV) in response to bath (extracellular) solutions at variable pH (see *Whole-cell patch clamp electrophysiology* section). The permeability of TMEM175 to $NMDG^+$ was imperceptible and so was ignored in the determination of P_H/P_{Na} and P_H/P_K.

Cytosolic pH imaging

Cytosolic pH dynamics were determined by time-lapse imaging using the genetic pH indicator pHluorin (Miesenbock et al., 1998) or the chemical sensor pHrodo™ Red. When binding H^+ intracellularly, the brightly fluorescent pHluorin is quenched to a lower level, while the dim fluorescence of pHrodo™ Red gets brighter.

The pHluorin plasmid was subcloned from NPY-pHluorin (a gift from Dr. Zhuan Zhou, Peking University, China) (Wang et al., 2017). Cells seeded on glass coverslips were transfected with pHluorin together with mCherry-TMEM175 (in pEZ-M55) or sham vector using Lipofectamine 2000 (Thermo Fisher Scientific). Twenty four hours after transfection, cells were washed with the imaging solution at pH 7.2 and imaged with a spinning-disk confocal microscope (IX81, Olympus; CSU-X1, Yokogawa) equipped with a 20 × objective lens and a temperature controller that kept the cells at 37 ^oC. The imaging solution at 7.2 or 4.6 usually contained 100 mM pH buffer (HEPES or MES) near its pKa supplemented with the either tetramethylammonium methanesulfonate (TMA-MSA), N-methyl-D-glucamine methanesulfonate (NMDG-MSA), potassium methanesulfonate (K-MSA) or sodium methanesulfonate (Na-MSA) to bring the osmolarity to ~ 300 mOsm. In a subset of experiments, Tyrode's solution at pH 7.4 (145 mM NaCl, 5 mM KCl, 2 mM $CaCl_2$, 1 mM $MgCl_2$, 10 mM HEPES and 10 mM glucose) and a modified Tyrode's-like solution at pH 4.6 (replacing HEPES with MES) were also used as imaging solutions. Prior to imaging, a single image was

acquired using excitation at 561 nm to identify the cells expressing mCherry-TMEM175 or sham vector. The fluorescence emissions excited by at 488 nm were then acquired every 5 seconds with an EMCCD camera (Andor, iXon ultra 897U) controlled by MetaMorph software. Undissociated acetic acid (HOAc) (150 mM NaCl, 10mM HEPES and 10 mM HOAc, pH 5.0 adjusted by NaOH) freely entering the cytosol, where it dissociates into a H^+ and an acetic ion (Ylitervo et al., 2014), served as a positive control to acidify the cytosol. Free NH_3 (NH_4Cl) (110mM NaCl, 50 mM NH_4Cl, 20 mM HEPES, pH 7.2 adjusted by NaOH) may enter cytosol, where it associates with H^+ to generate NH_4^+, served as an alkalizing agent to confirm the availability of pHluorin (Decoursey, 2003).

The chemical based intracellular pH indicator, pHrodo™ Red AM (P35372, Invitrogen), was also used to determine intracellular pH. Cells seeded on glass coverslips were transfected with EGFP-TMEM175 (pEZ-M29, GeneCopoeia) or sham vector using Lipofectamine 2000 (Thermo Fisher Scientific). Twenty-four hours after transfection, cells were loaded with the pHrodo™ Red AM according to the manufacturer's instructions and washed with the imaging solution at pH 7.2. In these experiments, a single image was acquired using excitation at 488 nm to identify the cells expressing EGFP-TMEM175 or sham vector. The fluorescence emissions excited by at 561 nm were then acquired every 5 seconds. The fluorescence intensity in cells was quantified with Fiji (ImageJ) software.

Lysosomal pH determination

Lysosomal pH measurement with the a ratiometric pH sensitive dye Oregon Green™ 488 conjugated dextran-10 kd (D7170, Molecular Probes) was performed as described previously (Christensen, 2002; Davis et al., 2012). In brief, cells seeded on glass coverslips were loaded with

150 μg/mL Oregon Green™ 488 Dextran overnight and chased in medium without dye for three hours before imaging. Cells were washed with Ringer's buffer (in mM: 155 NaCl, 5 KCl, 2 $CaCl_2$, 1 $MgCl_2$, 2 NaH_2PO_4, 10 HEPES, and 10 glucose, pH 7.4) and imaged using a Nikon TE300 inverted microscope equipped with a 60× objective lens (N.A. = 1.4) and a temperature-controlled stage. The fluorescence emission (530 nm) excited at 440 nm and 490 nm wavelengths were acquired with a cooled digital CCD camera (Quantix Photometrics) controlled by MetaMorph software. pH calibration was performed to generate the pH standard curve. pH standard buffers (in mM: 130 KCl, 1 $MgCl_2$, 15 HEPES and 15 MES) were prepared at variable pH ranging from 3.0 to 8.0 supplemented with 10 μM valinomycin and 10 μM nigericin. The ratio of fluorescence intensities excited at 440 nm and 490 nm in response to variable pH was fitted to sigmoidal equation to generate the pH standard curve. The lysosomal pH values were calculated with the resulting intensity ratio (440 nm / 490 nm) images based on the standard curve.

LysoTracker staining

For determination of lysosomal acidification, cells were cultured in a 24-well dish one (1) day before the experiment. To visualize the acidic organelles, 50 nM LysoTracker Red DND-99 (L7528; Thermo Fisher Scientific) was added into the cell culture medium with or without Baf-A1 (11038, Cayman Chemicals) and incubated at 37˚C for 30 min. Cells were then washed twice with Tyrode's solution and kept in Tyrode's for imaging. Images were acquired using an inverted fluorescence microscope (IX81, Olympus), and the fluorescence intensity of LysoTracker was quantified by Fiji (ImageJ).

Cathepsin B activity assay

Cathepsin B activity in the lysosome was determined using Magic Red Cathepsin B assay kit (937, ImmunoChemistry Technologies). Magic Red stock solution was prepared according to the manufacturer's instruction. Cells were incubated with Magic Red (1:1,000 dilution) at 37˚C for 1 hour and washed twice with Tyrode's solution before imaging. Images were taken using an inverted fluorescence microscope (IX81, Olympus) and the fluorescence intensity of Magic Red was quantified with Fiji (ImageJ).

Immunocytochemistry

Cells seeded on glass coverslips were washed with Phosphate-buffered saline (PBS) and fixed with 4% Paraformaldehyde (PFA) or cold anhydrous methanol. Afterwards, 0.3 % Triton-X 100 in block solution (PBS supplemented with 2% bovine serum albumin) was used to permeate the phospholipid membrane (only for PFA fixation). Protein blocking was performed on the cells via incubating with the block solution for one (1) hour. Cells were incubated with primary antibody overnight at 4 ℃ and with second antibody for one (1) hour at room temperature. Primary antibodies (anti-human LAMP1 (H4A3), DSHB, 1:200; anti-HA (3F10), 11867423001, Roche, 1:200) and second antibodies (anti-mouse conjugated to Texas Red, T862, Life Technologies, 1:500; anti-rat conjugated to Alexa Fluor 488, A11006, Life Technologies, 1:500) were diluted in the block solution proportionally as indicated. Coverslips were mounted on glass slides with Fluoromount-G (0100-01, Southern Biotech). Images were acquired with an inverted confocal microscope (IX81, Olympus) equipped with an oil 60 × objective lens.

Reagents

Unless otherwise noted, all reagents used for electrophysiology and fluorescent imaging were purchased from Millipore Sigma. DCPIB, 4-[(2-Butyl-6,7-dichloro-2-cyclopentyl-2,3-dihydro-1-oxo-1H-inden-5-yl)oxy]butanoic acid (Product # 1540) was purchased from Tocris Bioscience. Bafilomycin-A1 (Product # 11038) was purchased from Cayman Chemical.

Statistical analysis

Data are usually presented as mean ± SEM (standard error). When box plots were used, the box represents the 25-75% range, with the solid line within them indicating the mean level and the dashed line indicating the median level. The whiskers represent the standard deviation and all points outside the standard deviation are shown as individual dots.

For experiments with only two groups Student's t-test was used to check the significance, while for the experiments with more than two groups and multi-testing was required, one-way ANOVA with Sidak's test was adopted to reduce the type 1 error. Significance is indicated as NS (not significant), * p <0.05, ** p <0.01, *** p < 0.001.

III-6 Figures

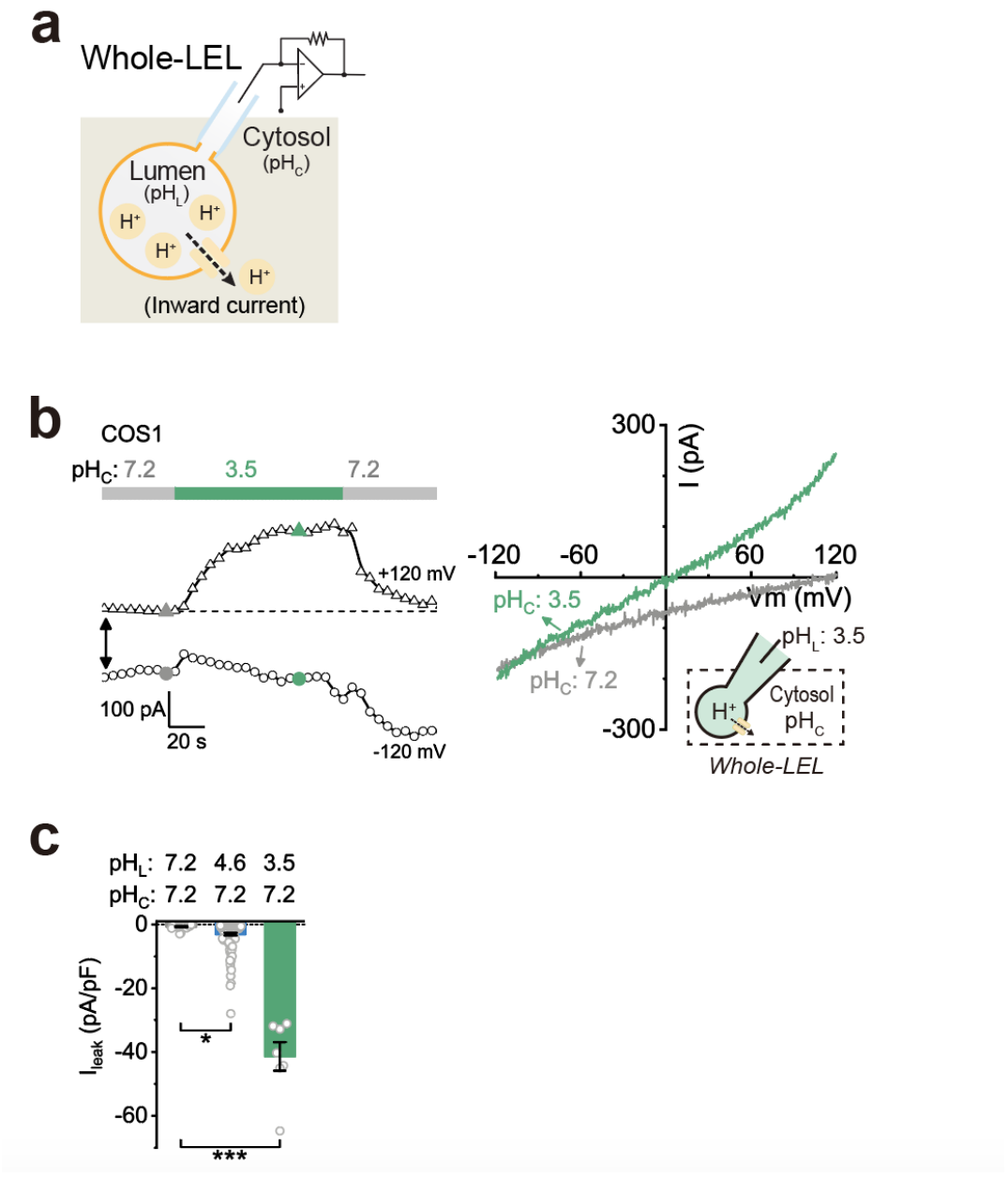


Figure 3.1 A proton "leak" channel exists in endosomes and lysosomes

(**a**)Diagram of Whole-LEL (late endosome and lysosome) recording method. Cation flow out of the LEL is defined as inward current. (**b**) Whole-LEL H^+ "leak" currents from a COS1 cell. Luminal pH_L was set to 3.5 and cytosolic pH_C varied as indicated. The double-sided arrow indicates the amplitude of "leak" current at pH_C 7.2. I-V relations at the time of the colored points

are illustrated. (**c**) Summary of whole-LEL "leak" current density at -120 mV from COS1 cells. (pH_L 7.2/4.6/3.5: n = 18/129/7, mean ± SEM, * p <0.05, *** p <0.001).

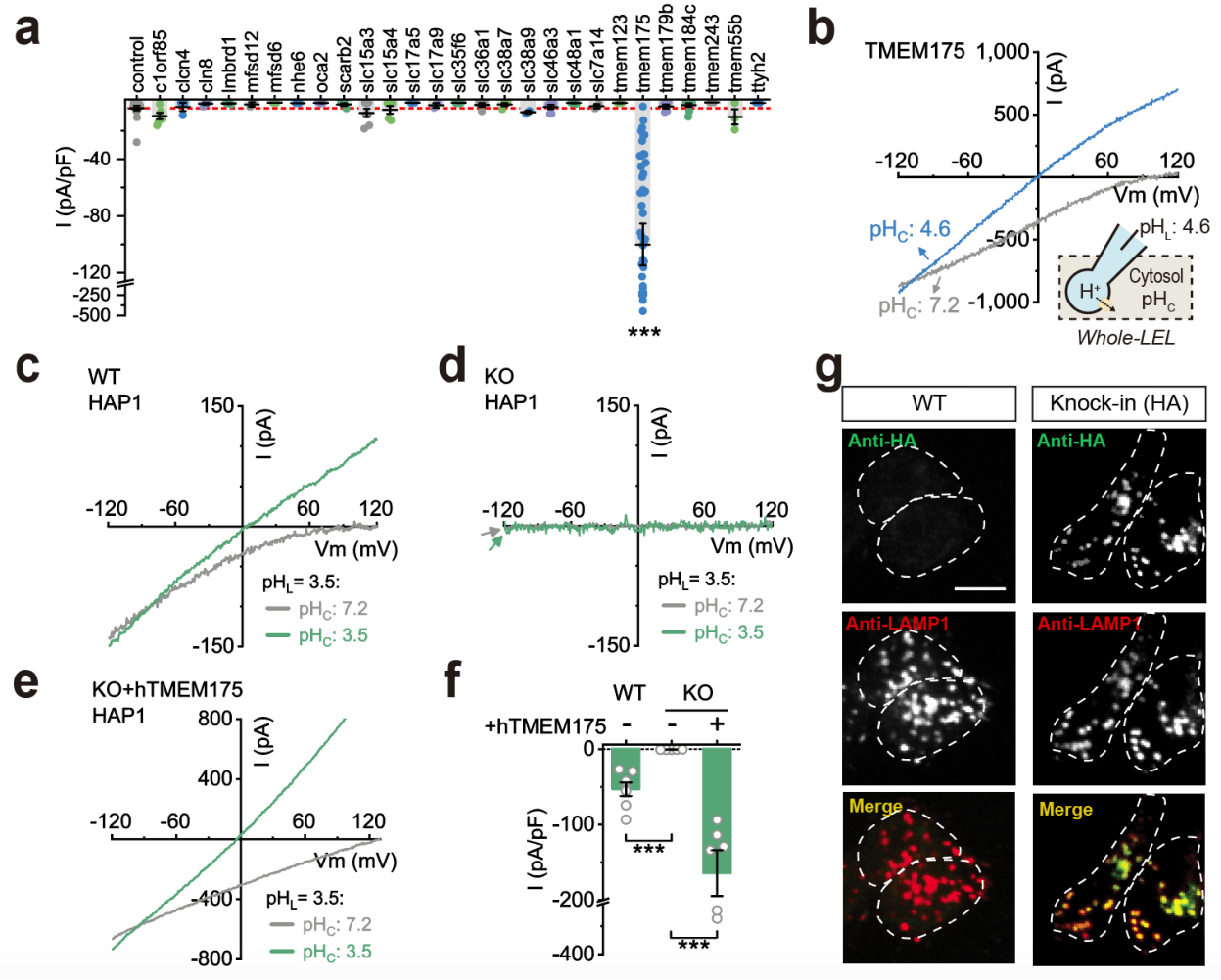


Figure 3.2 Lysosomal membrane protein TMEM175 is required for LyPAP currents

(**a**) Candidate screening revealed that only TMEM175 overexpression resulted in enhanced whole-LEL H^+ "leak" current from COS1 cells when luminal pH_L was 4.6 and cytosolic pH_C was 7.2. The red dashed line represents the mean level from non-transfected control LELs (Control/TMEM175/others: n = 16/39/2-9, mean ± SEM, *** p <0.001). (**b**) Typical whole-LEL H^+ "leak" currents from a COS1 cell overexpressing TMEM175. (**c-e**) Examples of whole-LEL H^+ "leak" currents from HAP1 WT cells, KO cells, and KO cells re-expressing human TMEM175. The luminal solution was set to pH_L 3.5. (**f**) Summary of current density at -120 mV from experiments as in (f-h) (WT/KO/KO+hTM175: n = 7/5/6, mean ± SEM, *** p <0.001). (**g**)

Assessment of colocalization of TMEM175 with LAMP1. TMEM175-HA knock-in HAP1 cells and homologous WT cells were immuno-stained by anti-HA and anti-LAMP1 antibodies. Dashed lines indicate cell perimeters. (Scale bar = 10 μm, confocal pinhole = 1.5 μm).

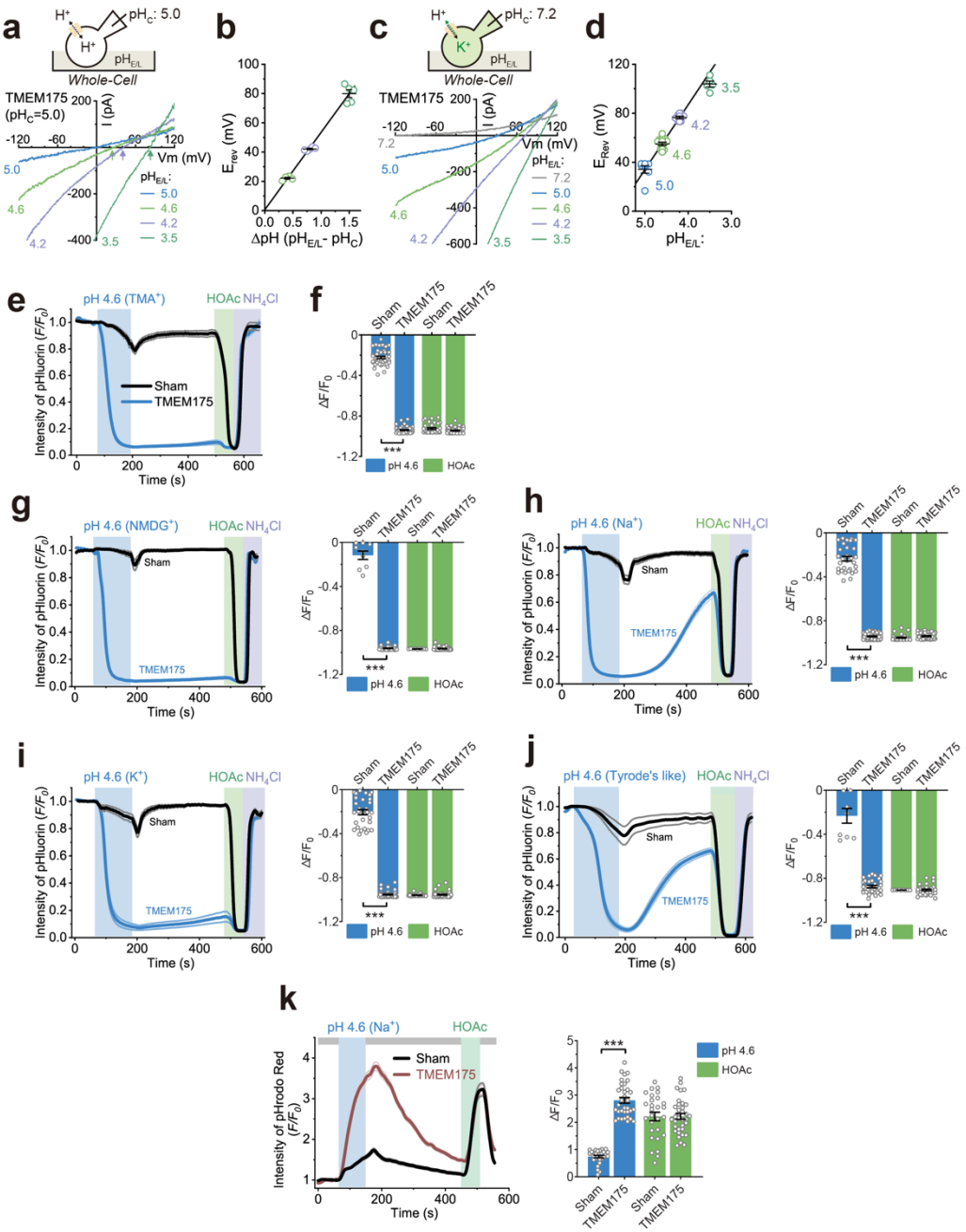


Figure 3.3 TMEM175 acts as a proton-activated, proton selective channel.

(a) E_{rev} measured in an HEK293T cell overexpressing TMEM175 when pH_C was set to 5.0 and $pH_{E/L}$ varied as indicated. (**b**) E_{rev} as a function of ΔpH from experiments as in (d). The line fit to the data had a slope of 53 mV/ΔpH and a y intercept of 0.58 mV (n = 4 - 5, mean ± SEM). (c) Erev detected in an HEK293T cell overexpressing TMEM175 under bi-ionic conditions. The cytosolic solution of pH_C 7.2 contained K-MSA instead of NMDG-MSA as the major ions. (d)

Analysis of the E_{rev} from experiments as in (c). The line is a least squares linear regression fit to the averages of the E_{rev} measured at $pH_{E/L}$ 5.0 to 4.2 (n = 5-11, slope = 53 mV/ΔpH, mean ± SEM). **(e-j)** Average pHlourin fluorescence in sham cells (*n* = 9-31, mean ± SEM, *** *p* <0.001) or TMEM175 transfected HEK293T cells (*n* = 31 – 45, mean ± SEM, *** *p* <0.001) in response to stimuli as indicated (See **Methods** for details of the imaging solutions). The summary of relative pHluorin fluorescence intensity in response to pH 4.6 and HOAc are shown in the right side of each panel. HOAc (pH 5.0) and NH4Cl (pH 7.2) 264 served as controls to acidify or alkalinize the cytosol. (**k**) The fluorescence intensity of the pHrodo™ Red was detected in TMEM175 transfected cells (*n* = 35, mean ± SEM) or sham cells (*n* = 25, *** *p* <0.001) in response to the stimuli as indicated.

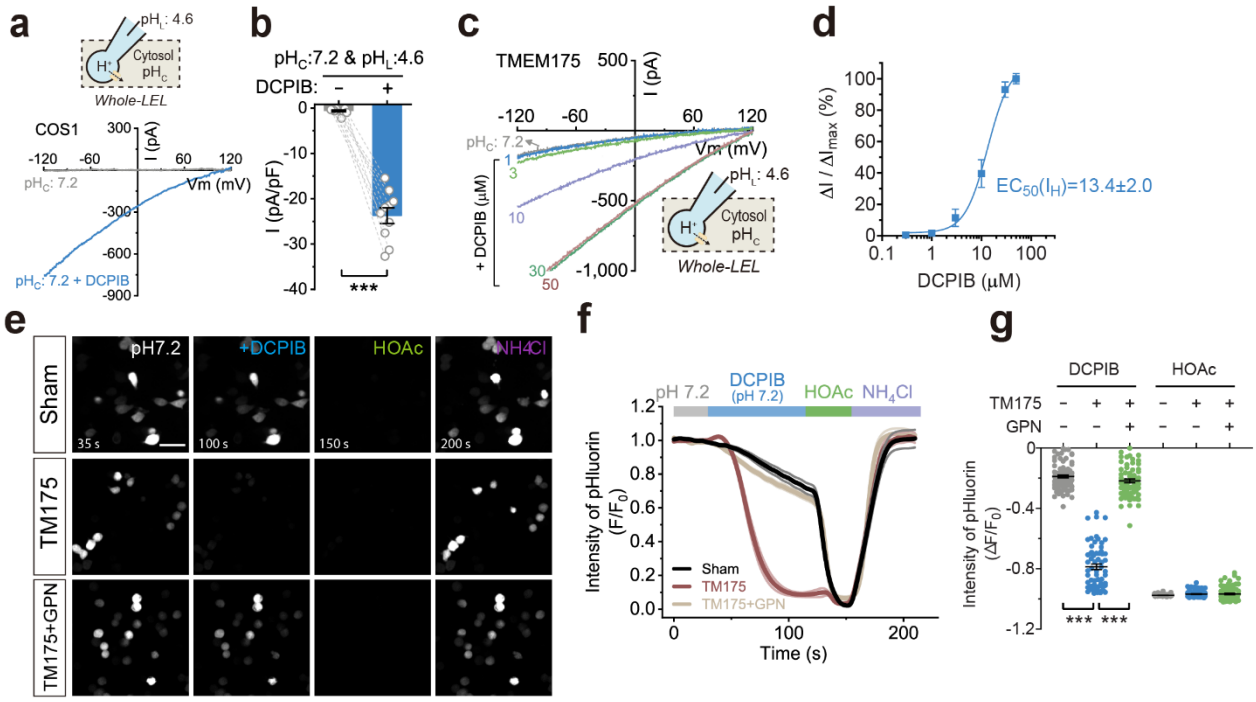


Figure 3.4 Activation of TMEM175 induces lysosome H^+ release

(a-b) Effect of DCPIB (100 μM) on whole-LEL H^+ currents in COS1 cells. Current density (-120 mV) is summarized in (b) (n = 10, mean ± SEM, *** p <0.001). **(c)** Effect of various concentrations of DCPIB on whole-LEL H^+ currents from a COS1 cell overexpressing TMEM175 when luminal pH_L was 4.6 and cytosolic pH_C was 7.2. (**d**) Summary of whole-LEL H^+ currents in response to various doses of DCPIB from experiments as in (c). (**e-f**) The fluorescence intensity of pHluorin in HEK293T cells overexpressing TMEM175 or in Sham cells in response to stimuli as indicated (scale bar = 50 μm). Imaging solution was set to pH 7.2 to eliminate H^+ influx across the plasma membrane. DCPIB (50 μM) was applied to potentiate TMEM175. Some cells were pre-treated with GPN (200 μM) one hour before imaging to abolish the H^+ gradient across the lysosome membrane. (**g**) Summary of relative pHluorin fluorescence intensity in response to DCPIB and HOAc (pH 5.0) (Sham/TM175/TM175+GPN, n = 88/63/73 cells; mean ± SEM, *** p <0.001).

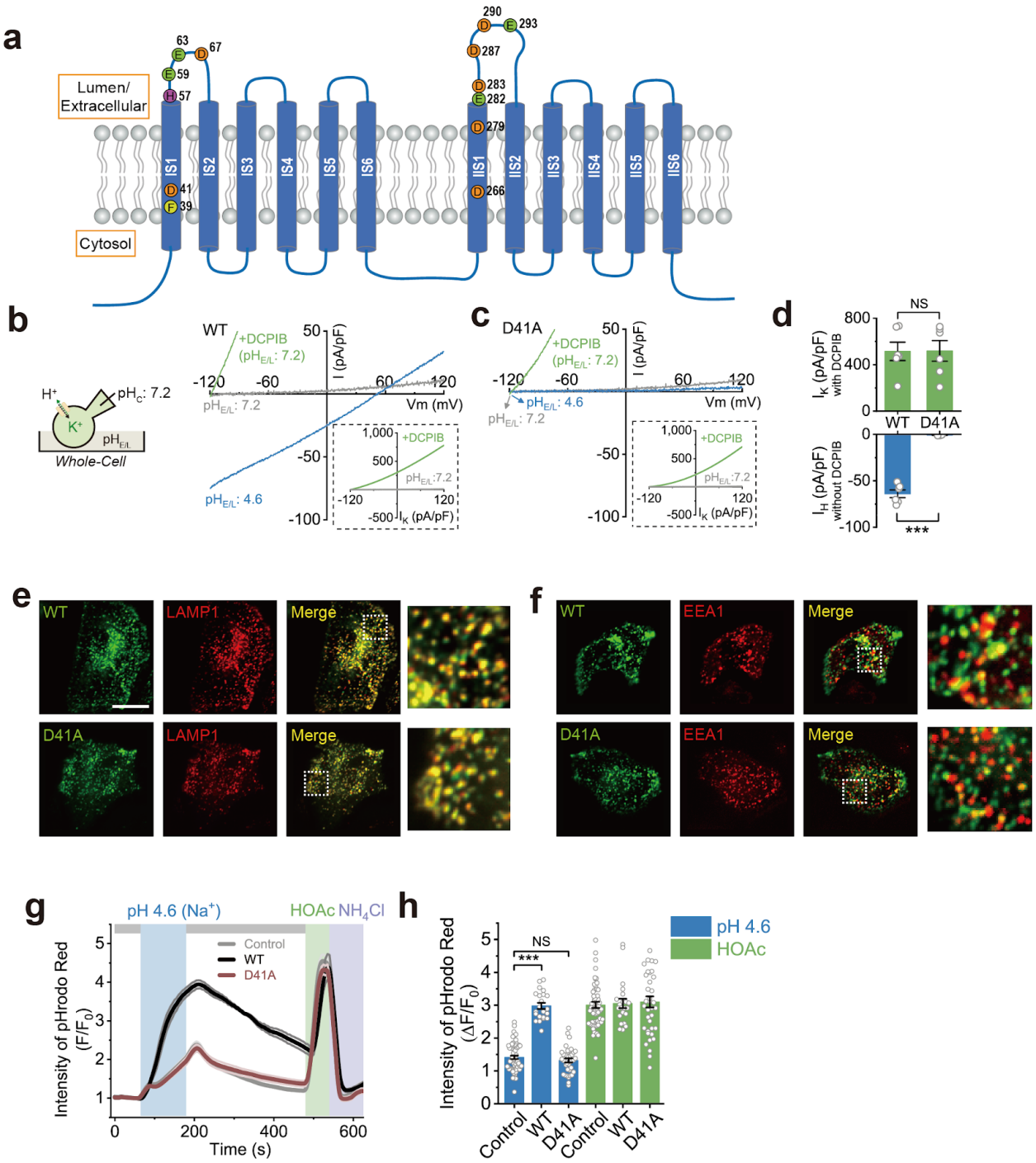


Figure 3.5 A single pore mutation in TMEM175 selectively eliminates its H^+ permeability without altering the K^+ permeability

(a) The topology of human TMEM175. This protein has two repeats, each of which contains six transmembrane domains (IS1-IS6 and IIS1-IIS6). The locations of aspartate (D), glutamate (E)

and histidine (H) sites in IS1, the IS1-IS2 loop, IIS1 and the IIS1-IIS2 loop are highlighted. F39, an amino acidic residue at which a mutation (F39V) is known to eliminate TMEM175 K^+ activity (Cang et al, 2015), is also highlighted. **(b-c)** Whole-cell currents recorded in an HEK293T cell overexpressing WT TMEM175 or the D41A mutant. The cytosolic solution contained K-MSA with pH_C set to 7.2. The large outward K^+ currents in the presence of DCPIB are shown on a different scale in the boxed inset. (**d**) Summary of H^+ (I_H) and K^+ (I_K) currents recorded in a series of cells from experiments as in (d-e). I_H was recorded at $pH_{E/L}$ 4.6 without any activators, and I_K was recorded in the presence of 50 μM DCPIB at $pH_{E/L}$ 7.2 (WT/D41A: n = 6/6 cells, mean ± SEM, *** p <0.001). (**e-f**) The subcellular localization of EGFP tagged WT TMEM175 and corresponding D41A mutants, determined using LAMP1-mCherry (late endosome and lysosome) and EEA1-mCherry (early endosome). Scale bars = 20 μm. (**g**) Average fluorescence emission of pHrodo™ Red stained HEK293T cells overexpressing WT TMEM175, D41A mutant and untransfected control cells in response to the stimuli as indicated. (**h**) Summary of the relative intensity of pHrodo™ Red in response to pH 4.6 and HOAc (control/WT/D41A, n = 65/25/38; mean ± SEM, *** p <0.001, NS p > 0.05)

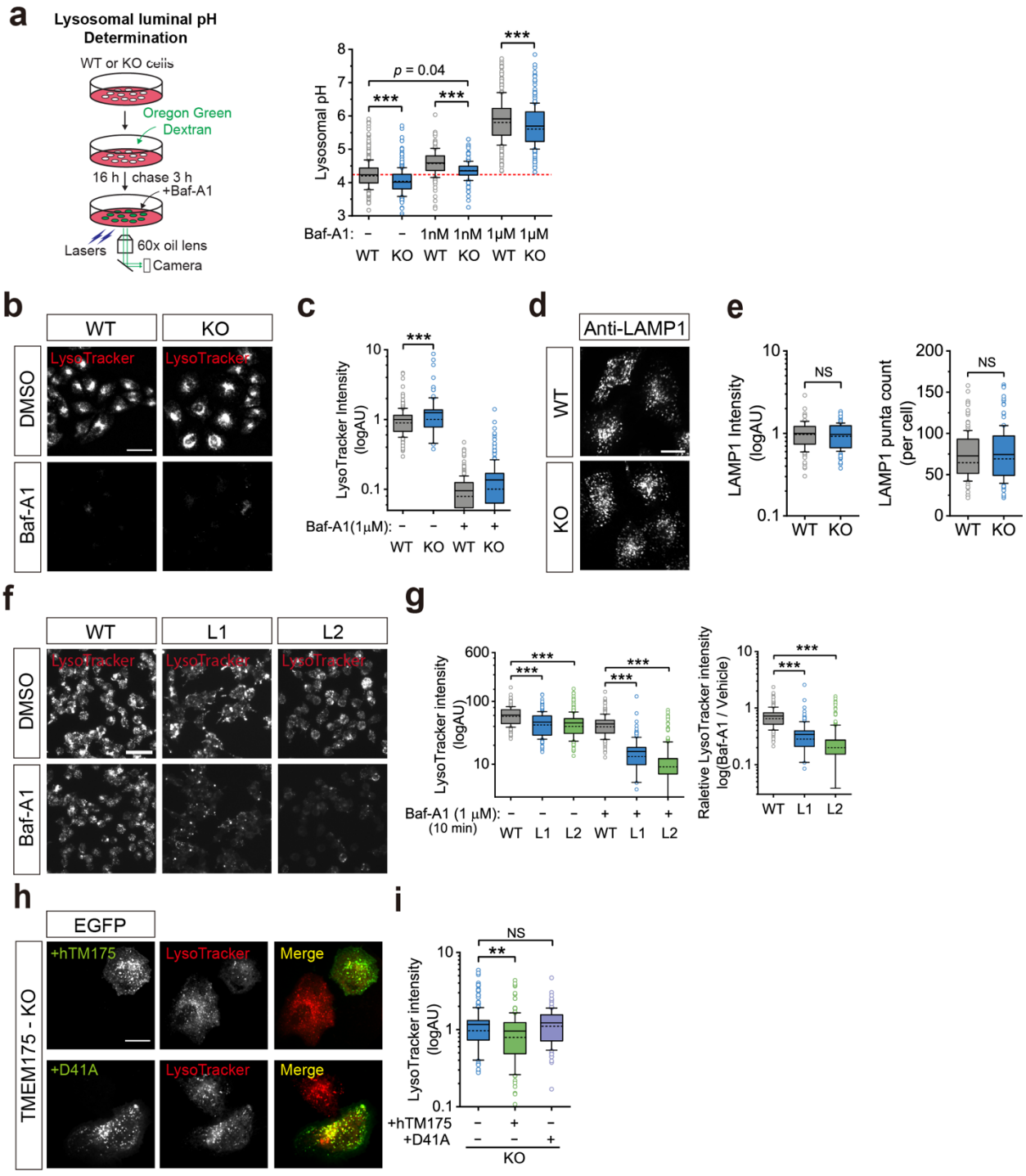
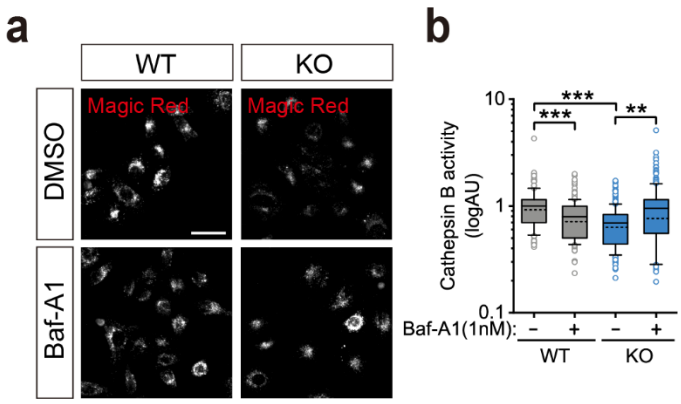


Figure 3.6 H^+ conductance through TMEM175 is required for lysosomal pH homeostasis.

(**a**) Lysosomal pH in WT and KO HeLa cells determined using Oregon Green Dextran. Baf-A1 was applied to block the V-ATPase and so alkalize the lysosome. Plots show the lysosomal pH

from three biological replicates of each condition. The red dashed line represents the mean level from WT cells (n = 177-487 cells per experiment, *** p <0.001). (**b-c**) Lysosomal acidity assessed by staining with LysoTracker (red) in WT and KO HeLa cells (scale bar = 50 μm). Plots show the LysoTracker intensity from three biological replicates (*n* = 165-228 cells per experiment, *** *p* <0.001). Cells incubated with 1 μM Baf-A1 for 1 hour served as a positive control. (**d-e**) Assessments of LAMP1 intensity (scale bar = 20 μm) and puncta count in WT and KO HeLa cells by immunostaining (WT, *n* = 80; KO, *n* = 81, NS *p* >0.05). (**f**) Representative fields of LysoTracker fluorescence in WT cells and two HEK293T cell lines stably expressing TMEM175 (L1 and L2) (scale bar = 50 μm). (**g**) Quantification of LysoTracker fluorescence intensity of all cells from three biological replicate experiments as in (f) (WT, *n* = 190; L1, *n* = 219; L2, *n* = 261, *** *p* <0.001, see **Methods** for the detail of box plots). Cells incubated with 1 μM Baf-A1 for 10 minutes immediately before imaging served as a positive control. In right panel, the relative LysoTracker intensity was calculated from the ratio between Baf-A1 groups and vehicle groups. (**h-i**) Lysosomal acidity assessed by staining with LysoTracker (red) in KO HeLa cells re-expressing EGFP-TMEM175 (WT) or the same construct carrying the D41A mutation (scale bar = 20 μm). Plots show LysoTracker intensity from three biological replicates (*n* = 108-308 cells per experiment, ** *p* <0.01, *** *p* <0.001).



3.7 TMEM175 is required for normal lysosome hydrolase activity.

(**a-b**) Lysosomal Cathepsin B activity estimated by staining with MagicRed in WT and KO HeLa cells (scale bar = 50 µm). Cells incubated with Baf-A1 (1 nM) for 1 hour served as the treatment group. Plots show average Magic Red intensity from three biological replicates (n = 128-266 cells per experiment, ** $p < 0.01$, *** $p < 0.001$).

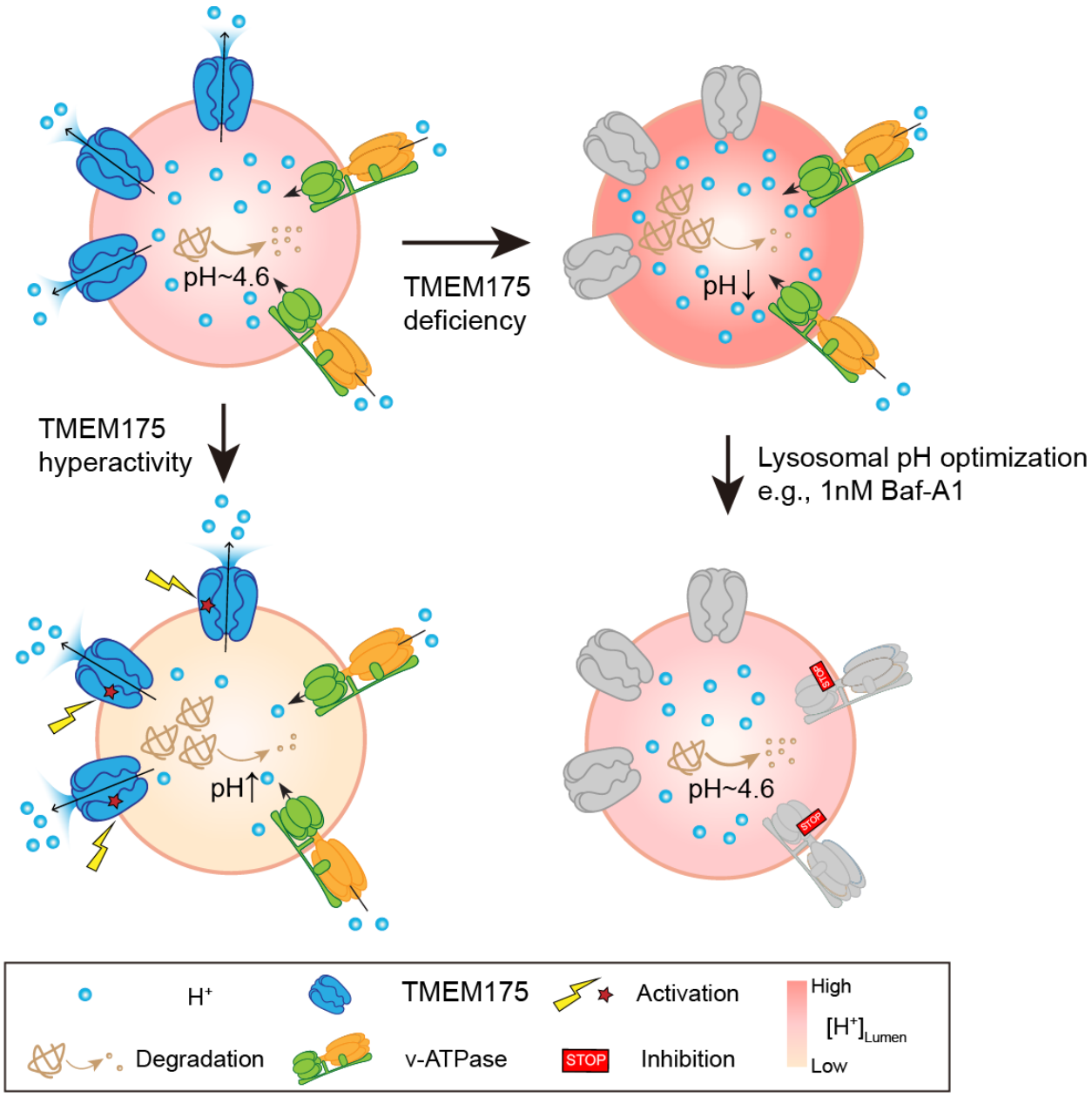


Fig. 3.8. Model for the role of TMEM175 in lysosomal pH homeostasis and lysosomal degradation. Lysosomal pH homeostasis, which is essential to macromolecule digestion in the lumen, requires the orchestration of V-ATPase pumping and TMEM175 leaking protons. Both TMEM175 deficiency and overactivity leads to lysosomal pH perturbation, which impairs lysosomal hydrolysis and causes macromolecules accumulation. Optimizing lysosomal pH, which can be

achieved by modulating V-ATPase activity or TMEM175 activity, may provide a new therapeutic target for lysosomal storage diseases and neurodegenerative diseases.

Chapter IV

Summary and Future Directions

IV-1 Summary of the study and significance

Lysosomes serve as intracellular signaling and degradation centers and maintain lysosome homeostasis in part through the use of lysosomal ion channels. Building upon the work of my collaborators who identified Lyso-VRAC and TMEM175 currents in lysosomes, the major goal of my studies was to elucidate the regulatory processes of Lyso-VRAC in maintaining proper cellular volume, and the mechanisms of TMEM175 in maintaining lysosomal pH homeostasis.

In chapter II, I showed that cells encountering physiological stresses often become vacuolated. Prior to our work the source of the vacuoles and their role in causing or ameliorating necrotic cell death was unclear. We demonstrated that in cells responding to hypo-osmotic stress, vacuoles are derived from lysosomes, and that many vacuoles subsequently undergo exocytosis. Furthermore, blocking either vacuolation or vacuole exocytosis by genetic or pharmacological approaches led to greatly increased necrotic cell death. By storing and then expelling excess water, lysosome-derived vacuoles maintain cytosolic water homeostasis and relieve membrane stress. This basic cellular function was present in all mammalian cell types tested, and required ionic-strength-sensitive ion channels formed from LRRC8 proteins on lysosomal membranes (Lyso-VRACs) acting in parallel with plasma membrane VRAC channels.

In chapter III, we extended already existing knowledge that lysosomal pH homeostasis is essential for metabolite degradation and other organelle functions, by demonstrating that the

optimal acidic environment within lysosomes is maintained by a V-type H^+ ATPase and a rapid proton efflux through TMEM175. When TMEM175 was deleted, cells showed hyper-acidification and impairment of degradation in lysosomes was restored by lysosomal pH optimization. Because TMEM175 has been identified as a genetic risk factor for Parkinson's Disease, this result not only builds on a novel concept on lysosomal pH regulation but also lays the groundwork necessary for therapeutic studies of PD.

IV-2 Potential Future Directions

2.1 Lyso-VRAC and cell death

The presence of LRRC8A on both the plasma membrane and the lysosomes suggests that common mechanisms may regulate both cell and organelle volume. We demonstrated clearly that lysosomal LRRC8A, but not PM LRRC8A, is essential for lysosomal vacuolation. VRAC channels are suspected to be permeable to water, in addition to anion (Nilius, 2004). Hence, certain unique properties of Lyso-VRAC, e.g., Γ_i-dependent gating and the water permeability of Lyso-VRAC are required for lysosomal vacuolation and RVD. It is necessary to determine the effect of initial vacuolation on the net driving force of Cl^- flux across lysosomal membranes, and to reveal the connections between Lyso-VRAC and lysosomal water permeability, vacuolation, and necrosis protection.

Because inflammation, which is reportedly associated with necrosis (Hotchkiss et al., 2009; Galluzzi et al., 2018), is prominent in most lysosomal storage diseases (LSDs) (Marques and Saftig, 2019), we wonder whether the lysosomal vacuolation-water sequestration-lysosomal exocytosis-water extrusion pathway may contribute to LSD pathologies. By screening a panel of LSD patient-derived human fibroblasts, we may be able to find if hypotonicity induced lysosomal vacuolation

is impaired in certain LSD fibroblasts compared with WT fibroblasts, so LSD cells may be more susceptible to necrotic cell death. Besides, it is worth mentioning that cholesterol, the primary storage material in NPC and many other LSDs (Marques and Saftig, 2019), is a reported inhibitor of VRAC (Romanenko et al., 2004). Hence, the Lyso-VRAC-mediated mechanism is likely to be impaired at least in some lysosomal diseases.

Our identification of LRRC8A as a lysosomal osmo-sensitive channel provides a molecular foundation upon which to explore the links between lysosomal physiology, lysosome and cell volume regulation, intracellular water regulation, necrosis, and pathologies of human diseases. Necrotic cell death is known to contribute significantly to stroke/trauma, brain inflammation, cancer, and many neurodegenerative disorders (Hotchkiss et al., 2009; Golstein and Kroemer, 2007) to which manipulating lysosome function and Lyso-VRAC activity may represent a general therapeutic strategy.

2.2 The Role of TMEM175

Impaired lysosome degradation function due to abnormal lysosomal pH leads to a range of diseases. We demonstrated that the activity of one of the lysosomal hydrolases, cathepsin B, was reduced with TMEM175 deficiency. Previous studies have demonstrated that cathepsin B and D are essential to α-synuclein degradation in the lysosome, which may provide a potential link between TMEM175 and Parkinson's diseases (McGlinchey and Lee, 2015). Lysosomal pH manipulation or optimization has been adopted to treat the patients with lysosomal hyper-acidification (Nicoli et al., 2019). Our demonstration that pH optimization results in restoration of cathepsin B activity provides the proof of concept that modulation of TMEM175 activity in the lysosome could be the basis of new therapies for Parkinson Disease.

Our identification of TMEM175 mutant D41A, which blocks proton and retains normal potassium currents, provides a unique opportunity to study the specific role of proton of TMEM175 in α-synuclein degradation. Generating D41A transgenic mice would be a novel model to study the physiological relevance of TMEM175 as a proton leak channel including lysosome degradation and α-synuclein aggregation *in vivo*. Moreover, a well-established assay, seeding of preformed α-synuclein fibrils (PFF) into the striatum, can be used to observe α-synuclein aggregation (Cover and Blanke, 2005). More and similar phosphorylated α-synuclein aggregation may occur in striatum and cortex of TMEM175 KO and D41A transgenic mice compared with WT mice, considering TMEM175 plays an essential role in lysosomal pH regulation and degradation. This study may potentially help to develop new therapeutic strategies in Parkinson Disease.

References

Al-Habori, M., A. Raman, M. J. Lawrence, and P. Skett. "In vitro effect of fenugreek extracts on intestinal sodium-dependent glucose uptake and hepatic glycogen phosphorylase A." International journal of experimental diabetes research 2 (2001).

Andrejewski, Nicole, Eeva-Liisa Punnonen, Gundula Guhde, Yoshitaka Tanaka, Renate Lüllmann-Rauch, Dieter Hartmann, Kurt Von Figura, and Paul Saftig. "Normal lysosomal morphology and function in LAMP-1-deficient mice." Journal of Biological Chemistry 274, no. 18 (1999): 12692-12701.

Ballabio, Andrea, and Juan S. Bonifacino. "Lysosomes as dynamic regulators of cell and organismal homeostasis." Nature Reviews Molecular Cell Biology 21, no. 2 (2020): 101-118.

Beertsen, Wouter, Marion Willenborg, Vincent Everts, Angelika Zirogianni, Rainer Podschun, Bernd Schröder, Eeva-Liisa Eskelinen, and Paul Saftig. "Impaired phagosomal maturation in neutrophils leads to periodontitis in lysosomal-associated membrane protein-2 knockout mice." The journal of immunology 180, no. 1 (2008): 475-482.

Beitz, Janice M. "Parkinson's disease: a review." Frontiers in bioscience (Scholar edition) 6 (2014): 65-74.

Borgnia, Mario, Søren Nielsen, Andreas Engel, and Peter Agre. "Cellular and molecular biology of the aquaporin water channels." Annual review of biochemistry 68, no. 1 (1999): 425-458.

Bourque, Charles W. "Central mechanisms of osmosensation and systemic osmoregulation." Nature Reviews Neuroscience 9, no. 7 (2008): 519-531.

Bowman, Emma Jean, Annette Siebers, and Karlheinz Altendorf. "Bafilomycins: a class of inhibitors of membrane ATPases from microorganisms, animal cells, and plant cells." Proceedings of the National Academy of Sciences 85, no. 21 (1988): 7972-7976.

Brady, Roscoe O. "Enzyme replacement for lysosomal diseases." Annu. Rev. Med. 57 (2006): 283-296.

Brunner, Janine D., Roman P. Jakob, Tobias Schulze, Yvonne Neldner, Anna Moroni, Gerhard Thiel, Timm Maier, and Stephan Schenck. "Structural basis for ion selectivity in TMEM175 K+ channels." Elife 9 (2020): e53683.

Cahalan, M., and R. S. Lewis. "Role of potassium and chloride channels in volume regulation by T lymphocytes: Cell Physiology of Blood, edited by R. Gunn and J. Parker." (1988): 281-301.

Cang, Chunlei, Biruk Bekele, and Dejian Ren. "The voltage-gated sodium channel TPC1 confers endolysosomal excitability." Nature chemical biology 10, no. 6 (2014): 463-469.

Cang, Chunlei, Kimberly Aranda, Young-jun Seo, Bruno Gasnier, and Dejian Ren. "TMEM175 is an organelle K+ channel regulating lysosomal function." Cell 162, no. 5 (2015): 1101-1112.

Cao, Qi, Xi Zoë Zhong, Yuanjie Zou, Zhu Zhang, Ligia Toro, and Xian-Ping Dong. "BK channels alleviate lysosomal storage diseases by providing positive feedback regulation of lysosomal Ca2+ release." Developmental cell 33, no. 4 (2015): 427-441.

Casey, Joseph R., Sergio Grinstein, and John Orlowski. "Sensors and regulators of intracellular pH." Nature reviews Molecular cell biology 11, no. 1 (2010): 50-61.

Chapel, Agnes, Sylvie Kieffer-Jaquinod, Corinne Sagne, Quentin Verdon, Corinne Ivaldi, Mourad Mellal, Jaqueline Thirion et al. "An extended proteome map of the lysosomal membrane reveals novel potential transporters." Molecular & Cellular Proteomics 12, no. 6 (2013): 1572-1588.

Chen, Cheng-Chang, Chunlei Cang, Stefanie Fenske, Elisabeth Butz, Yu-Kai Chao, Martin Biel, Dejian Ren, Christian Wahl-Schott, and Christian Grimm. "Patch-clamp technique to characterize ion channels in enlarged individual endolysosomes." nature protocols 12, no. 8 (2017): 1639.

Cheng, Xiping, Dongbiao Shen, Mohammad Samie, and Haoxing Xu. "Mucolipins: intracellular TRPML1-3 channels." FEBS letters 584, no. 10 (2010): 2013-2021.

Chou, Cheng-Yang, Meng-Ru Shen, and Sheng-Nan Wu. "Volume-sensitive chloride channels associated with human cervical carcinogenesis." Cancer research 55, no. 24 (1995): 6077-6083.

Chou, Kelvin L., Jennifer L. Taylor, and Parag G. Patil. "The MDS− UPDRS tracks motor and non-motor improvement due to subthalamic nucleus deep brain stimulation in Parkinson disease." Parkinsonism & related disorders 19, no. 11 (2013): 966-969.

Christensen, Kenneth A., Jesse T. Myers, and Joel A. Swanson. "pH-dependent regulation of lysosomal calcium in macrophages." Journal of cell science 115, no. 3 (2002): 599-607.

Churchill, Kathleen A., Barbara Holaway, and Heven Sze. "Separation of two types of electrogenic H+-pumping ATPases from oat roots." Plant physiology 73, no. 4 (1983): 921-928.

Churchill, Kathleen A., and Heven Sze. "Anion-sensitive, H+-pumping ATPase in membrane vesicles from oat roots." Plant physiology 71, no. 3 (1983): 610-617.

Conus, Sébastien, and Hans-Uwe Simon. "Cathepsins: key modulators of cell death and inflammatory responses." Biochemical pharmacology 76, no. 11 (2008): 1374-1382.

Cover, Timothy L., and Steven R. Blanke. "Helicobacter pylori VacA, a paradigm for toxin multifunctionality." Nature Reviews Microbiology 3, no. 4 (2005): 320-332.

Davis, Michael J., Brian Gregorka, Jason E. Gestwicki, and Joel A. Swanson. "Inducible renitence limits Listeria monocytogenes escape from vacuoles in macrophages." The Journal of Immunology 189, no. 9 (2012): 4488-4495.

Dawson, Ted M., Han Seok Ko, and Valina L. Dawson. "Genetic animal models of Parkinson's disease." Neuron 66, no. 5 (2010): 646-661.

Decher, Niels, Hans J. Lang, Bernd Nilius, Andrea Brüggemann, Andreas E. Busch, and Klaus Steinmeyer. "DCPIB is a novel selective blocker of ICl, swell and prevents swelling-induced shortening of guinea-pig atrial action potential duration." British journal of pharmacology 134, no. 7 (2001): 1467-1479.

Decoursey, Thomas E. "Voltage-gated proton channels and other proton transfer pathways." Physiological reviews (2003).

Decressac, Mickael, Bengt Mattsson, Pia Weikop, Martin Lundblad, Johan Jakobsson, and Anders Björklund. "TFEB-mediated autophagy rescues midbrain dopamine neurons from α-synuclein toxicity." Proceedings of the National Academy of Sciences 110, no. 19 (2013): E1817-E1826.

Delpire, Eric, and Kenneth B. Gagnon. "Water homeostasis and cell volume maintenance and regulation." In Current topics in membranes, vol. 81, pp. 3-52. Academic Press, 2018.

Deneka, Dawid, Marta Sawicka, Andy KM Lam, Cristina Paulino, and Raimund Dutzler. "Structure of a volume-regulated anion channel of the LRRC8 family." Nature 558, no. 7709 (2018): 254-259.

Dixon, Scott J., Kathryn M. Lemberg, Michael R. Lamprecht, Rachid Skouta, Eleina M. Zaitsev, Caroline E. Gleason, Darpan N. Patel et al. "Ferroptosis: an iron-dependent form of nonapoptotic cell death." Cell 149, no. 5 (2012): 1060-1072.

Dong, Xian-ping, Dongbiao Shen, Xiang Wang, Taylor Dawson, Xinran Li, Qi Zhang, Xiping Cheng et al. "PI (3, 5) P2 controls membrane trafficking by direct activation of mucolipin Ca2+ release channels in the endolysosome." Nature communications 1, no. 1 (2010): 1-11.

Dong, Xian-Ping, Xiang Wang, and Haoxing Xu. "TRP channels of intracellular membranes." Journal of neurochemistry 113, no. 2 (2010): 313-328.

Dong, Xian-Ping, Xiping Cheng, Eric Mills, Markus Delling, Fudi Wang, Tino Kurz, and Haoxing Xu. "The type IV mucolipidosis-associated protein TRPML1 is an endolysosomal iron release channel." Nature 455, no. 7215 (2008): 992-996.

Dou, Ying, Hang-jun Wu, Hui-quan Li, Song Qin, Yin-er Wang, Jing Li, Hui-fang Lou et al. "Microglial migration mediated by ATP-induced ATP release from lysosomes." Cell research 22, no. 6 (2012): 1022-1033.

Dubois, Jean-Marc, and Béatrice Rouzaire-Dubois. "Roles of cell volume in molecular and cellular biology." Progress in biophysics and molecular biology 108, no. 3 (2012): 93-97.

Edsall, John T., and Jeffries Wyman. "Jeffries Wyman and myself: a story of two interacting lives." In Comprehensive biochemistry, vol. 36, pp. 99-195. Elsevier, 1986.

Eskelinen, Eeva-Liisa, Christine Katrin Schmidt, Silja Neu, Marion Willenborg, Graciela Fuertes, Natalia Salvador, Yoshitaka Tanaka et al. "Disturbed cholesterol traffic but normal proteolytic function in LAMP-1/LAMP-2 double-deficient fibroblasts." Molecular biology of the cell 15, no. 7 (2004): 3132-3145

Fehrenbacher, Nicole, Lone Bastholm, Thomas Kirkegaard-Sørensen, Bo Rafn, Trine Bøttzauw, Christina Nielsen, Ekkehard Weber, Senji Shirasawa, Tuula Kallunki, and Marja Jäättelä. "Sensitization to the lysosomal cell death pathway by oncogene-induced down-regulation of lysosome-associated membrane proteins 1 and 2." Cancer research 68, no. 16 (2008): 6623-6633.

Finbow, Malcolm E., and Michael A. Harrison. "The vacuolar H+-ATPase: a universal proton pump of eukaryotes." Biochemical Journal 324, no. 3 (1997): 697-712.

Fishbein, Ianai, Yien-Ming Kuo, Benoit I. Giasson, and Robert L. Nussbaum. "Augmentation of phenotype in a transgenic Parkinson mouse heterozygous for a Gaucher mutation." Brain 137, no. 12 (2014): 3235-3247.

Galluzzi, Lorenzo, Ilio Vitale, Stuart A. Aaronson, John M. Abrams, Dieter Adam, Patrizia Agostinis, Emad S. Alnemri et al. "Molecular mechanisms of cell death: recommendations of the Nomenclature Committee on Cell Death 2018." Cell Death & Differentiation 25, no. 3 (2018): 486-541.

Golstein, Pierre, and Guido Kroemer. "Cell death by necrosis: towards a molecular definition." Trends in biochemical sciences 32, no. 1 (2007): 37-43.

Graves, Austin R., Patricia K. Curran, Carolyn L. Smith, and Joseph A. Mindell. "The Cl-/H+ antiporter ClC-7 is the primary chloride permeation pathway in lysosomes." Nature 453, no. 7196 (2008): 788-792.

Hazama, A. K. I. H. I. R. O., and Y. A. S. U. N. O. B. U. Okada. "Ca2+ sensitivity of volume-regulatory K+ and Cl- channels in cultured human epithelial cells." The Journal of Physiology 402, no. 1 (1988): 687-702.

Hille, Bertil. "Ionic channels in excitable membranes. Current problems and biophysical approaches." Biophysical Journal 22, no. 2 (1978): 283-294.

Hille, Bertil. "Ion channels of excitable membranes (3rd edition, Sinauer, Sunderland, MA)." (2001).

Hoffmann, Else K., Ian H. Lambert, and Stine F. Pedersen. "Physiology of cell volume regulation in vertebrates." Physiological reviews 89, no. 1 (2009): 193-277.

Hotchkiss, Richard S., Andreas Strasser, Jonathan E. McDunn, and Paul E. Swanson. "Cell death." New England Journal of Medicine 361, no. 16 (2009): 1570-1583.

Huynh, Chau, and Norma W. Andrews. "The small chemical vacuolin-1 alters the morphology of lysosomes without inhibiting Ca2+-regulated exocytosis." EMBO reports 6, no. 9 (2005): 843-847.

Huynh, Kassidy K., Eeva-Liisa Eskelinen, Cameron C. Scott, Anatoly Malevanets, Paul Saftig, and Sergio Grinstein. "LAMP proteins are required for fusion of lysosomes with phagosomes." The EMBO journal 26, no. 2 (2007): 313-324.

Ishida, Yoichi, Smita Nayak, Joseph A. Mindell, and Michael Grabe. "A model of lysosomal pH regulation." Journal of General Physiology 141, no. 6 (2013): 705-720.

Jackson, PAUL S., and K. E. V. I. N. Strange. "Volume-sensitive anion channels mediate swelling-activated inositol and taurine efflux." American Journal of Physiology-Cell Physiology 265, no. 6 (1993): C1489-C1500.

Jadot, Michel, Christine Colmant, Simone Wattiaux-De Coninck, and Robert Wattiaux. "Intralysosomal hydrolysis of glycyl-L-phenylalanine 2-naphthylamide." Biochemical Journal 219, no. 3 (1984): 965-970.

Jentsch, Thomas J. "VRACs and other ion channels and transporters in the regulation of cell volume and beyond." Nature Reviews Molecular Cell Biology 17, no. 5 (2016): 293-307.

Jentsch, Thomas J., and Michael Pusch. "CLC chloride channels and transporters: structure, function, physiology, and disease." Physiological reviews 98, no. 3 (2018): 1493-1590.

Jeong, Jeeyon, and David J. Eide. "The SLC39 family of zinc transporters." Molecular aspects of medicine 34, no. 2-3 (2013): 612-619.

Jinn, Sarah, Cornelis Blauwendraat, Dawn Toolan, Cheryl A. Gretzula, Robert E. Drolet, Sean Smith, Mike A. Nalls, Jacob Marcus, Andrew B. Singleton, and David J. Stone. "Functionalization of the TMEM175 p. M393T variant as a risk factor for Parkinson disease." Human molecular genetics 28, no. 19 (2019): 3244-3254.

Jinn, Sarah, Robert E. Drolet, Paige E. Cramer, Andus Hon-Kit Wong, Dawn M. Toolan, Cheryl A. Gretzula, Bhavya Voleti et al. "TMEM175 deficiency impairs lysosomal and mitochondrial function and increases α-synuclein aggregation." Proceedings of the National Academy of Sciences 114, no. 9 (2017): 2389-2394.

Kasper, Dagmar, Rosa Planells-Cases, Jens C. Fuhrmann, Olaf Scheel, Oliver Zeitz, Klaus Ruether, Anja Schmitt et al. "Loss of the chloride channel ClC-7 leads to lysosomal storage disease and neurodegeneration." The EMBO journal 24, no. 5 (2005): 1079-1091.

Kefauver, Jennifer M., Kei Saotome, Adrienne E. Dubin, Jesper Pallesen, Christopher A. Cottrell, Stuart M. Cahalan, Zhaozhu Qiu et al. "Structure of the human volume regulated anion channel." Elife 7 (2018): e38461.

Kern, David M., SeCheol Oh, Richard K. Hite, and Stephen G. Brohawn. "Cryo-EM structures of the DCPIB-inhibited volume-regulated anion channel LRRC8A in lipid nanodiscs." Elife 8 (2019): e42636.

Kim, Hyun Jin, Qin Li, Sandra Tjon-Kon-Sang, Insuk So, Kirill Kiselyov, Abigail A. Soyombo, and Shmuel Muallem. "A novel mode of TRPML3 regulation by extracytosolic pH absent in the varitint-waddler phenotype." The EMBO journal 27, no. 8 (2008): 1197-1205.

Kima, Peter E., Barbara Burleigh, and Norma W. Andrews. "Surface-targeted lysosomal membrane glycoprotein-1 (Lamp-1) enhances lysosome exocytosis and cell invasion by Trypanosoma cruzi." Cellular microbiology 2, no. 6 (2000): 477-486.

Kovacs, Gabor G. "Concepts and classification of neurodegenerative diseases." In Handbook of clinical neurology, vol. 145, pp. 301-307. Elsevier, 2018.

Lang, Florian, Gillian L. Busch, Markus Ritter, Harald Volkl, Siegfried Waldegger, Erich Gulbins, and Dieter Haussinger. "Functional significance of cell volume regulatory mechanisms." Physiological reviews 78, no. 1 (1998): 247-306.

Lang, Florian. "Mechanisms and significance of cell volume regulation." Journal of the American college of nutrition 26, no. sup5 (2007): 613S-623S.

Lee, Changkeun, Jiangtao Guo, Weizhong Zeng, Sunghoon Kim, Ji She, Chunlei Cang, Dejian Ren, and Youxing Jiang. "The lysosomal potassium channel TMEM175 adopts a novel tetrameric architecture." Nature 547, no. 7664 (2017): 472-475.

Lewis, C. A. "Ion-concentration dependence of the reversal potential and the single channel conductance of ion channels at the frog neuromuscular junction." The Journal of Physiology 286, no. 1 (1979): 417-445.

Lichko, L. P., and L. A. Okorokov. "Some properties of membrane-bound, solubilized and reconstituted into liposomes H+-ATPase of vacuoles of Saccharomyces carlsbergensis." FEBS letters 174, no. 2 (1984): 233-237.

Lie, Pearl PY, and Ralph A. Nixon. "Lysosome trafficking and signaling in health and neurodegenerative diseases." Neurobiology of disease 122 (2019): 94-105.

Lill, Christina M., Johnni Hansen, Jørgen H. Olsen, Harald Binder, Beate Ritz, and Lars Bertram. "Impact of Parkinson's disease risk loci on age at onset." Movement disorders 30, no. 6 (2015): 847-850.

Lockwood, Thomas D. "Lysosomal metal, redox and proton cycles influencing the CysHis cathepsin reaction." Metallomics 5, no. 2 (2013): 110-124.

Mackenzie, Bryan, and Jeffrey D. Erickson. "Sodium-coupled neutral amino acid (System N/A) transporters of the SLC38 gene family." Pflügers Archiv 447, no. 5 (2004): 784-795.

Marques, André RA, and Paul Saftig. "Lysosomal storage disorders–challenges, concepts and avenues for therapy: beyond rare diseases." Journal of Cell Science 132, no. 2 (2019).

McGlinchey, Ryan P., and Jennifer C. Lee. "Cysteine cathepsins are essential in lysosomal degradation of α-synuclein." Proceedings of the National Academy of Sciences 112, no. 30 (2015): 9322-9327.

Miesenböck, Gero, Dino A. De Angelis, and James E. Rothman. "Visualizing secretion and synaptic transmission with pH-sensitive green fluorescent proteins." Nature 394, no. 6689 (1998): 192-195.

Mindell, Joseph A. "Lysosomal acidification mechanisms." Annual review of physiology 74 (2012): 69-86.

Morgan, Anthony J., Frances M. Platt, Emyr Lloyd-Evans, and Antony Galione. "Molecular mechanisms of endolysosomal Ca2+ signalling in health and disease." Biochemical Journal 439, no. 3 (2011): 349-378.

Morgan, Deri, Melania Capasso, Boris Musset, Vladimir V. Cherny, Eduardo Ríos, Martin JS Dyer, and Thomas E. DeCoursey. "Voltage-gated proton channels maintain pH in human neutrophils during phagocytosis." Proceedings of the National Academy of Sciences 106, no. 42 (2009): 18022-18027.

Nalls, Mike A., Nathan Pankratz, Christina M. Lill, Chuong B. Do, Dena G. Hernandez, Mohamad Saad, Anita L. DeStefano et al. "Large-scale meta-analysis of genome-wide association data identifies six new risk loci for Parkinson's disease." Nature genetics 46, no. 9 (2014): 989-993.

Neher, Erwin. "Correction for liquid junction potentials in patch clamp experiments." Methods in enzymology 207 (1992): 123-131.

Nicoli, Elena-Raluca, Mary R. Weston, Mary Hackbarth, Alissa Becerril, Austin Larson, Wadih M. Zein, Peter R. Baker II et al. "Lysosomal storage and albinism due to effects of a de novo CLCN7 variant on lysosomal acidification." The American Journal of Human Genetics 104, no. 6 (2019): 1127-1138.

Nilius, Bernd. "Is the volume-regulated anion channel VRAC a “water-permeable” channel?" Neurochemical research 29, no. 1 (2004): 3-8.

Nilius, Bernd, Jan Eggermont, Thomas Voets, Gunnar Buyse, Vangelis Manolopoulos, and Guy Droogmans. "Properties of volume-regulated anion channels in mammalian cells." Progress in biophysics and molecular biology 68, no. 1 (1997): 69-119.

Nishino, Ichizo, Jin Fu, Kurenai Tanji, Takeshi Yamada, Sadatomo Shimojo, Tateo Koori, Marina Mora et al. "Primary LAMP-2 deficiency causes X-linked vacuolar cardiomyopathy and myopathy (Danon disease)." Nature 406, no. 6798 (2000): 906-910.

Nixon, Ralph A. "Niemann-Pick Type C disease and Alzheimer's disease: the APP-endosome connection fattens up." The American journal of pathology 164, no. 3 (2004): 757-761.

Oh, SeCheol, Navid Paknejad, and Richard K. Hite. "Gating and selectivity mechanisms for the lysosomal K+ channel TMEM175." Elife 9 (2020): e53430.

Ohkuma, Shoji, YOSHINOlu Moriyama, and Tatsuya Takano. "Identification and characterization of a proton pump on lysosomes by fluorescein-isothiocyanate-dextran fluorescence." Proceedings of the National Academy of Sciences 79, no. 9 (1982): 2758-2762.

Parenti, Giancarlo, Generoso Andria, and Andrea Ballabio. "Lysosomal storage diseases: from pathophysiology to therapy." Annual review of medicine 66 (2015): 471-486.

Parkinson-Lawrence, Emma J., Tetyana Shandala, Mark Prodoehl, Revecca Plew, Glenn N. Borlace, and Doug A. Brooks. "Lysosomal storage disease: revealing lysosomal function and physiology." Physiology 25, no. 2 (2010): 102-115.

Pedersen, Stine F., Yasunobu Okada, and Bernd Nilius. "Biophysics and physiology of the volume-regulated anion channel (VRAC)/volume-sensitive outwardly rectifying anion channel (VSOR)." Pflügers Archiv-European Journal of Physiology 468, no. 3 (2016): 371-383.

Pisoni, Ronald L., and Jess G. Thoene. "The transport systems of mammalian lysosomes." Biochimica Et Biophysica Acta (BBA)-Reviews on Biomembranes 1071, no. 4 (1991): 351-373.

Platt, Frances M., and Terry D. Butters. "Substrate reduction therapy." In Lysosomal Storage Disorders, pp. 153-168. Springer, Boston, MA, 2007.

Poehler, Anne-Maria, Wei Xiang, Philipp Spitzer, Verena Elisabeth Luise May, Holger Meixner, Edward Rockenstein, Oldriska Chutna et al. "Autophagy modulates SNCA/α-synuclein release, thereby generating a hostile microenvironment." Autophagy 10, no. 12 (2014): 2171-2192.

Pu, Jing, Carlos M. Guardia, Tal Keren-Kaplan, and Juan S. Bonifacino. "Mechanisms and functions of lysosome positioning." Journal of cell science 129, no. 23 (2016): 4329-4339.

Pungerčar, Jerica Rozman, Dejan Caglič, Mohammed Sajid, Marko Dolinar, Olga Vasiljeva, Urška Požgan, Dušan Turk, Matthew Bogyo, Vito Turk, and Boris Turk. "Autocatalytic processing of procathepsin B is triggered by proenzyme activity." The FEBS journal 276, no. 3 (2009): 660-668.

Qiu, Zhaozhu, Adrienne E. Dubin, Jayanti Mathur, Buu Tu, Kritika Reddy, Loren J. Miraglia, Jürgen Reinhardt, Anthony P. Orth, and Ardem Patapoutian. "SWELL1, a plasma membrane protein, is an essential component of volume-regulated anion channel." Cell 157, no. 2 (2014): 447-458.

Quraishi, Omar, Dorit K. Nägler, Ted Fox, J. Sivaraman, Miroslaw Cygler, John S. Mort, and Andrew C. Storer. "The occluding loop in cathepsin B defines the pH dependence of inhibition by its propeptide." Biochemistry 38, no. 16 (1999): 5017-5023.

Rastall, David Pw, and Andrea Amalfitano. "Recent advances in gene therapy for lysosomal storage disorders." The application of clinical genetics 8 (2015): 157.

Ramsey, I. Scott, Magdalene M. Moran, Jayhong A. Chong, and David E. Clapham. "A voltage-gated proton-selective channel lacking the pore domain." Nature 440, no. 7088 (2006): 1213-1216.

Ran, F. Ann, Patrick D. Hsu, Jason Wright, Vineeta Agarwala, David A. Scott, and Feng Zhang. "Genome engineering using the CRISPR-Cas9 system." Nature protocols 8, no. 11 (2013): 2281-2308.

Rodríguez, Ana, Paul Webster, Javier Ortego, and Norma W. Andrews. "Lysosomes behave as Ca2+-regulated exocytic vesicles in fibroblasts and epithelial cells." The Journal of cell biology 137, no. 1 (1997): 93-104.

Romanenko, Victor G., George H. Rothblat, and Irena Levitan. "Sensitivity of volume-regulated anion current to cholesterol structural analogues." The Journal of general physiology 123, no. 1 (2004): 77-88.

Samie, Mohammad Ali, and Haoxing Xu. "Lysosomal exocytosis and lipid storage disorders." Journal of lipid research 55, no. 6 (2014): 995-1009.

Sasaki, Mari, Masahiro Takagi, and Yasushi Okamura. "A voltage sensor-domain protein is a voltage-gated proton channel." Science 312, no. 5773 (2006): 589-592.

Savitt, Joseph M., Valina L. Dawson, and Ted M. Dawson. "Diagnosis and treatment of Parkinson disease: molecules to medicine." The Journal of clinical investigation 116, no. 7 (2006): 1744-1754.

Schröder, Bernd A., Christian Wrocklage, Andrej Hasilik, and Paul Saftig. "The proteome of lysosomes." Proteomics 10, no. 22 (2010): 4053-4076.

Schroder, B., C. Wrocklage, C. Pan, R. Jager, B. Kosters, H. Schafer, H. P. Elsasser, M. Mann, and A. Hasilik. "Integral and associated lysosomal membrane proteins Traffic 2007 8." N 12: 1676-1686.

Schulze, Heike, and Konrad Sandhoff. "Lysosomal lipid storage diseases." Cold Spring Harbor perspectives in biology 3, no. 6 (2011): a004804.

Schwake, Michael, Bernd Schröder, and Paul Saftig. "Lysosomal membrane proteins and their central role in physiology." Traffic 14, no. 7 (2013): 739-748.

Shea, L., and N. Raben. "Autophagy in skeletal muscle: implications for Pompe disease." International journal of clinical pharmacology and therapeutics 47, no. Suppl 1 (2009): S42.

Shen, Meng-Ru, Guy Droogmans, Jan Eggermont, Thomas Voets, J. Clive Ellory, and Bernd Nilius. "Differential expression of volume-regulated anion channels during cell cycle progression of human cervical cancer cells." The Journal of physiology 529, no. 2 (2000): 385-394.

Sherer, Todd B., Sohini Chowdhury, Katherine Peabody, and Deborah W. Brooks. "Overcoming obstacles in Parkinson's disease." Movement disorders 27, no. 13 (2012): 1606-1611.

Sidransky, Ellen, Michael A. Nalls, Jan O. Aasly, Judith Aharon-Peretz, Grazia Annesi, Egberto R. Barbosa, Anat Bar-Shira et al. "Multicenter analysis of glucocerebrosidase mutations in Parkinson's disease." New England Journal of Medicine 361, no. 17 (2009): 1651-1661.

Stefanis, Leonidas, Evangelia Emmanouilidou, Marina Pantazopoulou, Deniz Kirik, Kostas Vekrellis, and George K. Tofaris. "How is alpha-synuclein cleared from the cell?" Journal of neurochemistry 150, no. 5 (2019): 577-590.

Steinberg, Benjamin E., Kassidy K. Huynh, Alexandre Brodovitch, Sabrina Jabs, Tobias Stauber, Thomas J. Jentsch, and Sergio Grinstein. "A cation counterflux supports lysosomal acidification." Journal of Cell Biology 189, no. 7 (2010): 1171-1186.

Štrbák, Vladimí, and Monte A. Greer. "Regulation of hormone secretion by acute cell volume changes: Ca2+-independent hormone secretion." Cellular Physiology and Biochemistry 10, no. 5-6 (2000): 393-402.

Syeda, Ruhma, Zhaozhu Qiu, Adrienne E. Dubin, Swetha E. Murthy, Maria N. Florendo, Daniel E. Mason, Jayanti Mathur et al. "LRRC8 proteins form volume-regulated anion channels that sense ionic strength." Cell 164, no. 3 (2016): 499-511.

Tanaka, Yoshitaka, Gundula Guhde, Anke Suter, Eeva-Liisa Eskelinen, Dieter Hartmann, Renate Lüllmann-Rauch, Paul ML Janssen, Judith Blanz, Kurt Von Figura, and Paul Saftig.

"Accumulation of autophagic vacuoles and cardiomyopathy in LAMP-2-deficient mice." Nature 406, no. 6798 (2000): 902-906.

Tu, Yu-Hsiang, Alexander J. Cooper, Bochuan Teng, Rui B. Chang, Daniel J. Artiga, Heather N. Turner, Eric M. Mulhall, Wenlei Ye, Andrew D. Smith, and Emily R. Liman. "An evolutionarily conserved gene family encodes proton-selective ion channels." Science 359, no. 6379 (2018): 1047-1050.

Vílchez, M. Carmen, Marina Morini, David S. Peñaranda, Víctor Gallego, Juan F. Asturiano, and Luz Pérez. "Role of potassium and pH on the initiation of sperm motility in the European eel. Part A Molecular & integrative physiology." (2017).

Vitner, Einat B., Frances M. Platt, and Anthony H. Futerman. "Common and uncommon pathogenic cascades in lysosomal storage diseases." Journal of Biological Chemistry 285, no. 27 (2010): 20423-20427.

Voss, Felizia K., Florian Ullrich, Jonas Münch, Katina Lazarow, Darius Lutter, Nancy Mah, Miguel A. Andrade-Navarro, Jens P. von Kries, Tobias Stauber, and Thomas J. Jentsch. "Identification of LRRC8 heteromers as an essential component of the volume-regulated anion channel VRAC." Science 344, no. 6184 (2014): 634-638.

Wang, Wuyang, Qiong Gao, Meimei Yang, Xiaoli Zhang, Lu Yu, Maria Lawas, Xinran Li et al. "Up-regulation of lysosomal TRPML1 channels is essential for lysosomal adaptation to nutrient starvation." Proceedings of the National Academy of Sciences 112, no. 11 (2015): E1373-E1381.

Wang, Wuyang, Xiaoli Zhang, Qiong Gao, Maria Lawas, Lu Yu, Xiping Cheng, Mingxue Gu et al. "A voltage-dependent K+ channel in the lysosome is required for refilling lysosomal Ca2+ stores." Journal of Cell Biology 216, no. 6 (2017): 1715-1730.

Wang, Yeshi, Qihui Wu, Meiqin Hu, Bin Liu, Zuying Chai, Rong Huang, Yuan Wang et al. "Ligand-and voltage-gated Ca2+ channels differentially regulate the mode of vesicular neuropeptide release in mammalian sensory neurons." Science Signaling 10, no. 484 (2017).

WANG, Z-M., C-X. LI, D. Xing, Y-H. YU, N. Liu, R-D. XUE, Y-D. DONG, and T-Y. ZHAO. "Detection and widespread distribution of sodium channel alleles characteristic of insecticide resistance in Culex pipiens complex mosquitoes in China." Medical and veterinary entomology 26, no. 2 (2012): 228-232.

Wyant, Gregory A., Monther Abu-Remaileh, Evgeni M. Frenkel, Nouf N. Laqtom, Vimisha Dharamdasani, Caroline A. Lewis, Sze Ham Chan, Ivonne Heinze, Alessandro Ori, and David M. Sabatini. "NUFIP1 is a ribosome receptor for starvation-induced ribophagy." Science 360, no. 6390 (2018): 751-758.

Xilouri, Maria, and Leonidas Stefanis. "Autophagic pathways in Parkinson disease and related disorders." Expert reviews in molecular medicine 13 (2011).

Xiong, Jian, and Michael X. Zhu. "Regulation of lysosomal ion homeostasis by channels and transporters." Science China Life Sciences 59, no. 8 (2016): 777-791.

Xu, Haoxing, and Dejian Ren. "Lysosomal physiology." Annual review of physiology 77 (2015): 57-80.

Yang, Hong, Xiaohong Joe Zhou, Min-ming Zhang, Xu-ning Zheng, Yi-lei Zhao, and Jue Wang. "Changes in spontaneous brain activity in early Parkinson's disease." Neuroscience letters 549 (2013): 24-28.

Yang, Junhua, Jianan Chen, Maria del Carmen Vitery, James Osei-Owusu, Jiachen Chu, Haiyang Yu, Shuying Sun, and Zhaozhu Qiu. "PAC, an evolutionarily conserved membrane protein, is a proton-activated chloride channel." Science 364, no. 6438 (2019): 395-399.

Ylitervo, Päivi, Carl Johan Franzén, and Mohammad J. Taherzadeh. "Continuous ethanol production with a membrane bioreactor at high acetic acid concentrations." Membranes 4, no. 3 (2014): 372-387.

Yoshida, Asami, Megumi Ohta, Koichi Kuwahara, Min-Jie Cao, Kenji Hara, and Kiyoshi Osatomi. "Purification and characterization of cathepsin B from the muscle of horse mackerel Trachurus japonicus." Marine drugs 13, no. 11 (2015): 6550-6565.

Yu, Lu, Xiaoli Zhang, Yexin Yang, Dan Li, Kaiyuan Tang, Zifan Zhao, Wanwan He et al. "Small-molecule activation of lysosomal TRP channels ameliorates Duchenne muscular dystrophy in mouse models." Science advances 6, no. 6 (2020): eaaz2736.

Zhang, Lisha, Rui Sheng, and Zhenghong Qin. "The lysosome and neurodegenerative diseases." Acta biochimica et biophysica Sinica 41, no. 6 (2009): 437-445.

Zhang, Xiaoli, Meiqin Hu, Yexin Yang, and Haoxing Xu. "Organellar TRP channels." Nature structural & molecular biology 25, no. 11 (2018): 1009-1018.